Changes in ocean circulation during MIS3 inferred from radiocarbon records

Warren Beck, Doug Donahue, Tiffany McLamarrah, Dana Biddulph……*University of Arizona, USA*

David Richards, Peter Smart…….*University of Bristol*

Larry Edwards……………………..*University of Minnesota, USA*

Changes in ocean circulation during MIS3 inferred from radiocarbon records:
Inferences and implications from the ^{14}C record

Short background discussion of the modern carbon cycle

The radiocarbon record

- Long record from a stalagmite

Controls on radiocarbon production

- Galactic cosmic rays
- Solar electromagnetic field
- Geomagnetic field

Partitioning of radiocarbon in the carbon cycle

- Dominance of the oceans

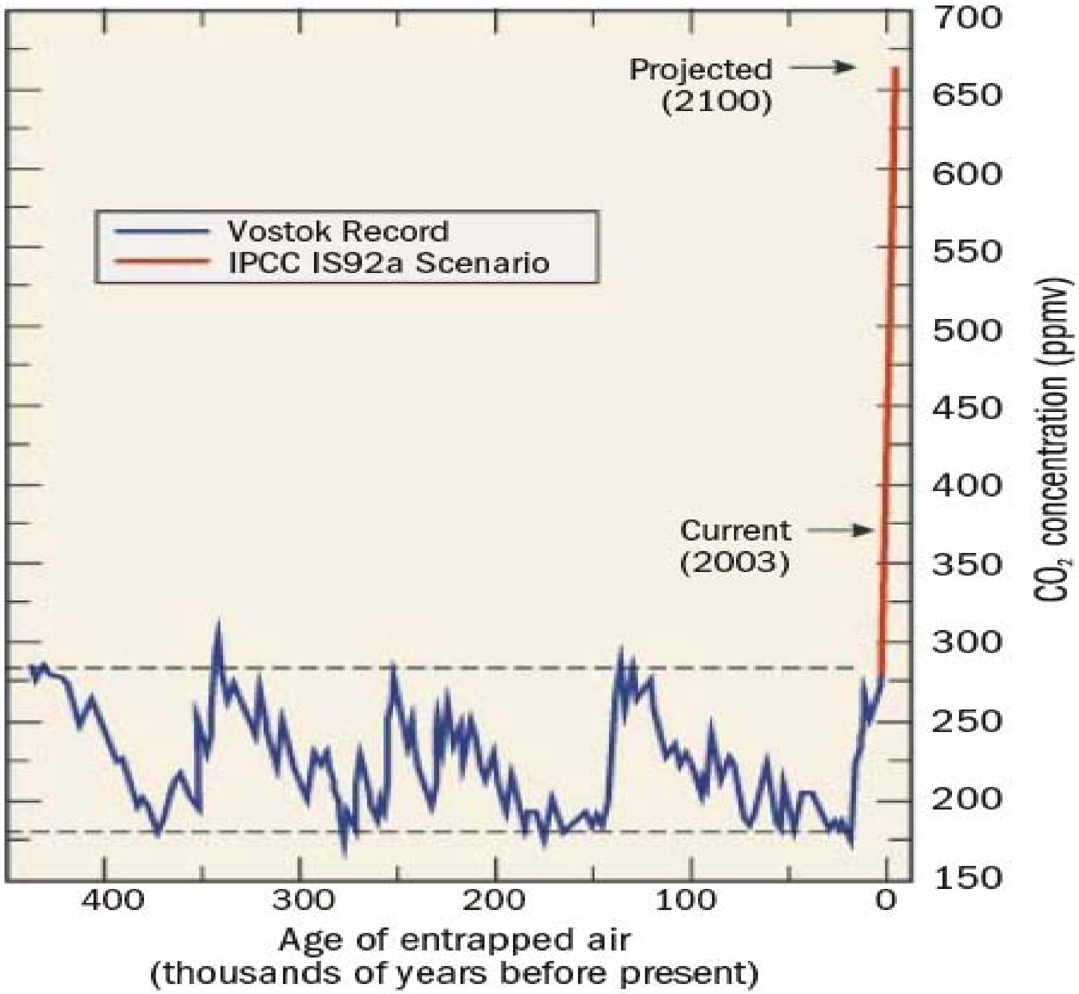

Figure 2

The Vostok ice core record for atmospheric concentration (Petit et al 1999) and the 'business as usual' prediction used in the IPCC third assessment (IPCC 2001a). The current concentration of atmospheric carbon dioxide (CO_2) is also indicated.

From The Global Carbon Project, ESSP Report #1.

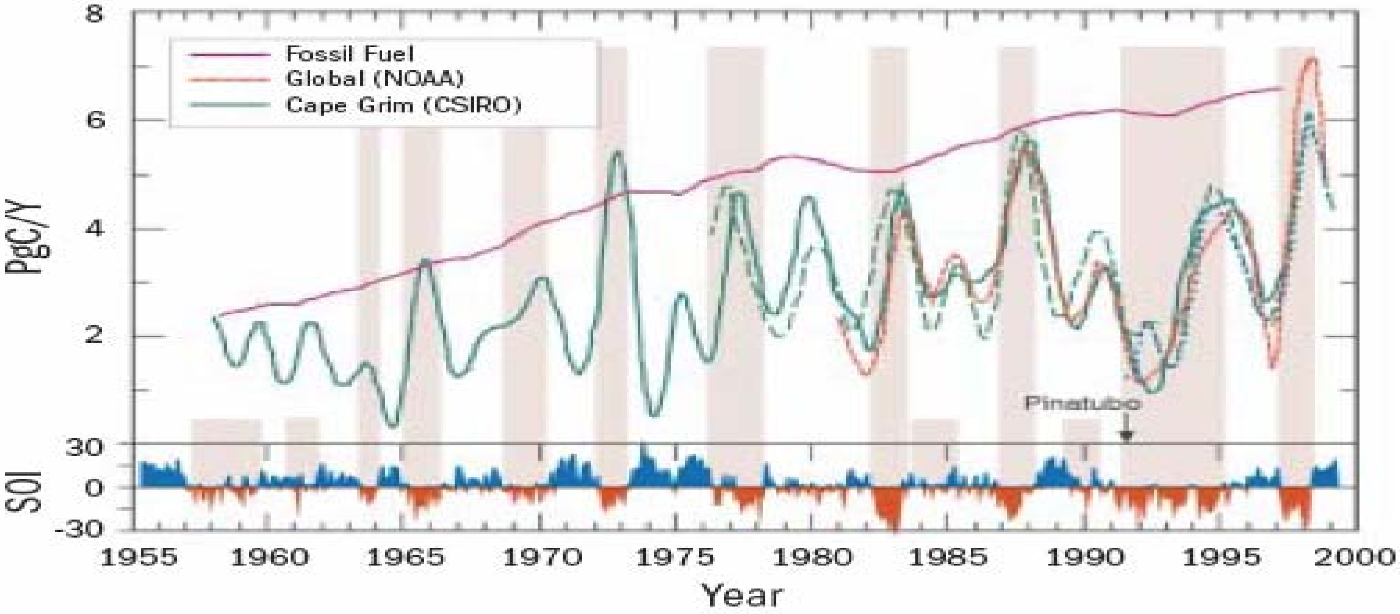

Figure 7

The CO_2 global growth rate (expressed here as 10^{15} g/yr of carbon accumulating in the atmosphere since the start of direct CO_2 monitoring) is compared to fossil fuel emissions over 4 decades. On average, 55% of the anthropogenic carbon is retained in the atmosphere, but with large interannual variability related to the southern oscillation index (SOI). (The very low growth following the Pinatubo volcanic explosion in 1991 is an exception). All CO_2 data are deseasonalised and smoothed over 650 days. The records collected by SIO/NOAA from Mauna Loa, by NOAA from 50 global sites, or by CSIRO from Cape Grim all closely track the global growth rates (Source: R J Francey, presented at the EC-IGBP-GTOS Terrestrial Carbon Meeting, 22-26 May 2000, Costa da Caparica, Portugal).

Table 1 Contemporary carbon budgets for the 1980s and 1990s

	1980s* (Gt C yr^{-1})	1990s* (Gt C yr^{-1})
Emissions (fossil-fuel burning, cement manufacture)	5.4 ± 0.3	6.3 ± 0.4
Atmospheric increase	3.3 ± 0.1	3.2 ± 0.1
Ocean–atmosphere flux	–1.9 ± 0.5	–1.7 ± 0.5
Land–atmosphere flux	–0.2 ± 0.7	–1.4 ± 0.7
Emissions due to land-use change	1.7 (0.6 to 2.5)†	Assume 1.6 ± 0.8‡
Residual terrestrial sink	–1.9 (–3.8 to 0.3)	–2 to –4 (Highly uncertain)

Negative values denote flux from the atmosphere, that is, ocean or land uptake.
* From ref. 4.
† The range of estimates available to IPCC 2001 (ref. 4).
‡ Based on the early 1990s only and not the full decade (ref. 24).

Methodologies

Inverse modelling techniques

- Δ $p(CO_2)$ method
- Inventory approach
- Atmospheric $\delta^{13}C$ method
- Atmospheric (O_2/N_2) Method
- Radiocarbon inventory

- Coupled OCGCM

Takahashi et al., 2002 DSR
(Climatology, non ENSO)

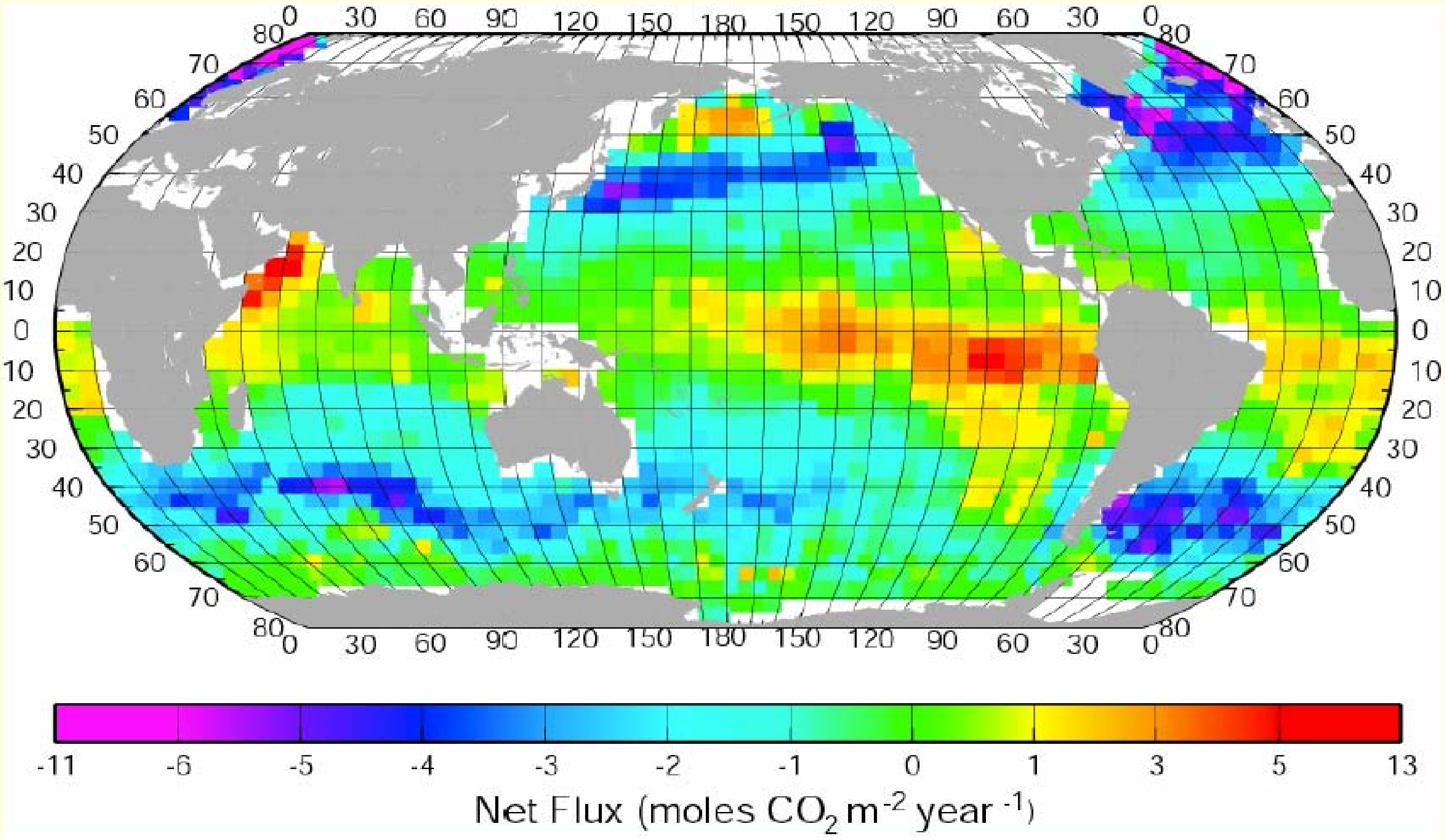

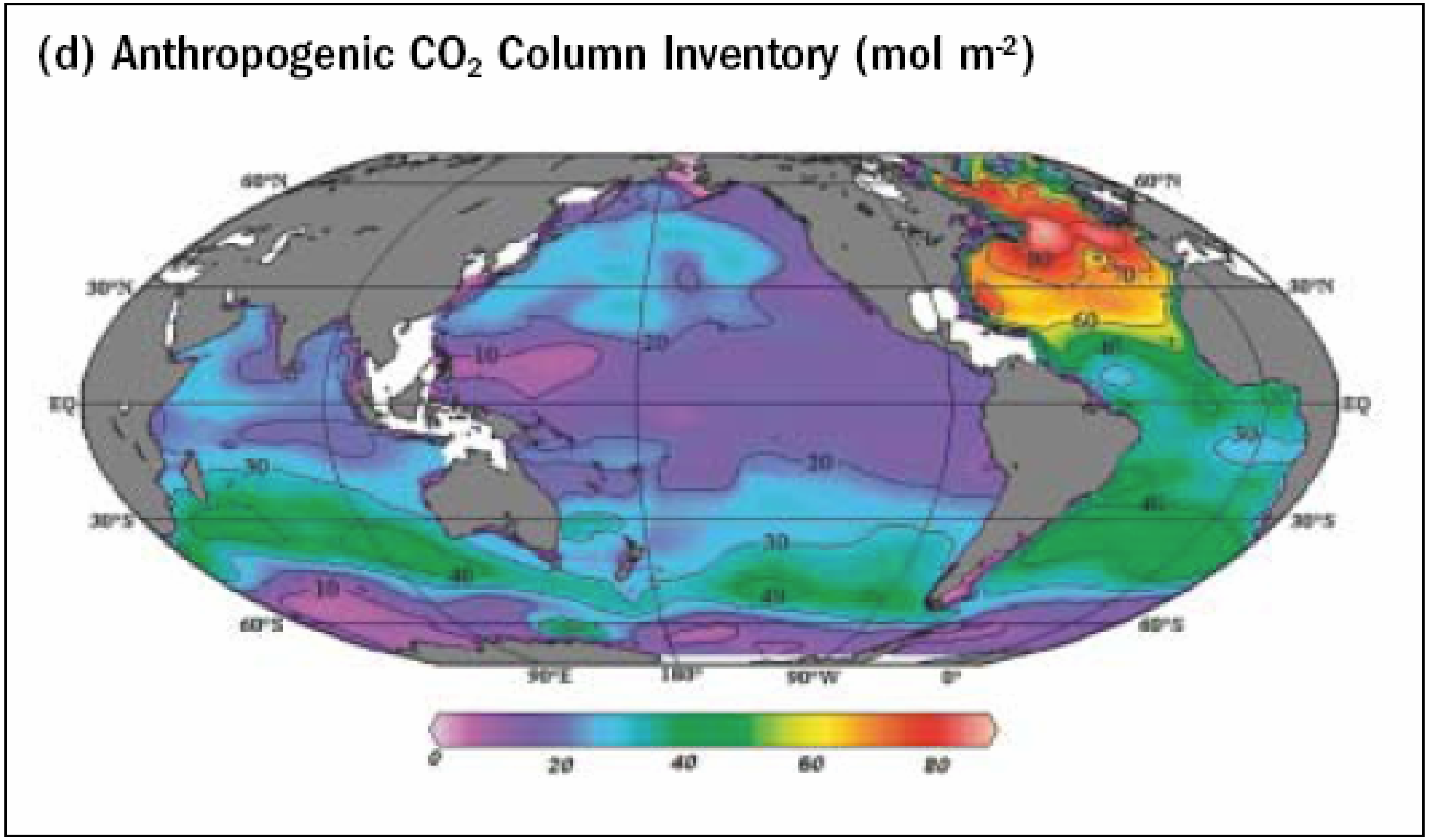

(Sabine et al., 2003)

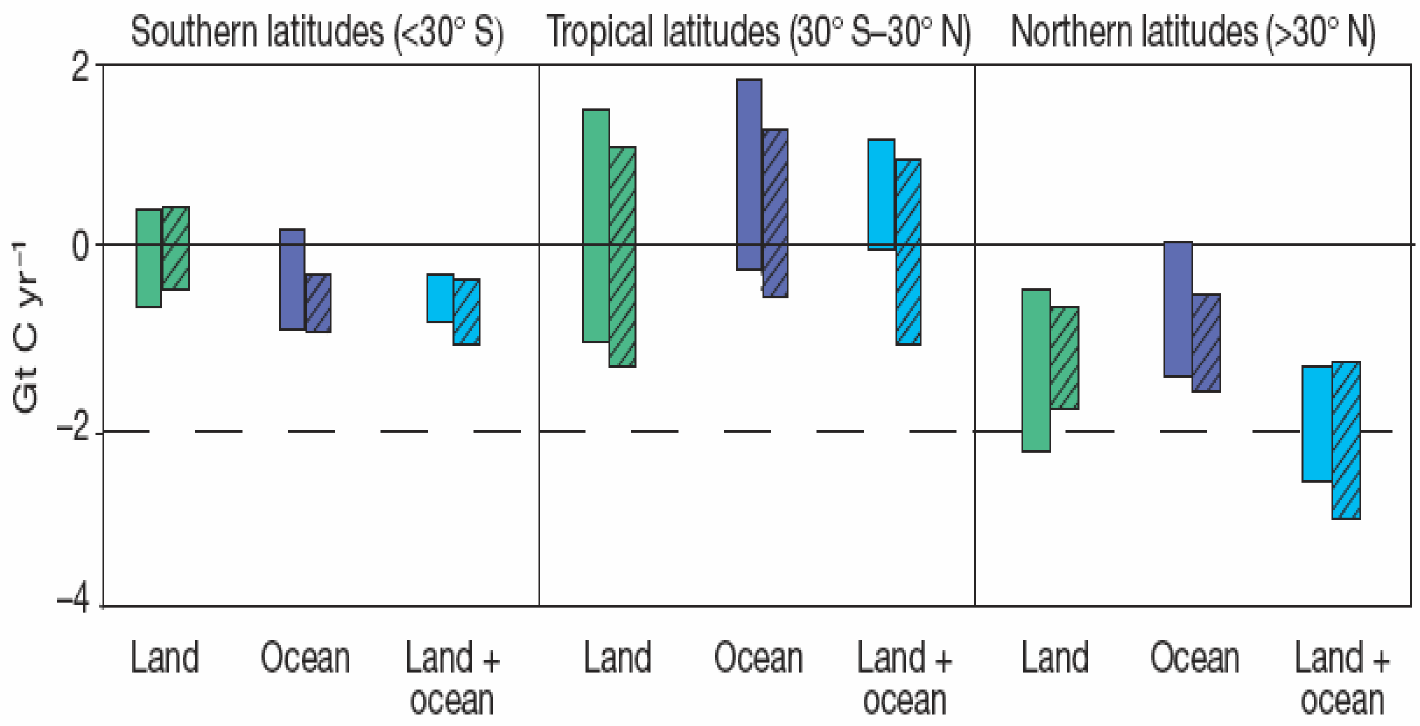

Figure 1 Zonal distribution of terrestrial and oceanic carbon fluxes. These data were deduced from eight inverse models using different techniques and sets of atmospheric observations after accounting for fossil-fuel emissions (not shown)[13]. Results are shown for the 1980s (plain bars) and for 1990–96 (hatched bars). The bars indicate the full range of results from the models. Positive numbers are fluxes to the atmosphere. Note that data and time-intervals are not precisely consistent with those used in other analyses presented in this Progress Article, and so the global totals may differ from those mentioned elsewhere.

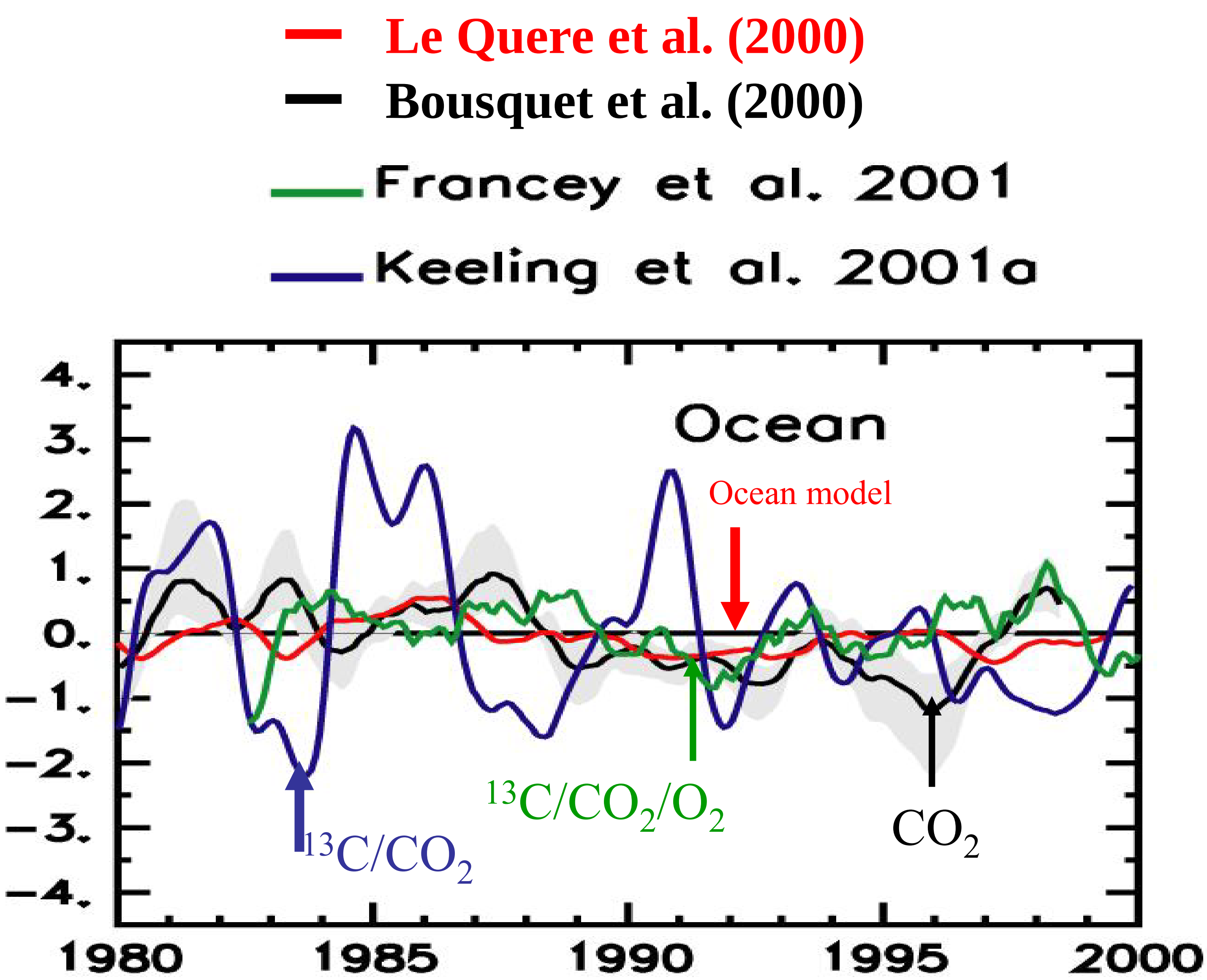

Le Quere et al. (2000)
Bousquet et al. (2000)
Francey et al. 2001
Keeling et al. 2001a
Ocean
Ocean model
4.
3.
2.
1.
0.
−1.
−2.
−3.
−4.
1980
1985
1990
1995
2000
$^{13}C/CO_2$
$^{13}C/CO_2/O_2$
CO_2

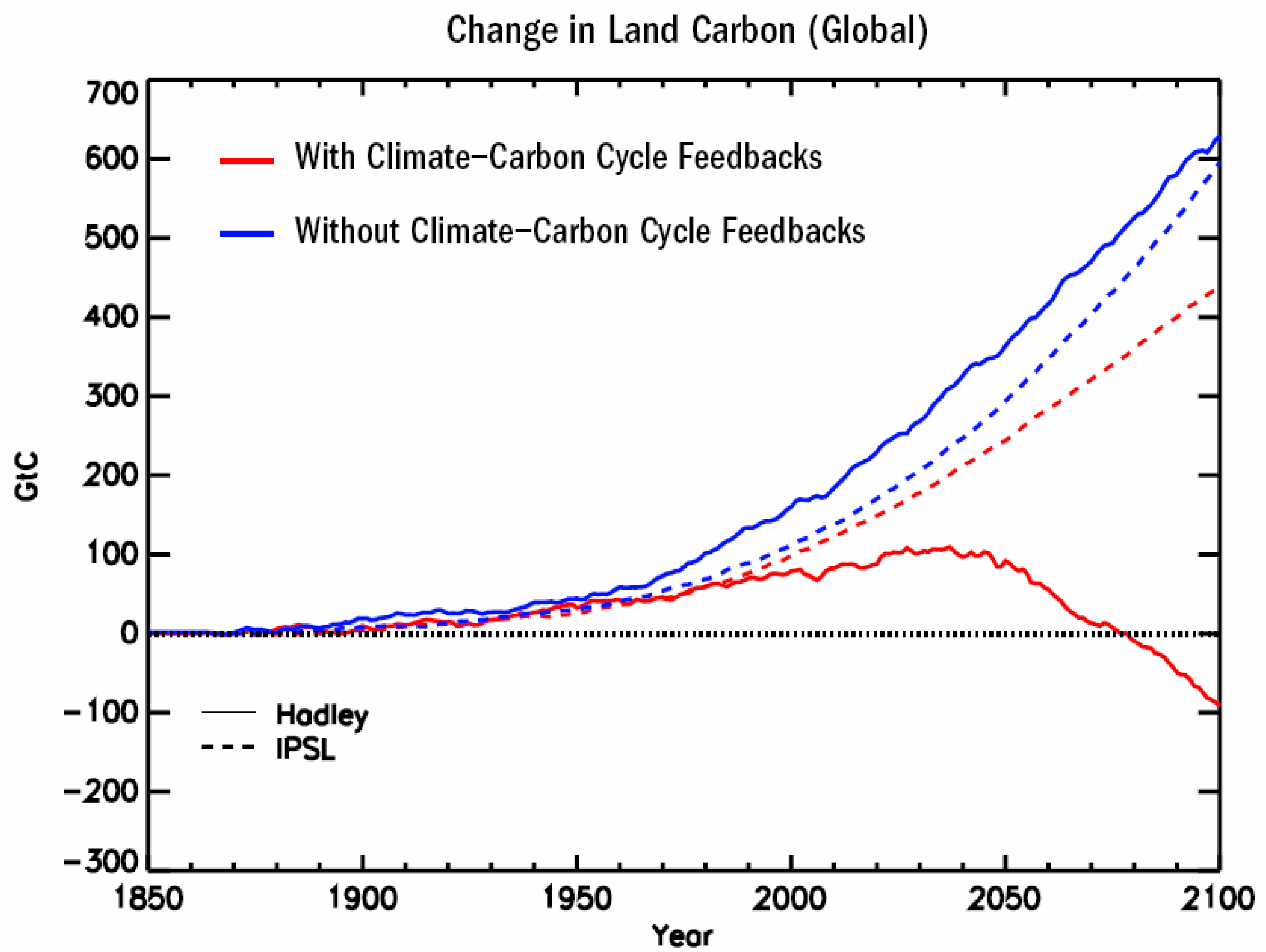

Figure 15

Predicted changes in global land carbon (vegetation plus soils) from two coupled climate-carbon cycle GCMs. Positive represents an increase in land storage. The Hadley Centre results are shown by the continuous lines and the IPSL model results by the dashed lines. Blue lines represent runs without climate change, and the red lines are from the fully coupled runs including climate-carbon cycle feedback (Cox et al 2000).

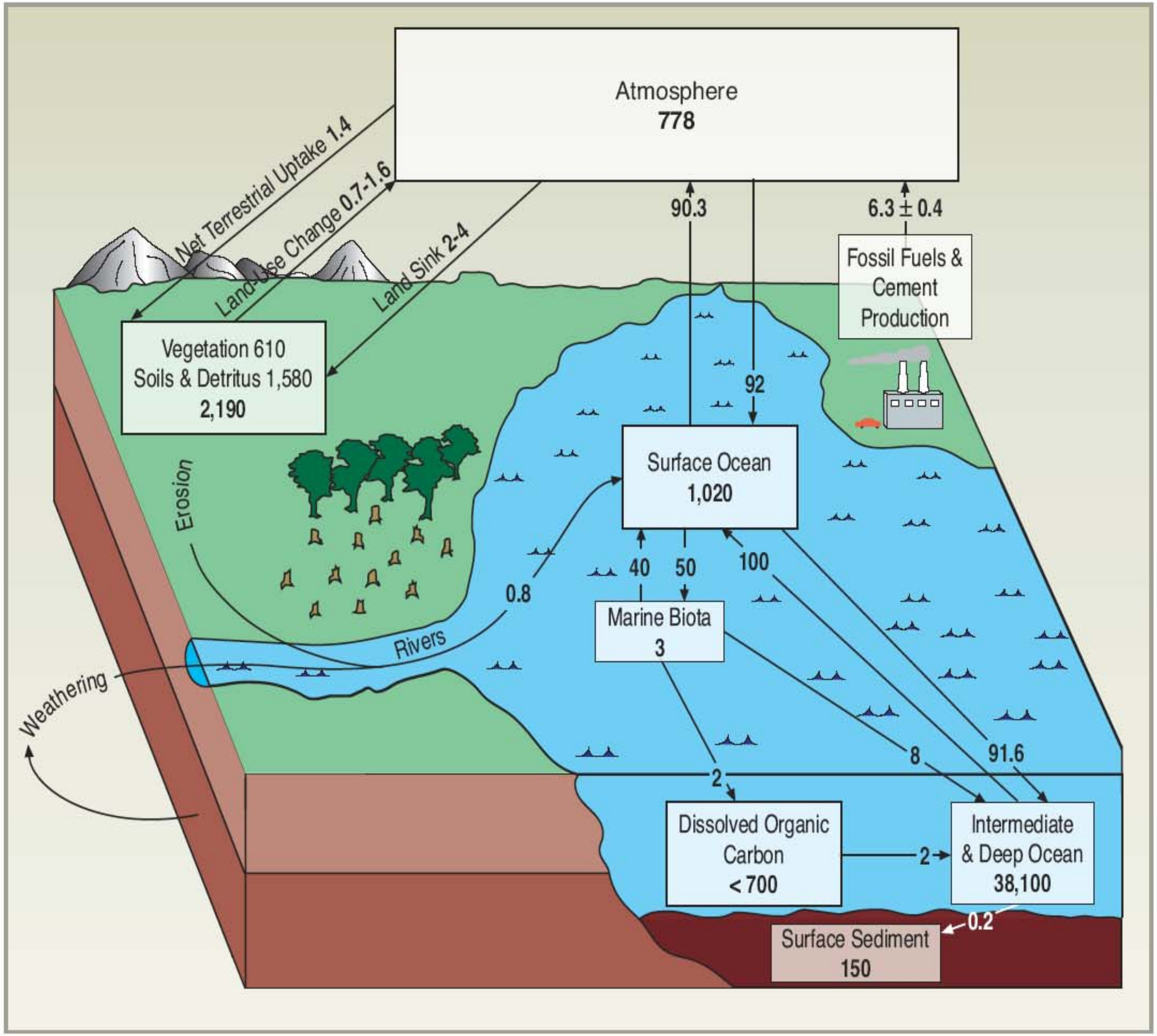

Figure 7-1: The global carbon cycle. Carbon is exchanged among the atmosphere, oceans, and land. This cycling of carbon is fundamental to regulating Earth's climate. In this static figure, the components are simplified and average values are presented. Storages [in petagrams carbon (PgC)] and fluxes (in PgC yr^{-1}) of carbon for the major components of the Earth's carbon cycle are estimated for the 1990s. For more information, see Annex C.

Futur Long-term variations of air-sea CO_2 flux: a view from a coupled model
IPSL: OPA-HAMOCC3-LMD-SLAVE-IS92a (L.Bopp)

2090-1990

Diff. Air-Sea Flux in mol m^{-2} $year^{-1}$

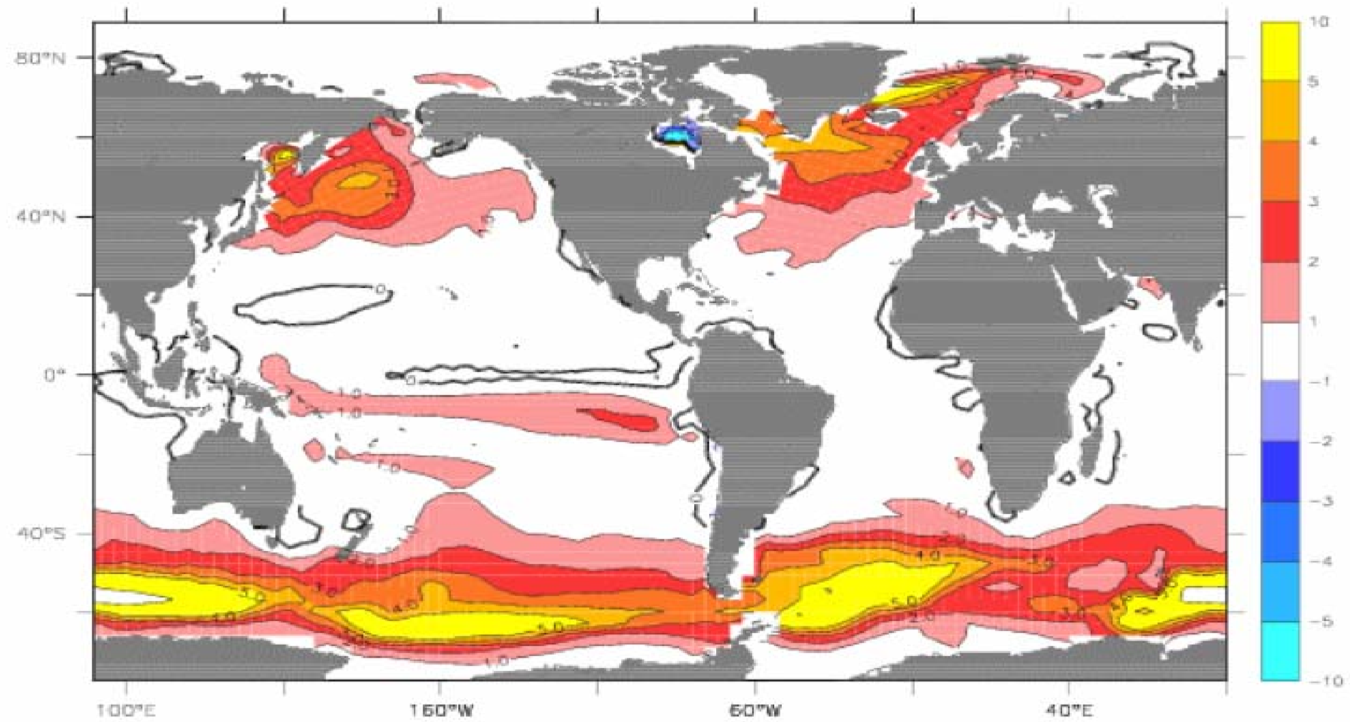

In the tropics, changes would occur in the eastern EQPAC region; why ?

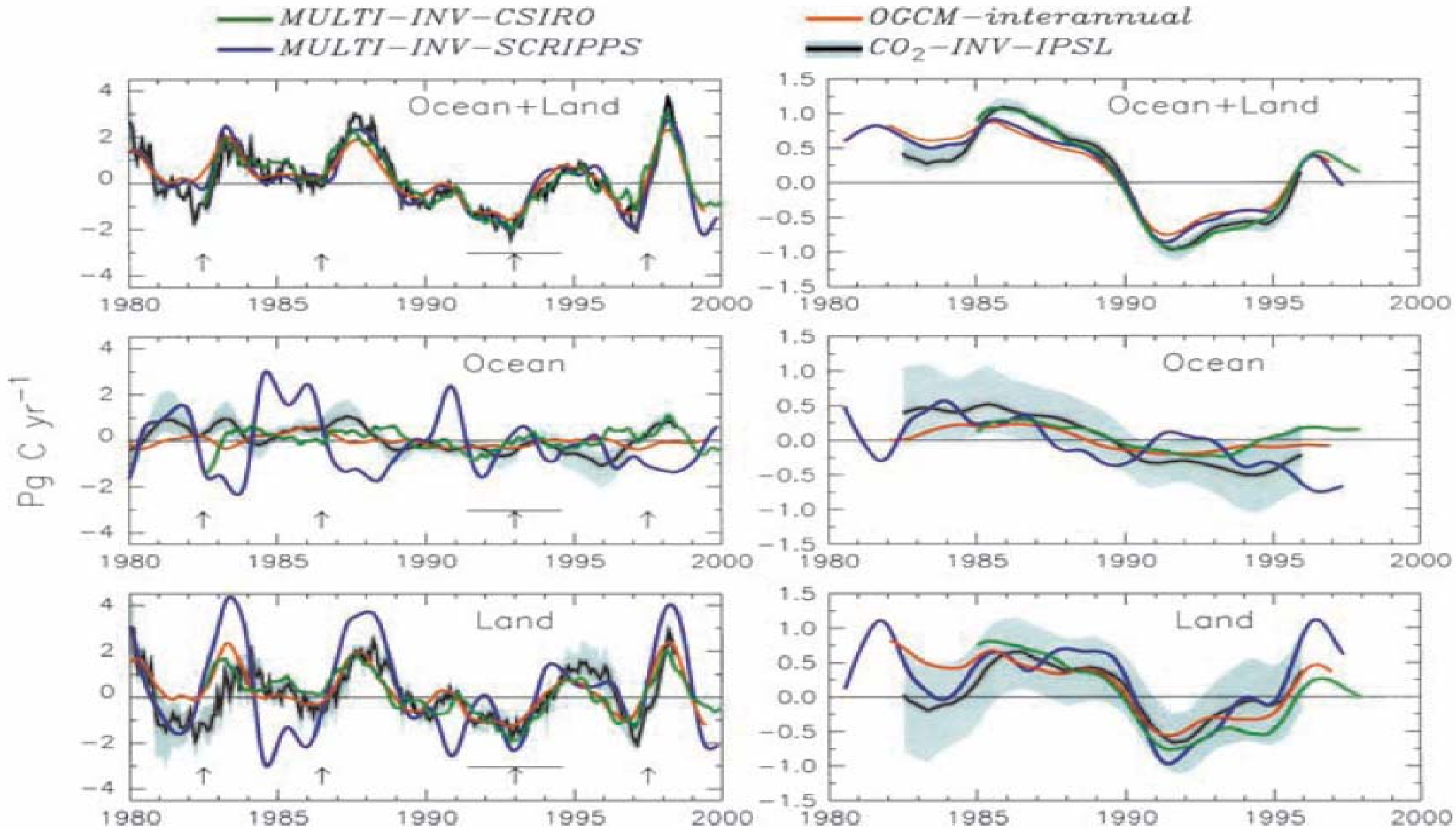

Fig. 2. Variability in ocean and land CO_2 fluxes in Pg C yr^{-1}. Positive values indicate a CO_2 flux anomaly from the ocean or land to the atmosphere, negative values a CO_2 flux anomaly from the atmosphere to the ocean or land. The curves are smoothed to remove variability less than 1 yr (left panels) and less than 5 yr (right panels). The mean of 1985–1995 is removed from each curve. Arrows indicate El Niño events. The different methods are described in the text.

From Le Quéré et al, Tellus (2003)

Radiocarbon is a passive tracer that can be used to understand the carbon cycle

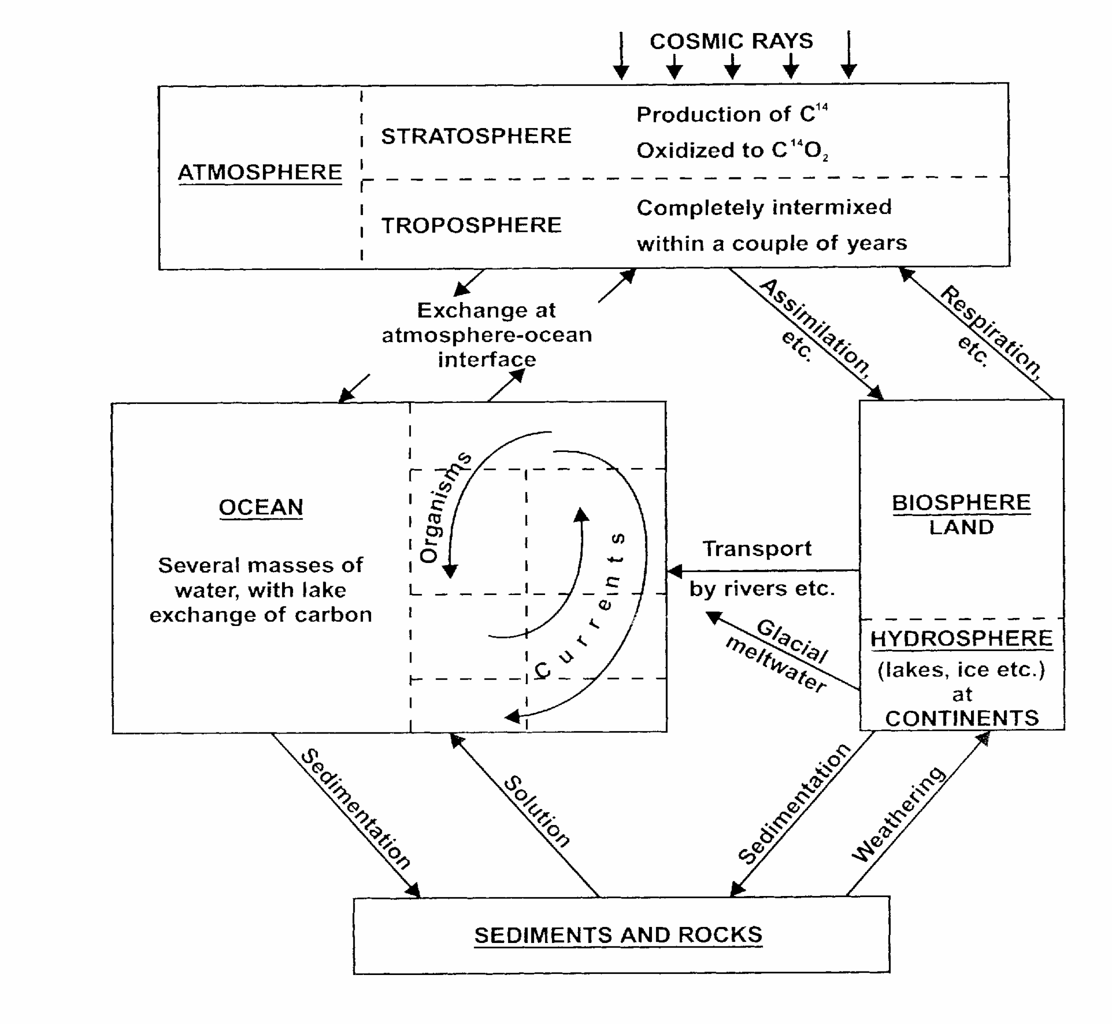

Carbon circulation in nature

[From Bradley (1999), and based on Mangerud (1972)]

Carbon cycle: reservoir sizes and fluxes (Gt C and Gt C yr^{-1}, from Siegenthaler and Sarmiento, 1993)

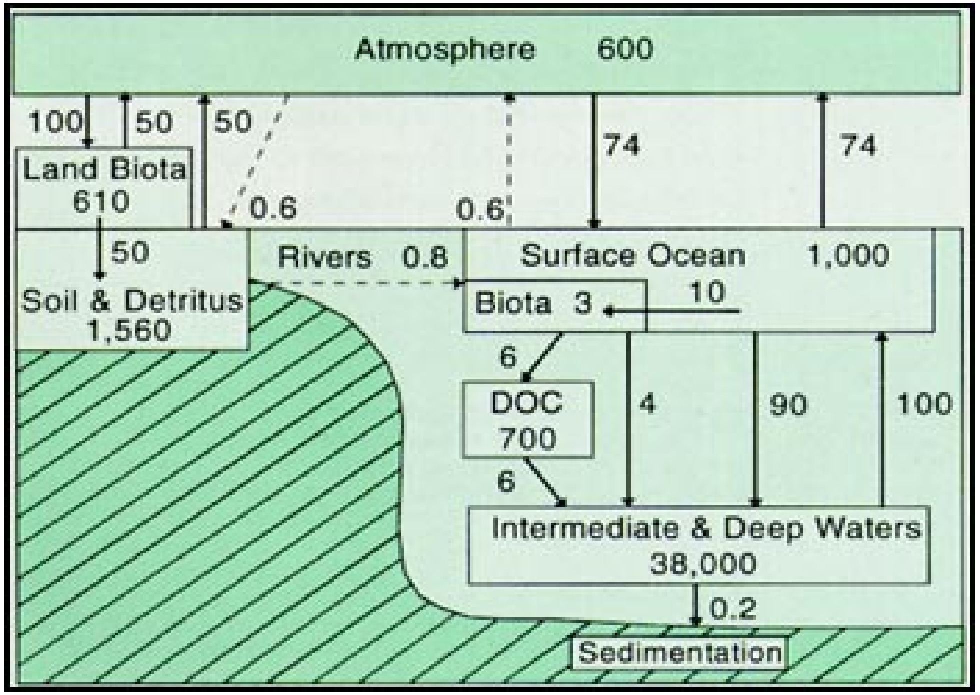

Atmosphere:
^{14}C short residence times and small reservoir

Deep ocean:
^{14}C long residence times and very large reservoir

By measuring the ^{14}C abbundance we learn something about the residence time and exchange rates of carbon amongst these reservoirs.

How do we obtain records of past ^{14}C abundance?

Radiocarbon records

- Tree rings
- Varved Lake sediments
- Varved Ocean sediments
- Speleothems

Tree-ring calibration

Overlapping sequences of tree-ring chronologies (dendrochronology) used to obtain continuous record of decadal estimates of past atmospheric concentration

11.85 ka ⟵

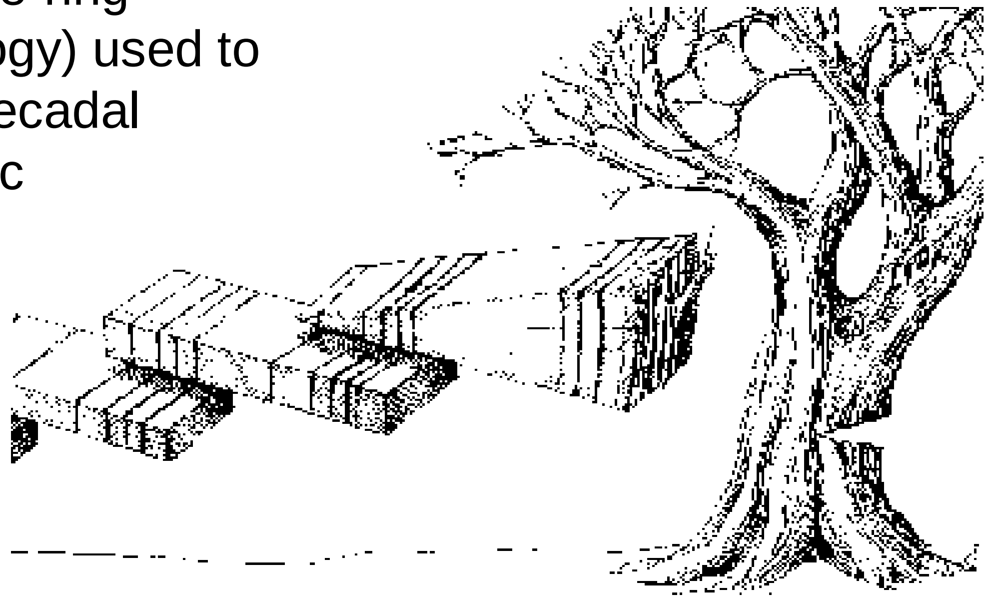

^{14}C age is compared with calendar age based on tree ring count

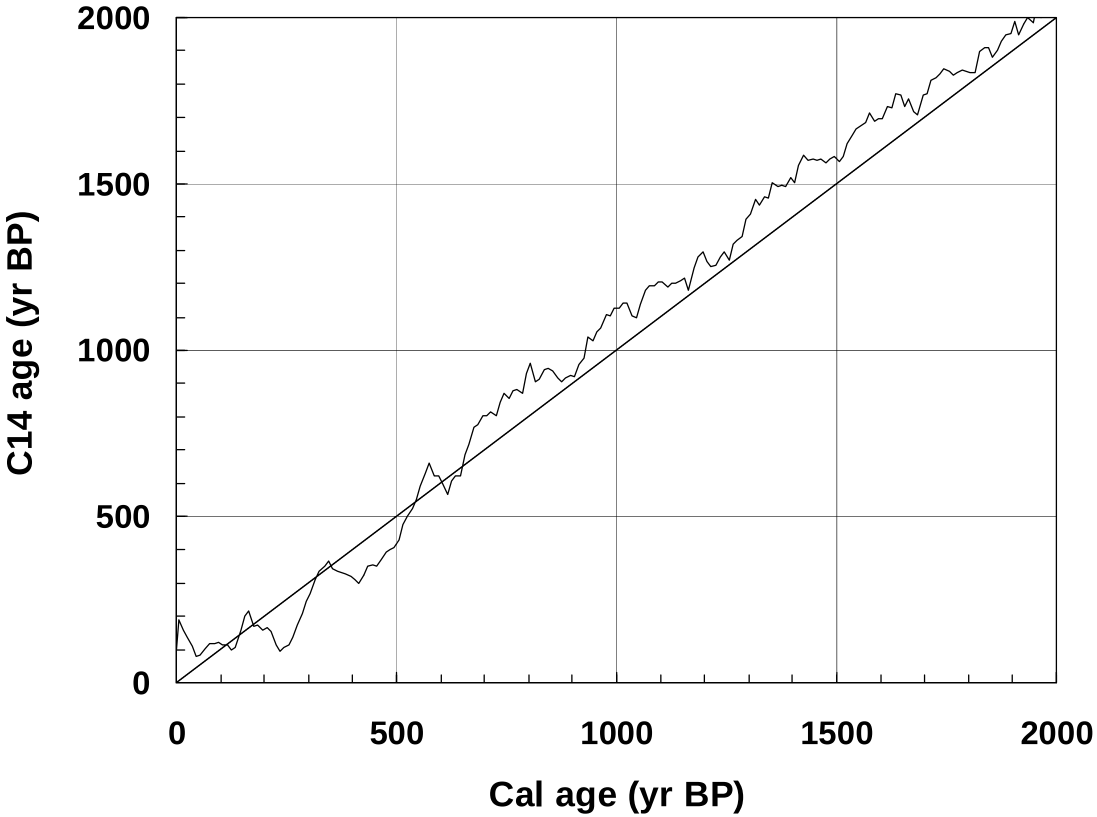
2000
1500
1000
500
0
C14 age (yr BP)
0
500
1000
1500
2000
Cal age (yr BP)

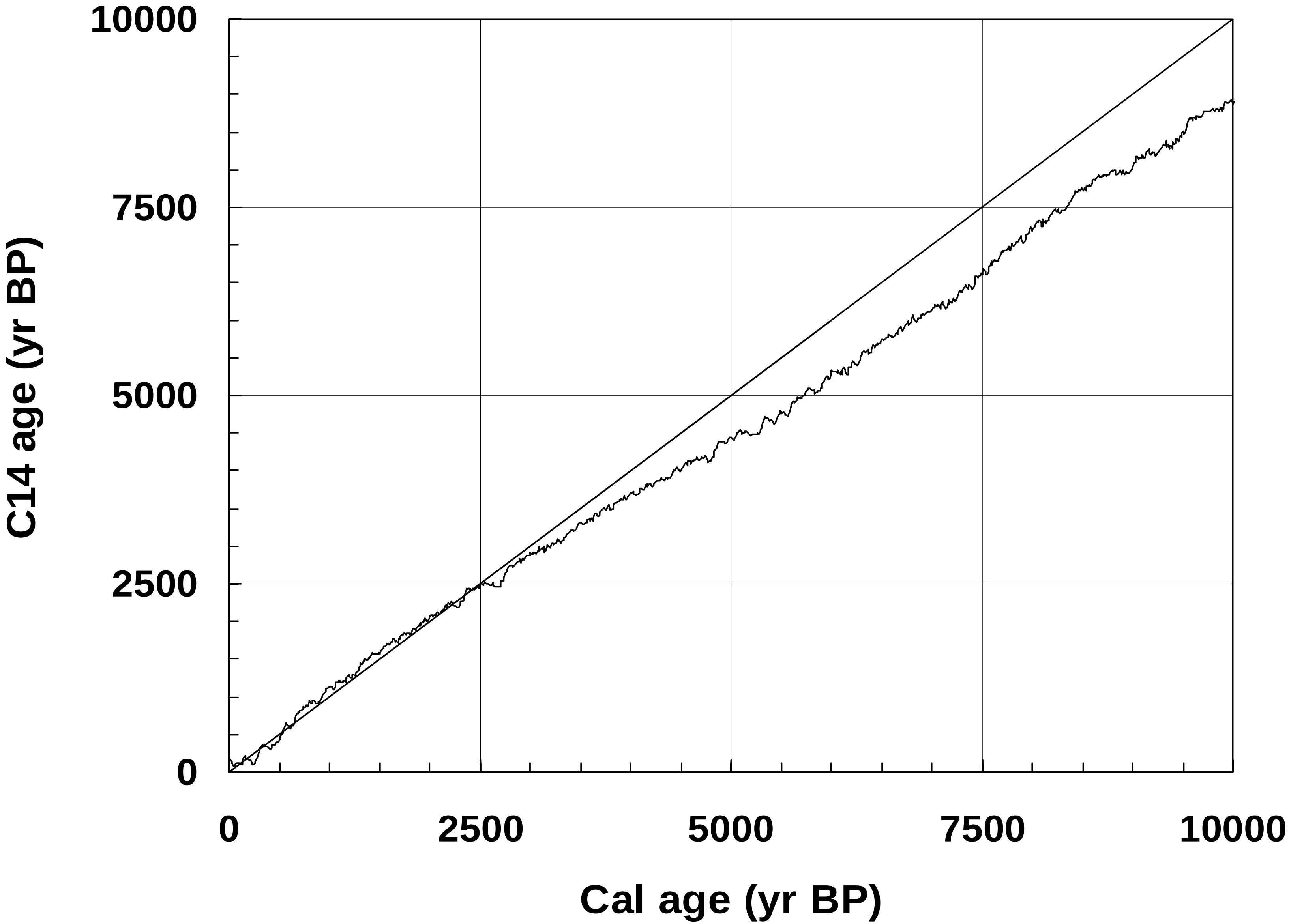
10000
7500
5000
2500
0
C14 age (yr BP)
0
2500
5000
7500
10000
Cal age (yr BP)

$\Delta^{14}C$ from corals

Sample 94-CB-1
Marau Sound
Guadalcanal,
Solomon Islands

Porites

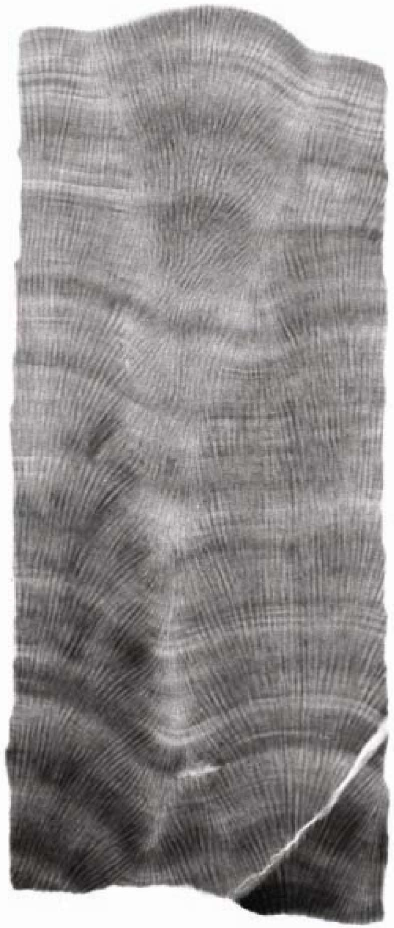

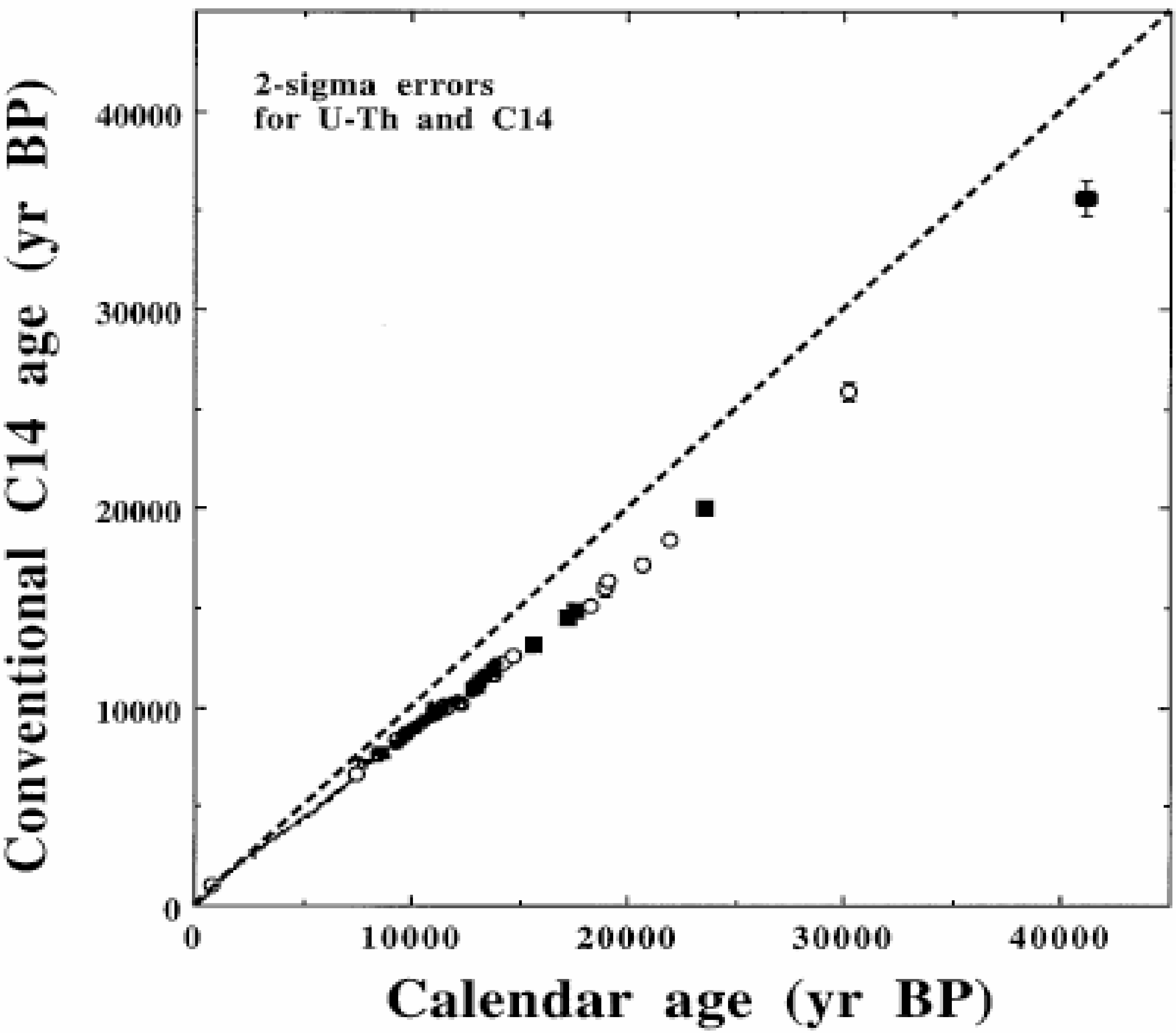

2-sigma errors
for U-Th and C14
Conventional C14 age (yr BP)
Calendar age (yr BP)
0
10000
20000
30000
40000

Lake sediments

^{14}C on terrestrial plant particles

Calendar ages from counting varves

(Kitagawa & van der Plicht, 2000)

Ocean sediments

^{14}C from planktonic foraminifera

Calendar ages from comparing $\delta^{18}O$ (or greyscale) with GISP2 $\delta^{18}O$

(Voelker et al., 2001; Hughen et al., 1997, 2004)

Speleothems (stalagmites)

Calendar ages from U/Th ages

Collecting speleothems from Grand Bahamas caves at 90m bsl, using He-rebreather apparatus

Rob Palmer
Rob Parker

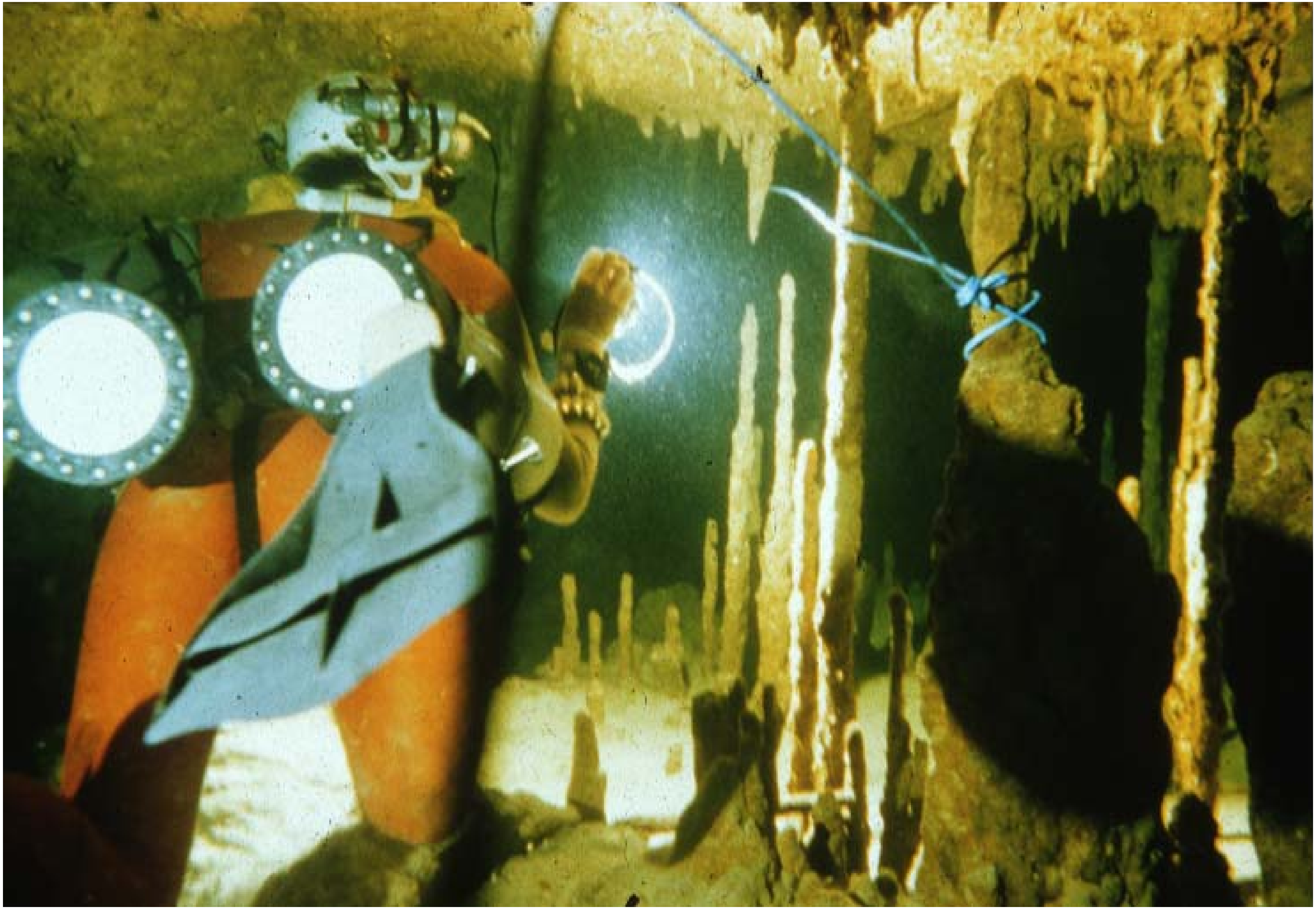

Stalagmite from Sagittarius blue hole, Grand Bahama

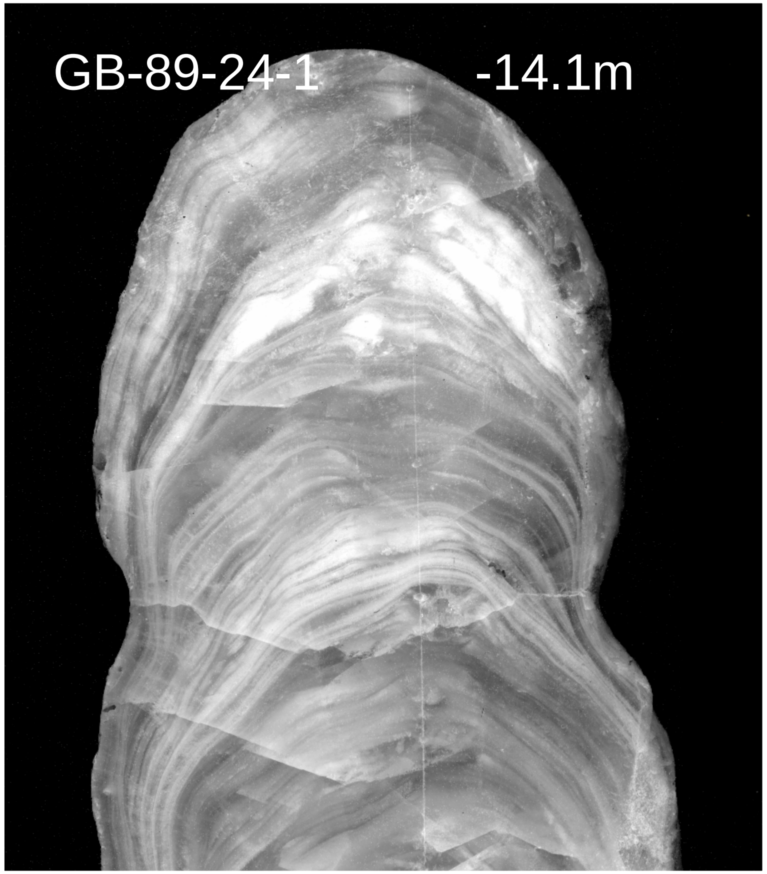

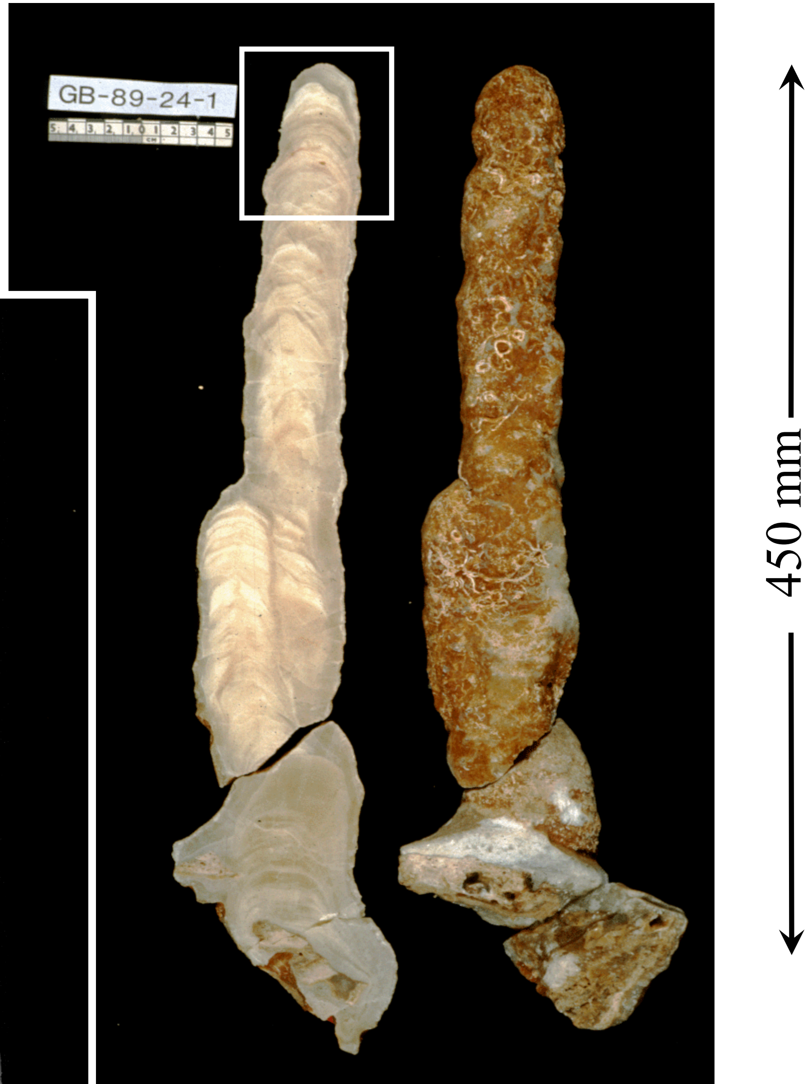

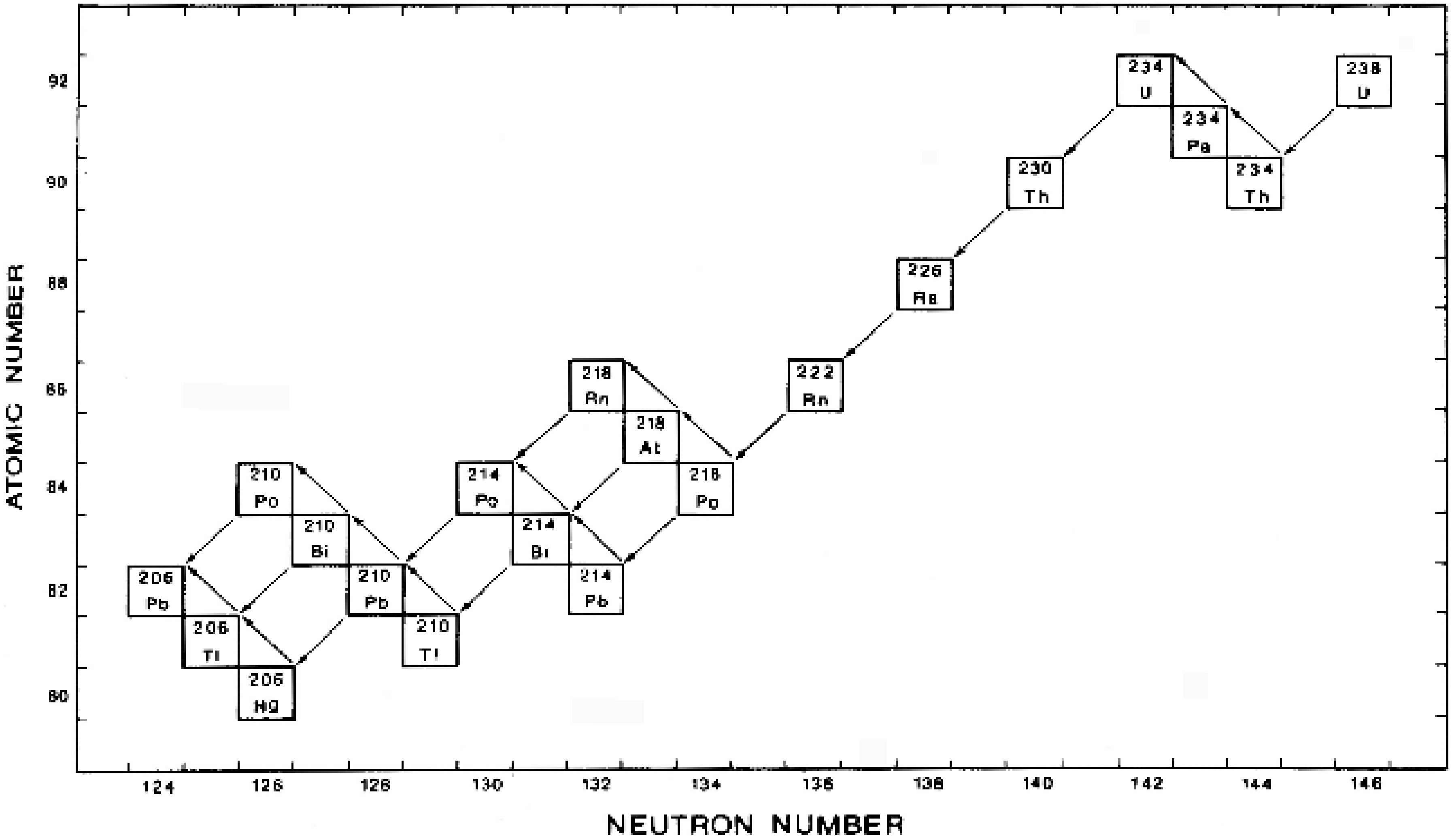

Figure 18.1 The decay of ^{238}U to stable ^{206}Pb.

Uranium-series disequilibrium

….on dissolution and subsequent precipitation of carbonate

(eg. coral or speleothem)

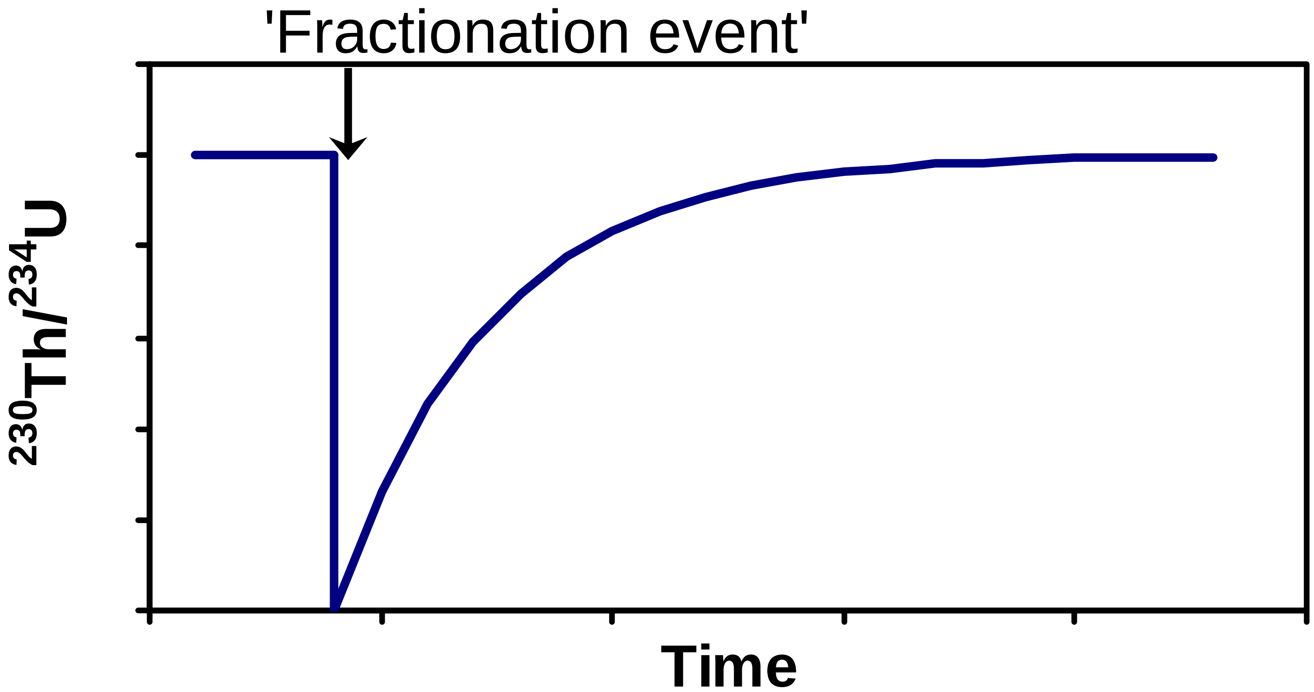

(Without derivation):

The new law governing ^{230}Th activity in the presence of excess ^{234}U becomes:

$$\left(\frac{^{230}\mathrm{Th}}{^{238}\mathrm{U}}\right)_A = 1 - e^{-\lambda_{230}T} + \left(\frac{\delta^{234}\mathrm{U(T)}}{1000}\right)\left(\frac{\lambda_{230}}{\lambda_{230} - \lambda_{234}}\right)\left(1 - e^{(\lambda_{234} - \lambda_{230})T}\right)$$

(assuming no initial ^{230}Th)

Can't solve analytically because T appears in two independent terms
Solve iteratively :

1) Pick a T, then compare to measured $(^{234}\mathrm{U}/^{238}\mathrm{U})_a$
2) Repeat until convergence.

Uranium-series ages along axis of growth

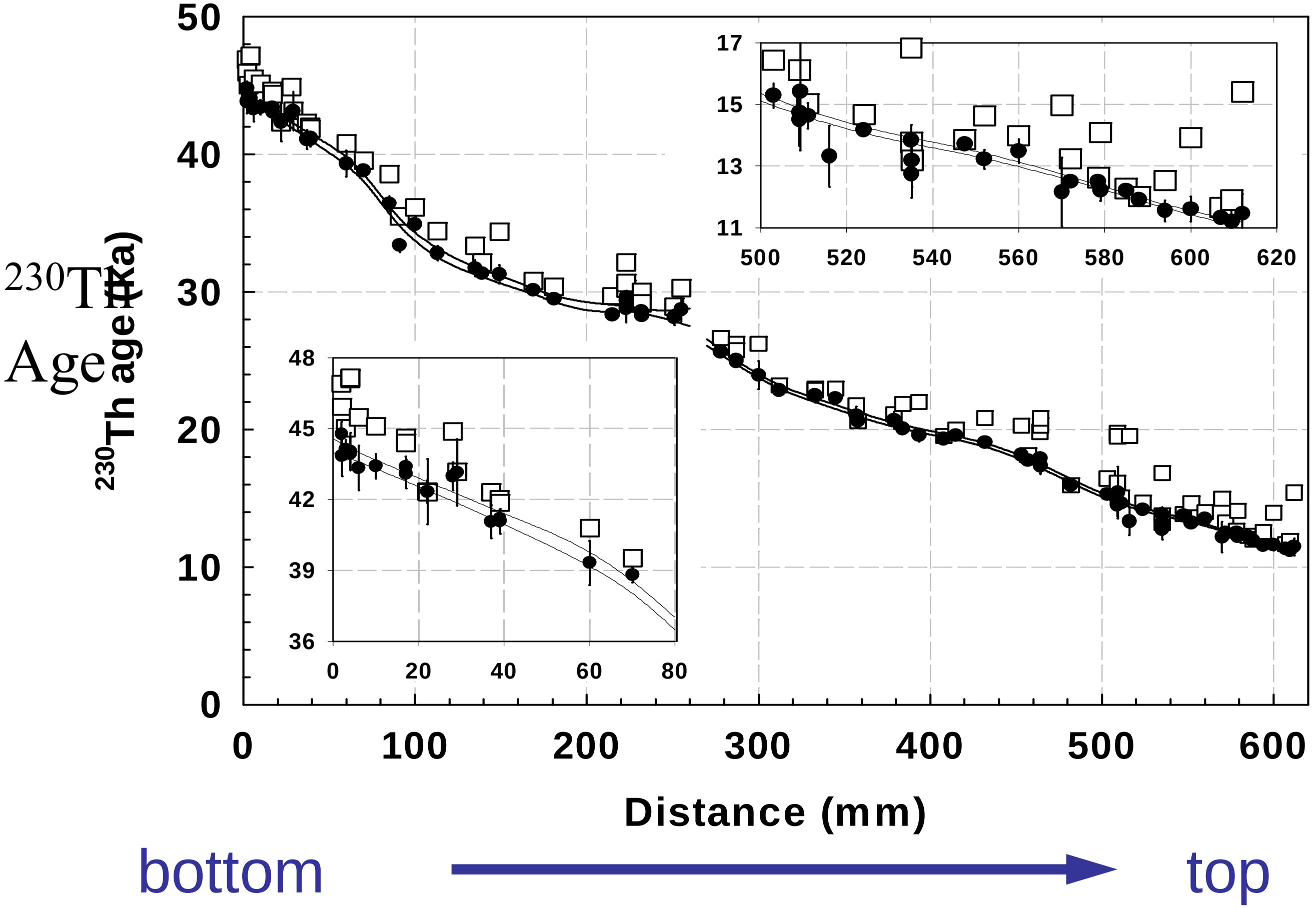

Smooth, curvilinear growth with break in deposition as drip site moved at 28 to 26 ka

Ages corrected for elevated $^{230}Th/^{232}Th$ based on isochrons

More U/Th approaches:

(1) No initial ^{230}Th and $\delta^{234}U = 0$ (i.e $^{234}U/^{238}U$ at secular equilibrium)

$$(^{230}Th/^{238}U)_a = 1 - e^{-(\lambda_{230}\, t)}$$

$$(^{231}Pa/^{235}U)_a = 1 - e^{-(\lambda_{231}\, t)}$$

(2) No initial ^{230}Th and $\delta^{234}U \neq 0$

$$\left(\frac{^{230}Th}{^{238}U}\right)_A = 1 - e^{-\lambda_{230}T} + \left(\frac{\delta^{234}U(T)}{1000}\right)\left(\frac{\lambda_{230}}{\lambda_{230}-\lambda_{234}}\right)\left(1 - e^{(\lambda_{234}-\lambda_{230})T}\right)$$

(3) Initial ^{230}Th present:

$$\left\{\left[\frac{^{230}Th}{^{238}U}\right] - \left[\frac{^{232}Th}{^{238}U}\right]\left[\frac{^{230}Th}{^{232}Th}\right]_i \left(e^{-\lambda_{230}t}\right)\right\} - 1 = - e^{-\lambda_{230}t} + \left(\frac{\delta^{234}U_m}{1000}\right)\left(\frac{\lambda_{230}}{\lambda_{230}-\lambda_{234}}\right)\left(1 - e^{-(\lambda_{230}-\lambda_{234})t}\right)$$

Isochron diagrams for GB-89-24-1

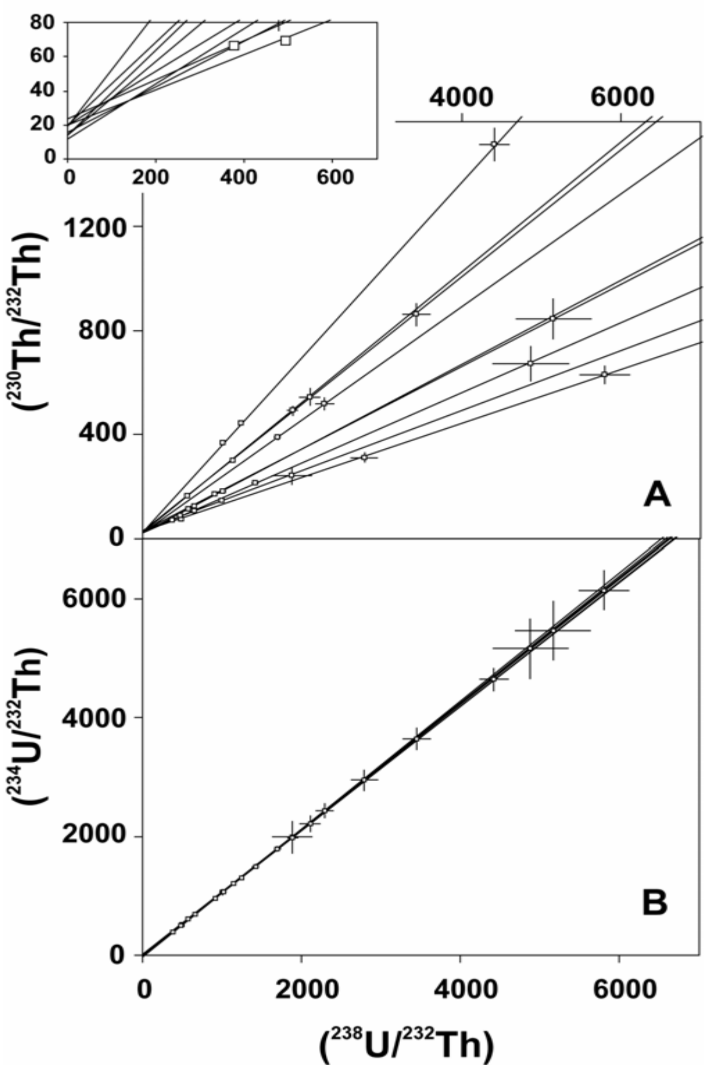

Intercept with y-axis is equivalent to initial $^{230}Th/^{232}Th$

Activity ratio = 18.6,

which is much greater than Bulk-Earth (0.8)

Uranium-series ages along axis of growth

^{230}Th Age

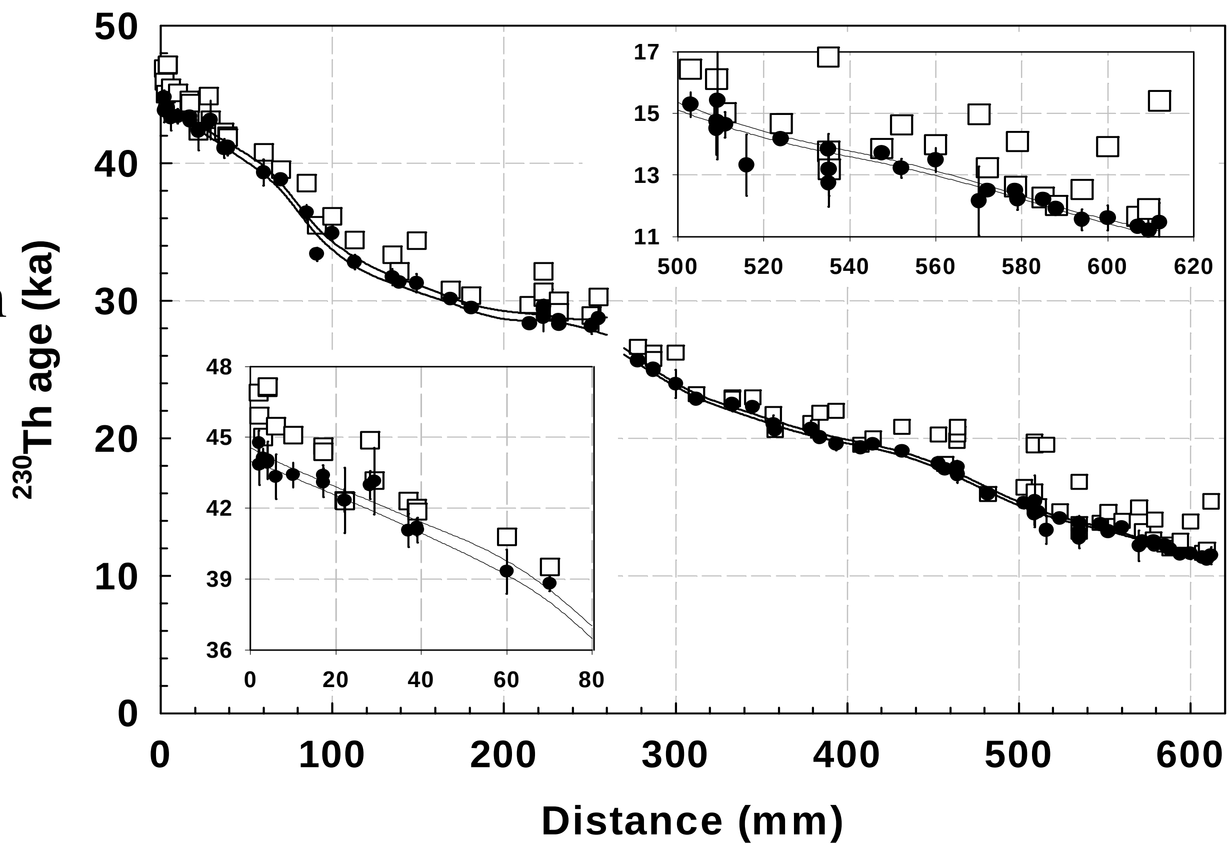

bottom → top

Smooth, curvilinear growth with break in deposition as drip site moved at 28 to 26 ka

Ages corrected for elevated ^{230}Th/^{232}Th based on isochrons

^{231}Pa *vs* ^{230}Th ages

^{231}Pa
Age (ka)

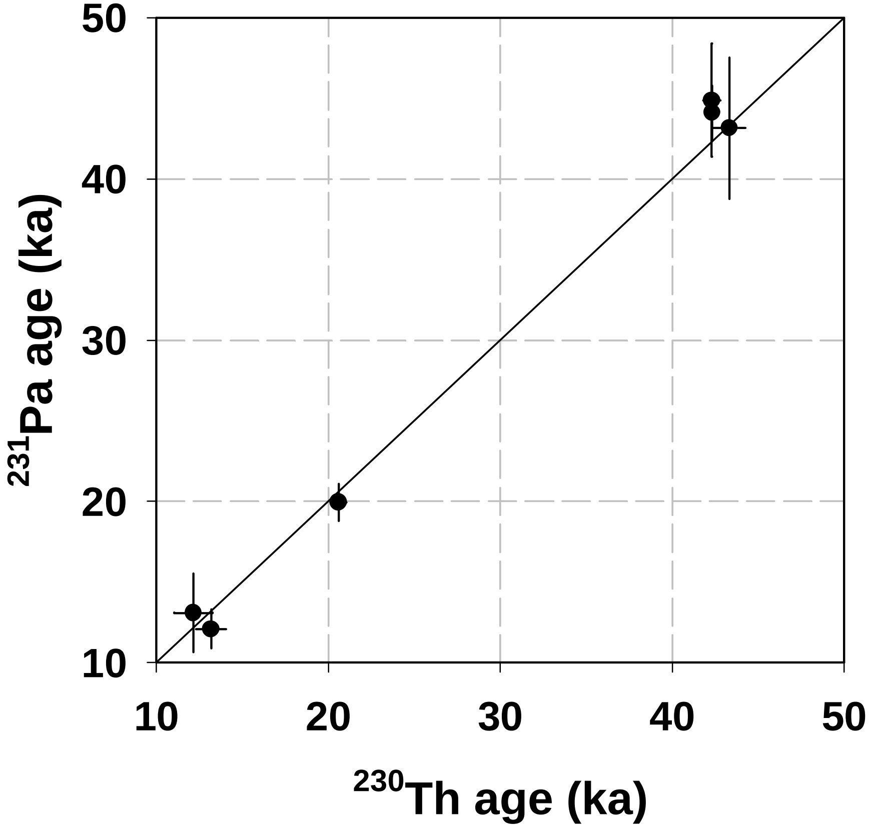

Arizona - NSF Accelerator Mass Spectrometry Facility

Radiocarbon age *vs* ^{230}Th age: 26 to 11 ka

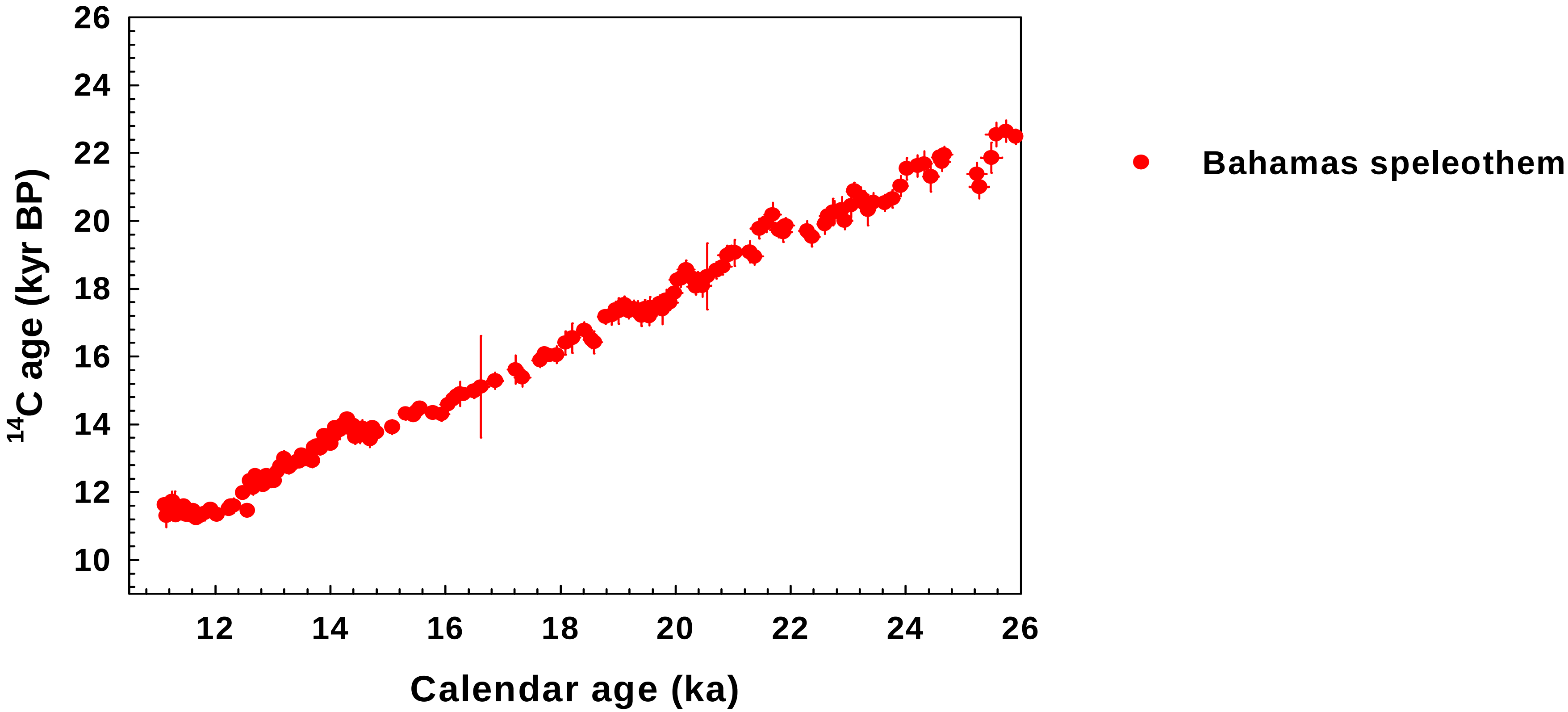

…plus corals from Vanuatu

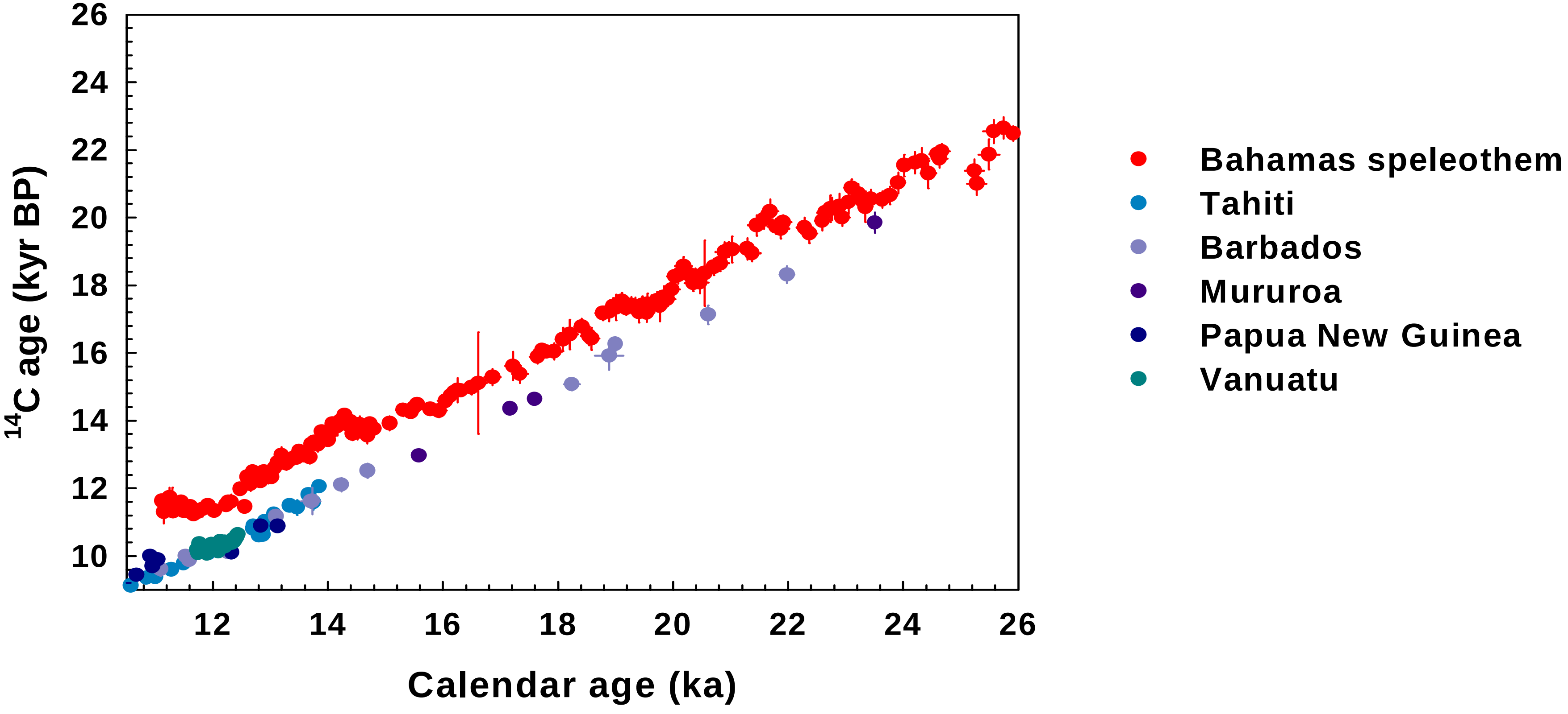

...plus varves from Cariaco

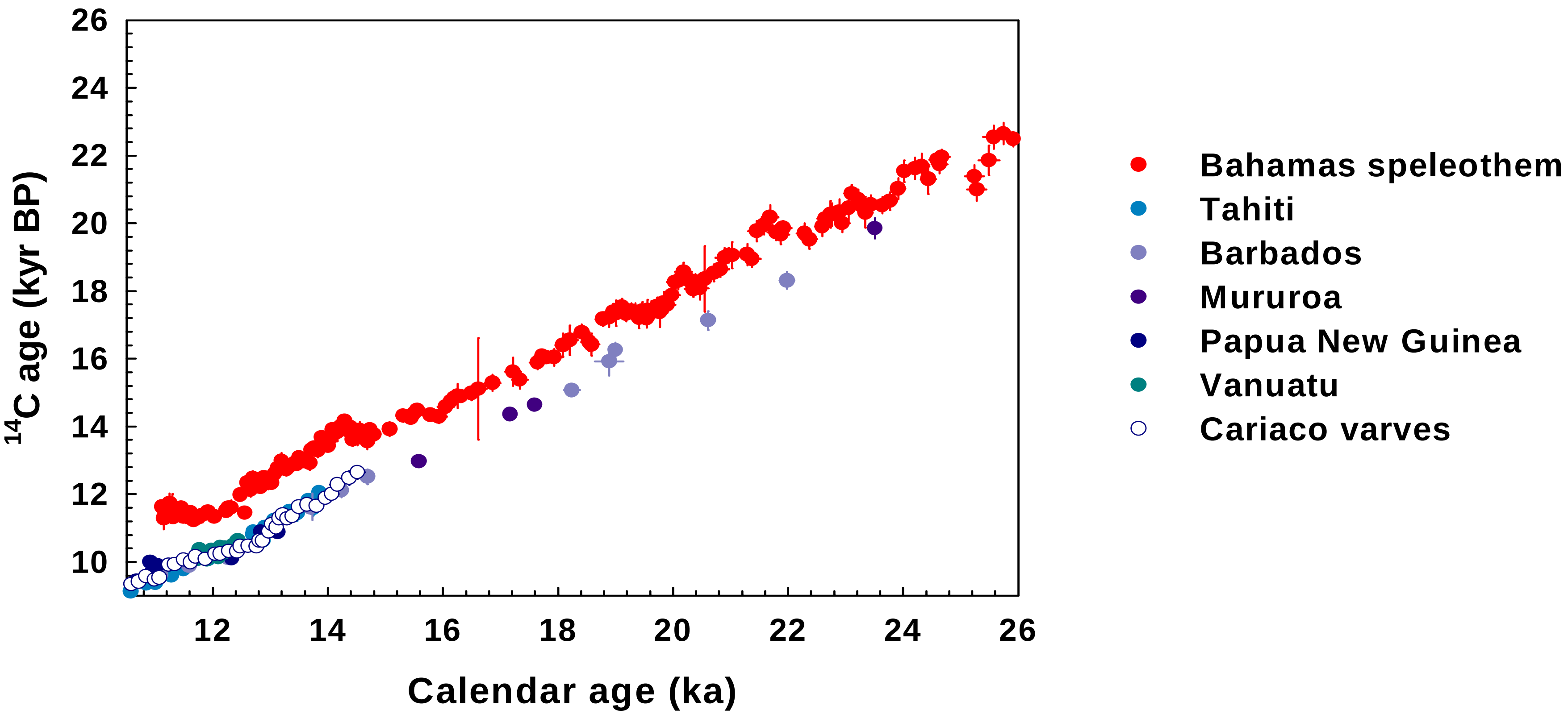

…plus corals from German tree rings

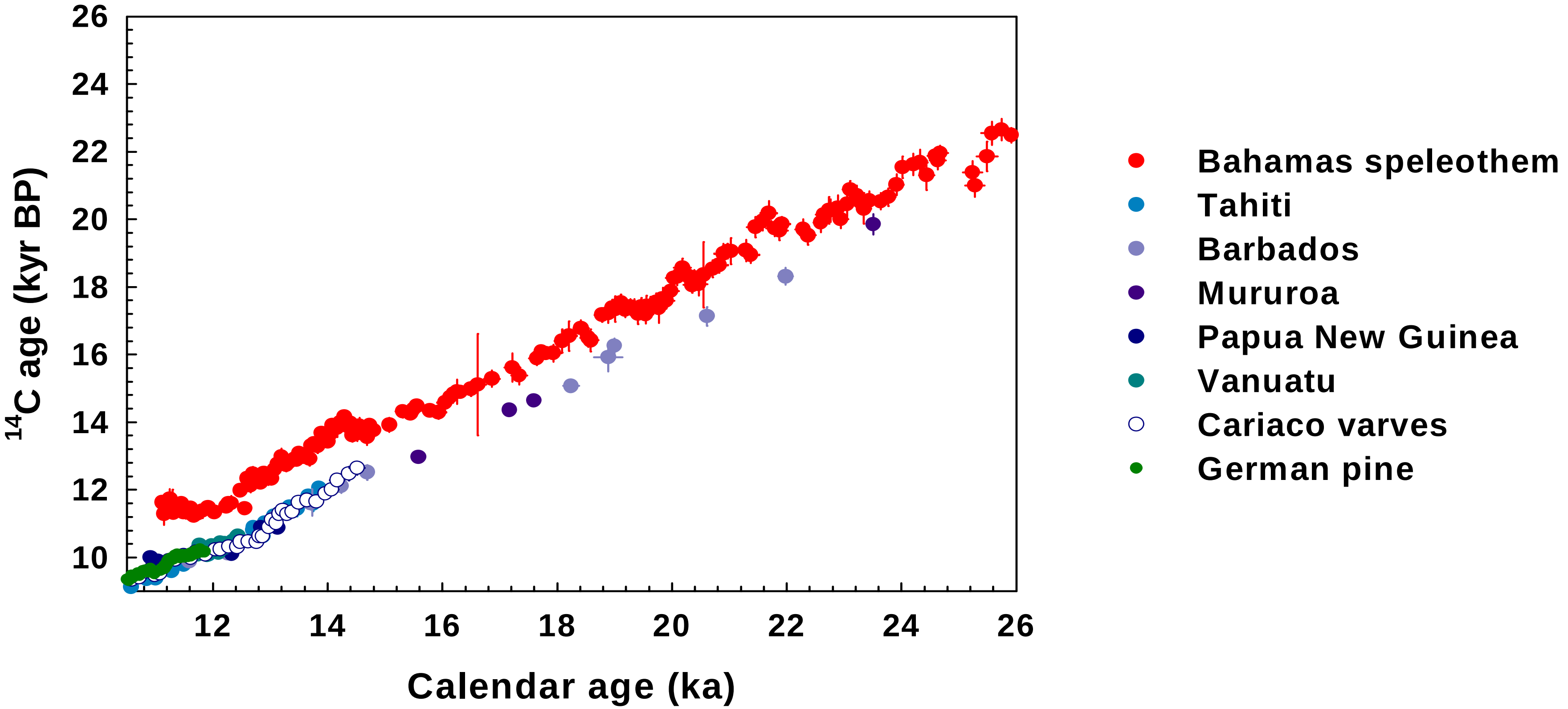

…INTCAL98 compilation

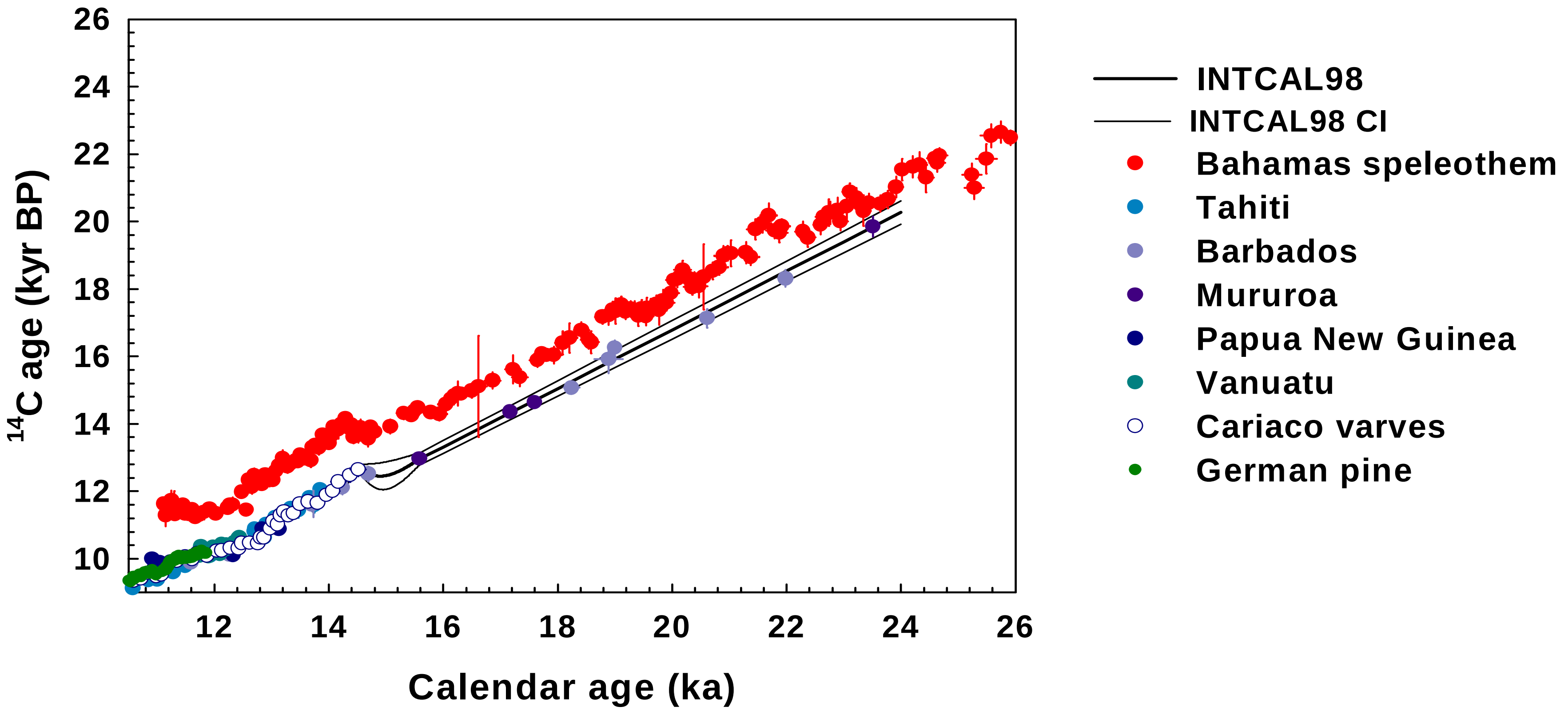

…plus varves from Lake Suigetsu, Japan

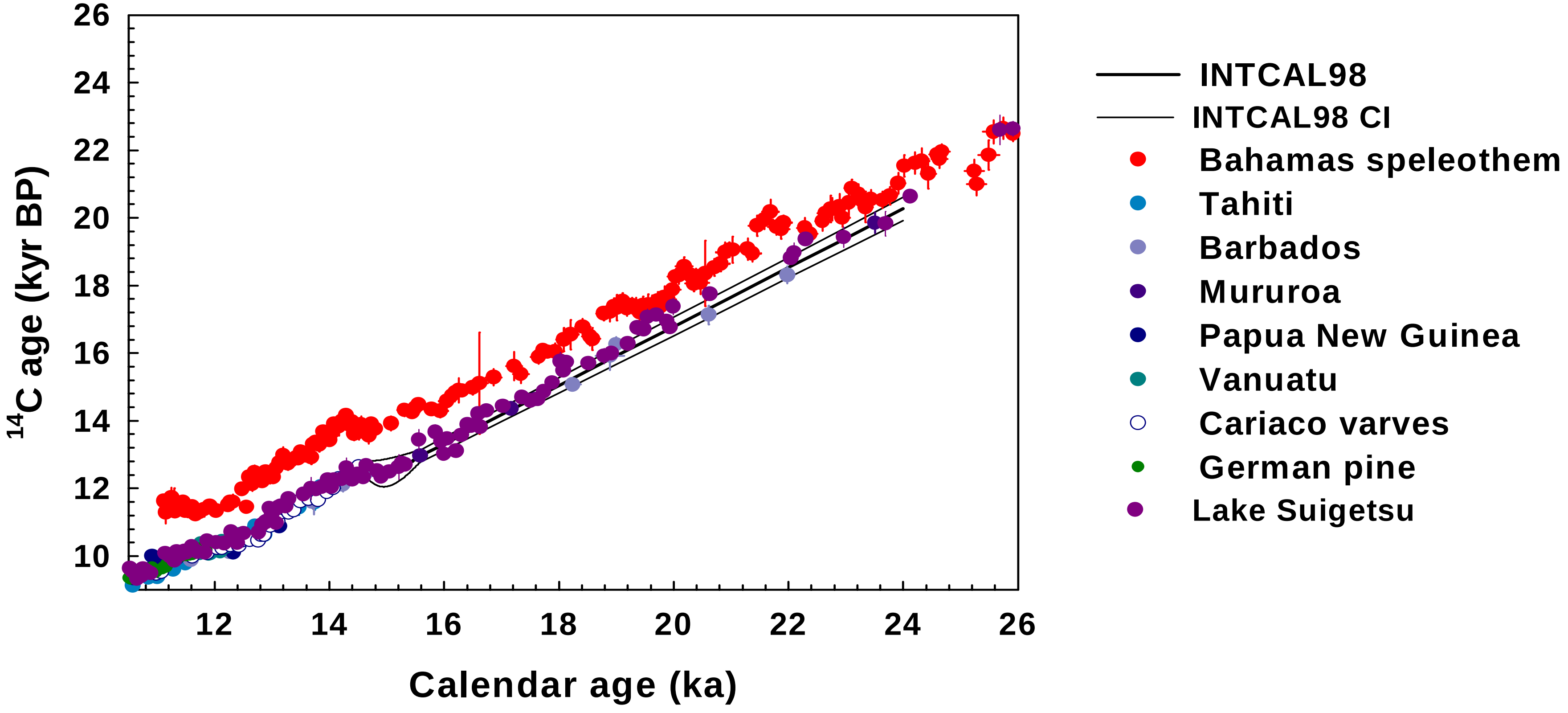

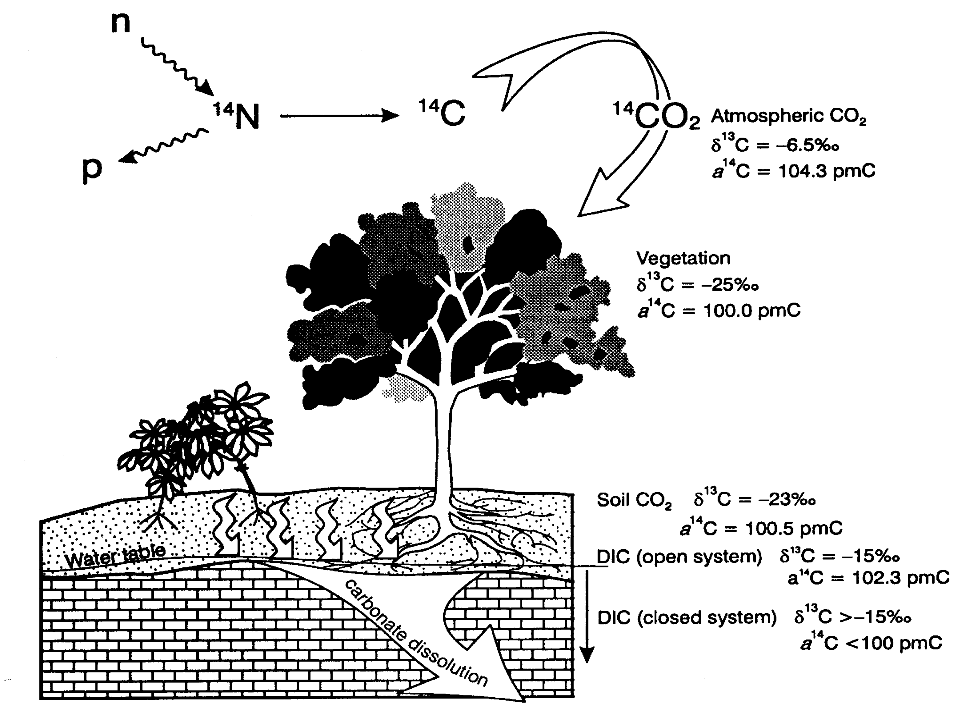

Dead carbon fraction

$$CaCO_3 + H_2O + CO_{2(g)} \Leftrightarrow Ca^{2+} + 2HCO_3^-$$

Host limestone, ^{14}C free or 'dead'

Soil gas, atmospheric ^{14}C

Dissolved bicarbonate, 'combination of two'

Collecting drips in Conch Bar Cave, Turks and Caicos

Investigation of modern ^{14}C concentrations in drip waters - work in progress

Constancy of dead carbon fraction

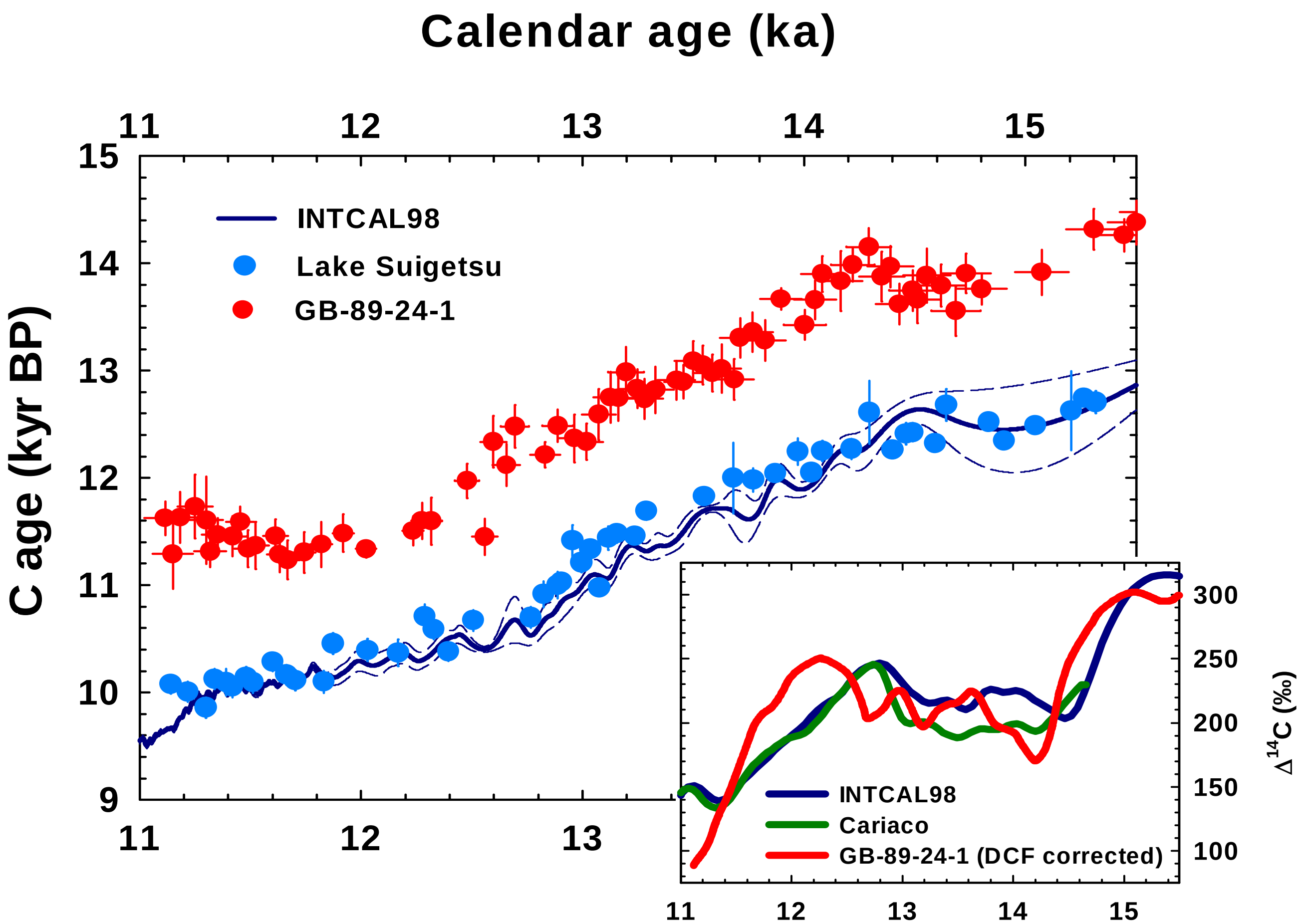

^{14}C Age

DCF-corrected ages *vs* calendar ages: 11 to 45 ka

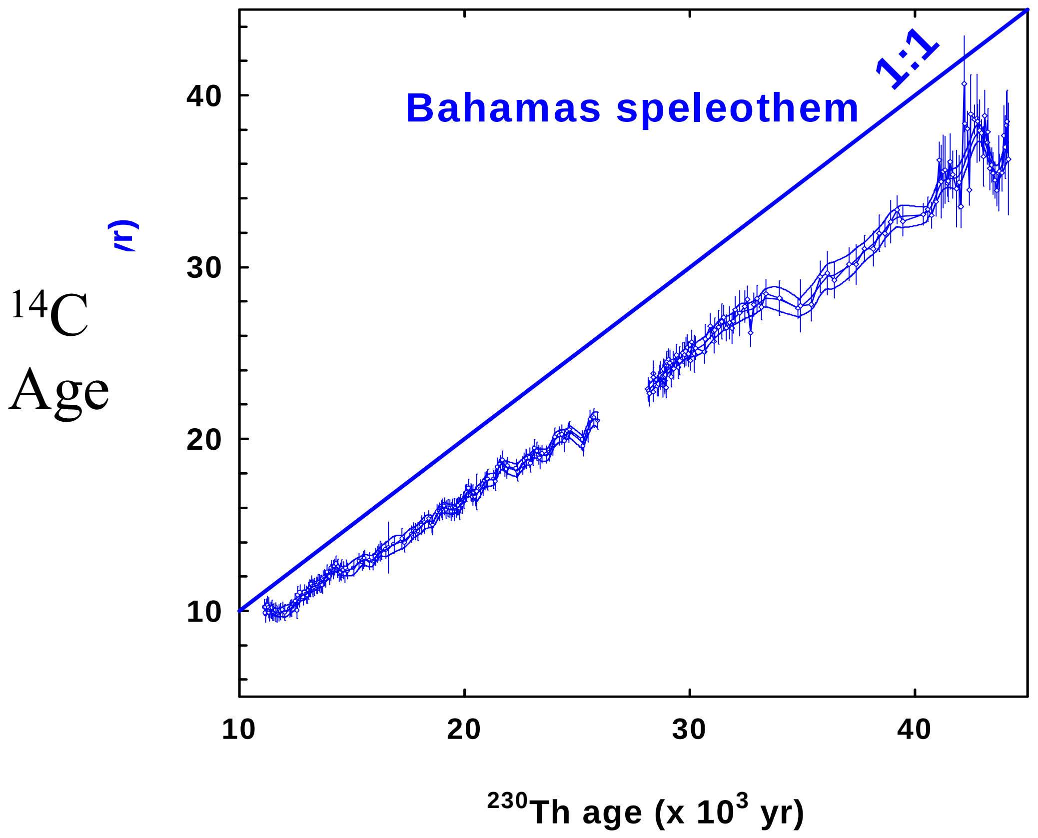

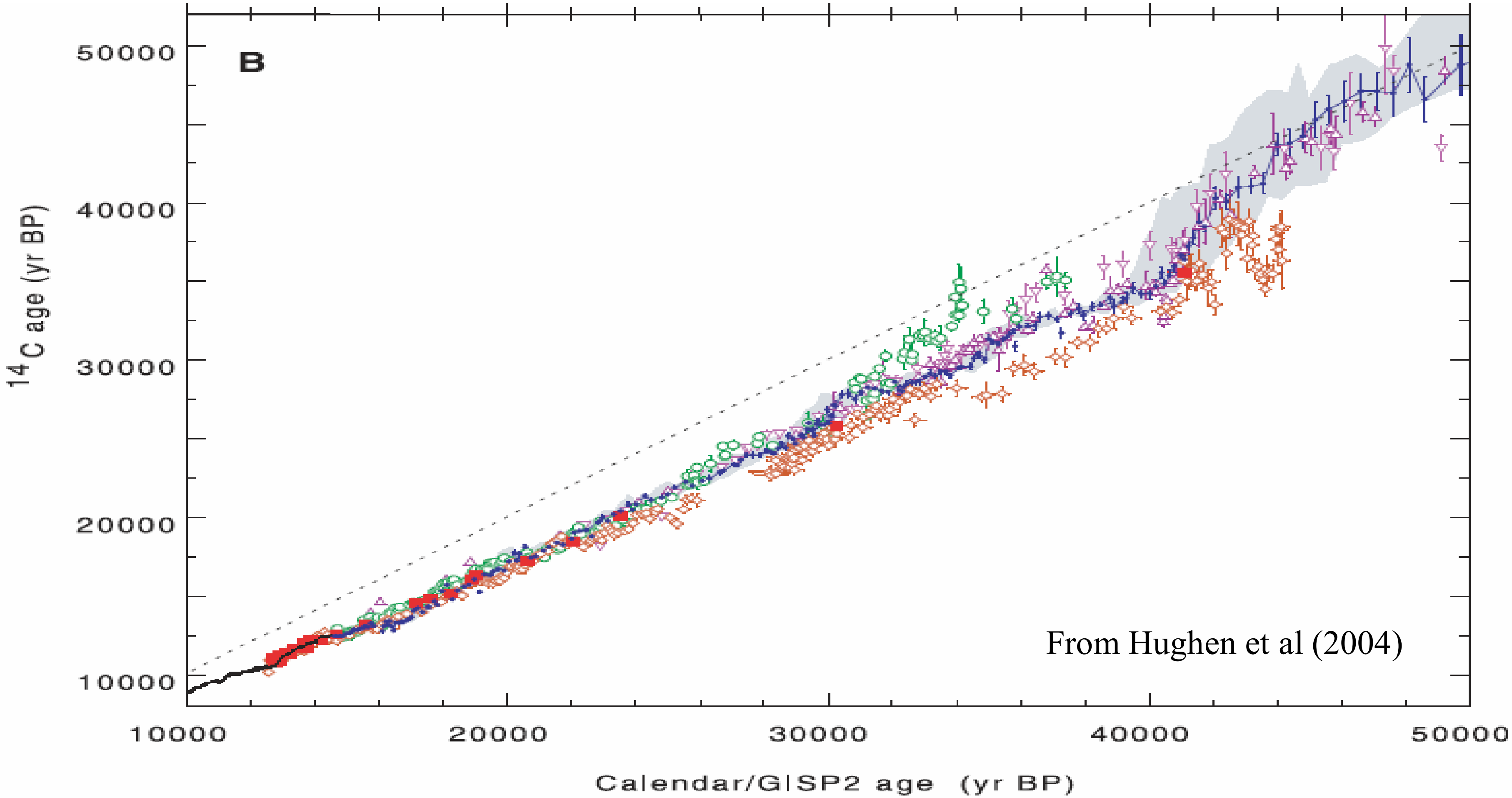

Fig. 2. Radiocarbon calibration data from various sources. **(A)** Calibration data from Cariaco leg 165, holes 1002D and 1002E (blue circles), plotted versus GISP2 calendar age (*12*) assigned by correlation of detailed paleoclimate records (*17*) (SOM Text and fig. S2). The thin black line is high-resolution calibration data from Intcal98 tree rings (*2, 3*) joined at ~12 cal. ka B.P. to the Cariaco PL07-58PC varve chronology (*13*). Red squares are paired ^{14}C-U/Th dates from corals (*5*). Replicate measurements, including overlap between 1002D and 1002E, have been averaged. Light gray shading represents the Cariaco calibration curve shifted within limits of calendar age uncertainty. Dashed line shows equal ^{14}C-calendar ages. Error bars are 1 σ. **(B)** Cariaco site 1002 data set plotted versus other published ^{14}C calibration data. Symbols are the same as above, with additional data from Lake Suigetsu varves (*6*) (open circles), Bahama speleothem U/Th (*7*) (open diamonds), and North Atlantic cores PS2644 (*9*) (upside-down triangles) and SO82-5 (*10*) (triangles) correlated to GISP2. Error bars for all records are 1 σ.

$\Delta^{14}C$ definition

$\Delta^{14}C = (F\, e^{\lambda t} - 1)\, 1000‰$

Where λ is the ^{14}C decay constant,
And t is the time time of sample formation
Relative to 1950 AD,

and

F= Fraction Modern = $(^{14}C/^{12}C)_s/(^{14}C/^{12}C)_{std}$

Thus, $\Delta^{14}C$ = 0‰ is the same ^{14}C concentration as the 1950 Atmosphere, 1000‰ is twice the ^{14}C concentration, etc..

Bahamas speleothem $\Delta^{14}C$

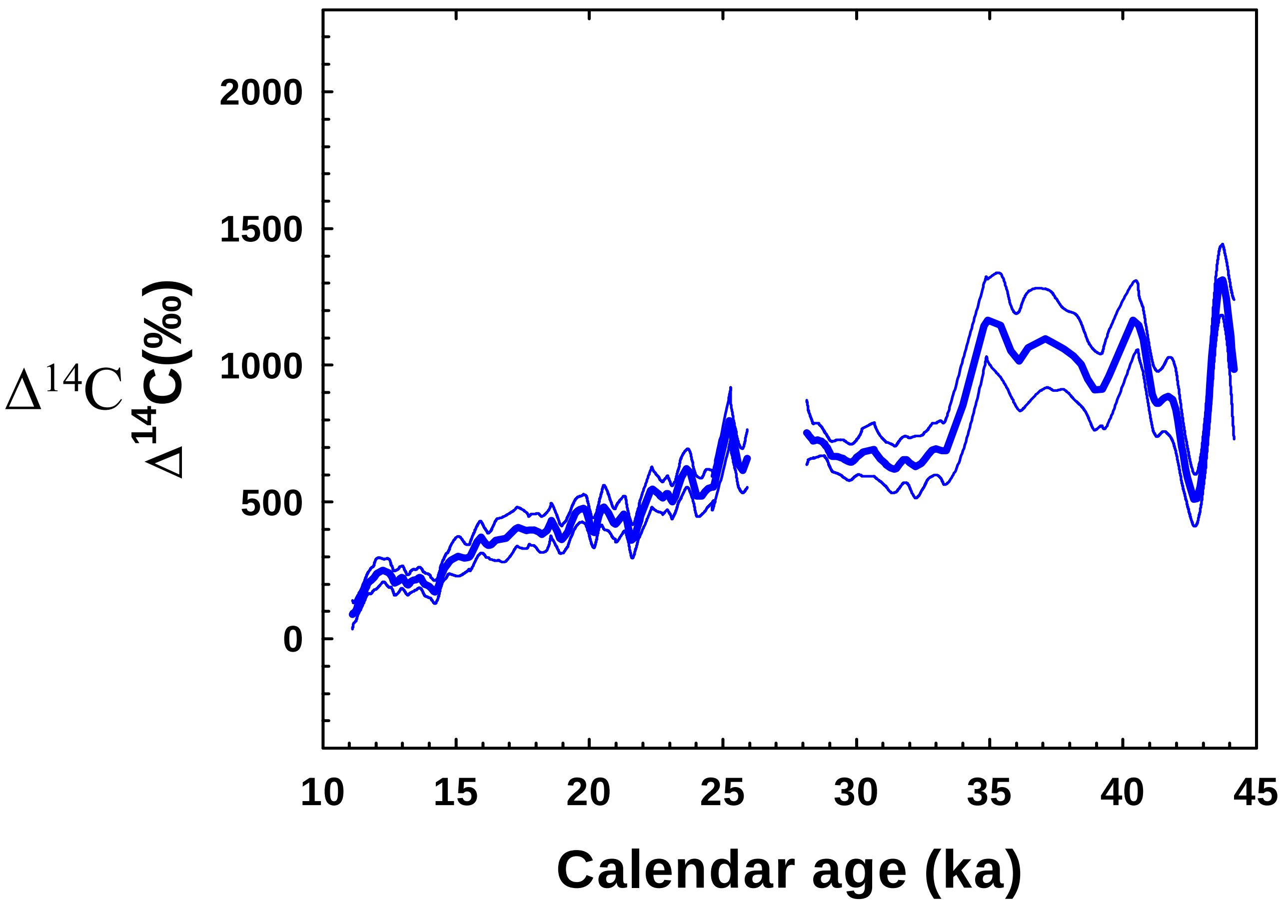

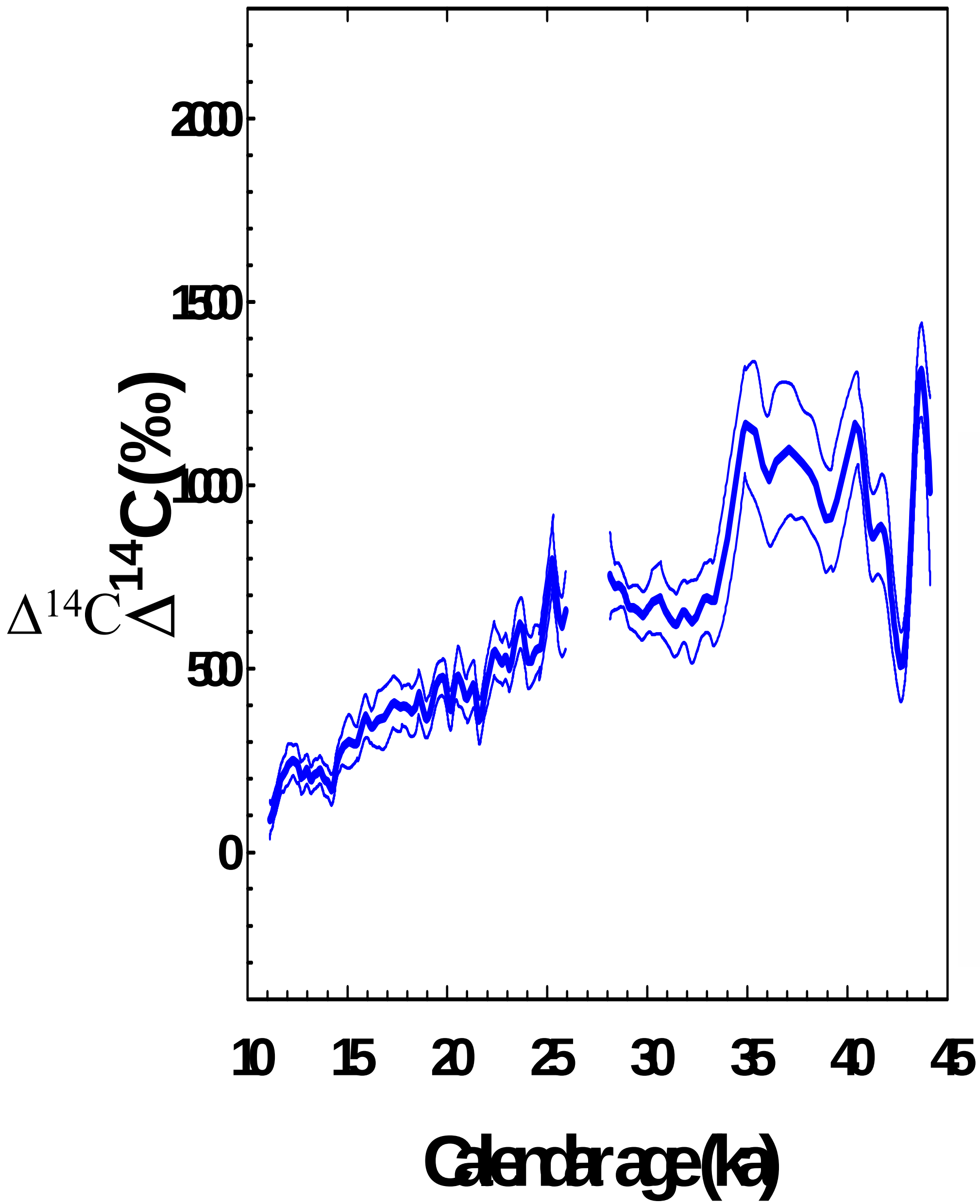
Δ14C
Δ14C (‰)
2000
1500
1000
500
0
10
15
20
25
30
35
40
45

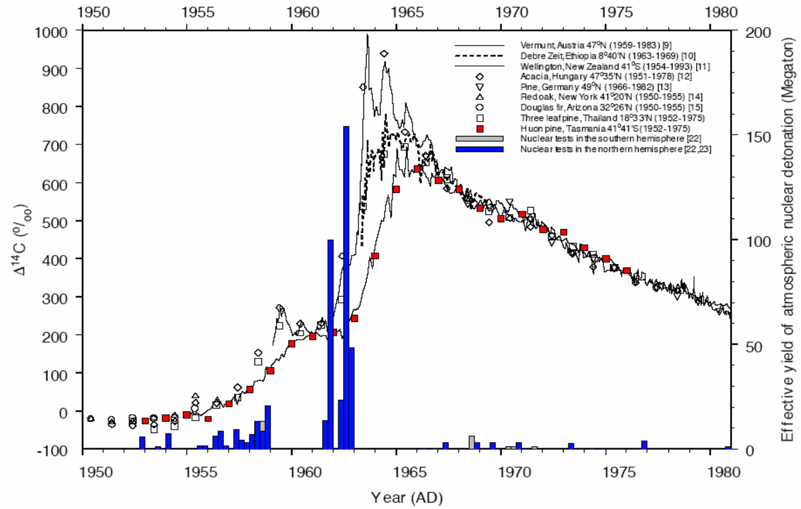
1950
1955
1960
1965
1970
1975
1980
Δ14C (‰)
1000
900
800
700
600
500
400
300
200
100
0
-100
200
150
100
50
0
Effective yield of atmospheric nuclear detonation (Megaton)
Year (AD)
Vermunt, Austria 47°N (1959-1983) [9]
Debre Zeit, Ethiopia 8°40'N (1963-1969) [10]
Wellington, New Zealand 41°S (1954-1993) [11]
Acacia, Hungary 47°35'N (1951-1978) [12]
Pine, Germany 49°N (1966-1982) [13]
Red oak, New York 41°20'N (1950-1955) [14]
Douglas fir, Arizona 32°26'N (1950-1955) [15]
Three leaf pine, Thailand 18°33'N (1952-1975)
Huon pine, Tasmania 41°41'S (1952-1975)
Nuclear tests in the southern hemisphere [22]
Nuclear tests in the northern hemisphere [22,23]

Why is $\Delta^{14}C$ so high during the last glacial age?

- Galactic cosmic ray flux was higher
- Geomagnetic field was lower
- Solar magnetic field was lower
- Ocean/atmosphere CO_2 exchange rate was significantly slower

Galactic Cosmic Rays (GCR)

•^{14}C is formed in the atmosphere by galactic cosmic rays.

•Galactic cosmic rays are high energy (up to 10^6 GeV) particles (usually protons) accelerated by celestial events such as super nova.

•GCR striking our atmosphere shatter their target atoms into free protons and neutrons.

•Free neutrons are gathered by other atoms in the atmosphere to make new nuclides, such as ^{14}C.

If GCR fluxes have varried in the past, then measurement of different cosmogenic nuclides with various halflifes (^{14}C, ^{10}Be, ^{41}Ca, ^{3}He, etc.) measured in unshielded materials (such as meteorites or lunar soils) should have different activities (N/λ).

Measurements show that all such nuclides have the same activity, thus GCR has Remained constant.

Earth's magnetosphere

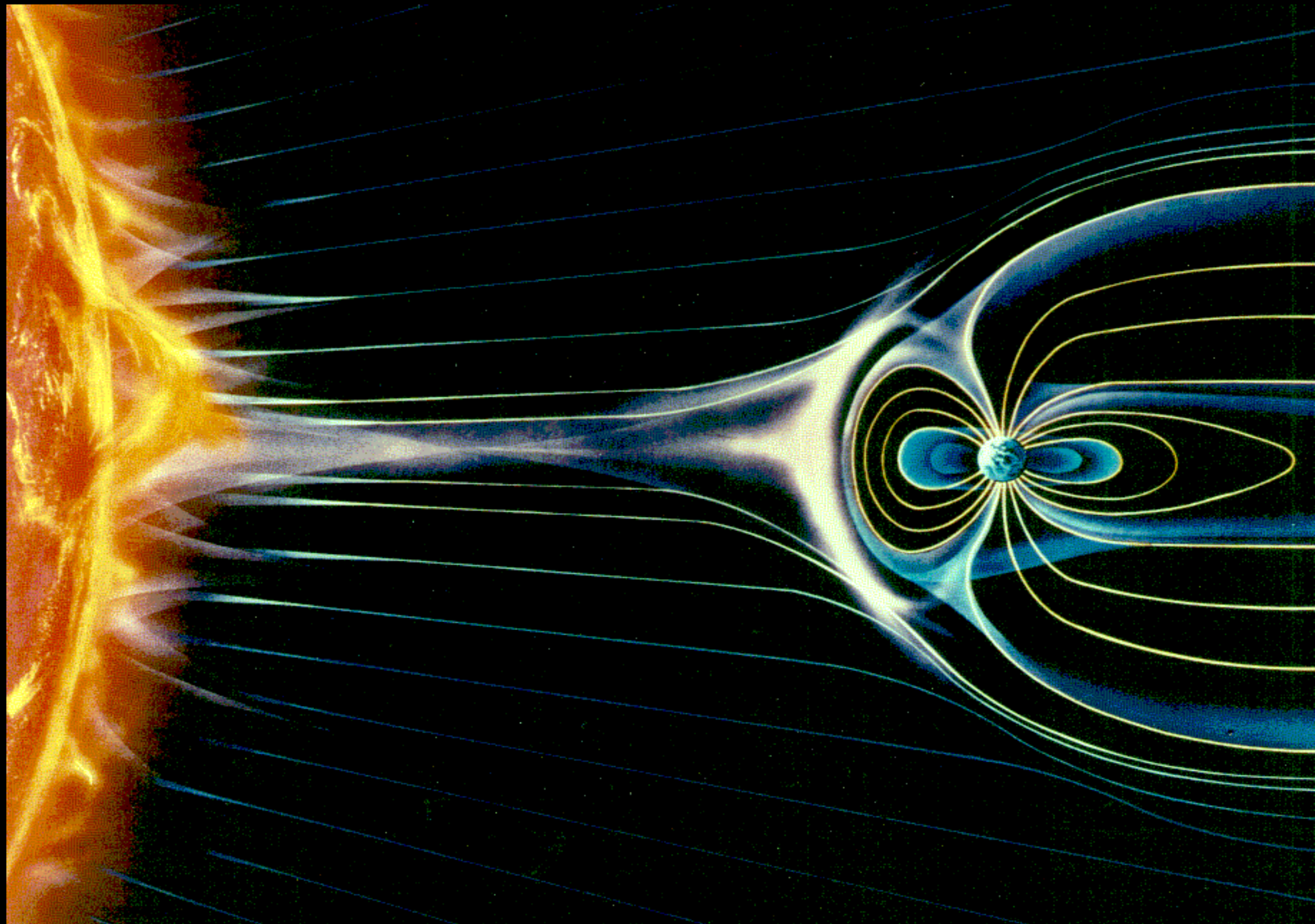

Comparison of $\Delta^{14}C$ and dipole moment from 10 ka to present

McElhinny and Senanayake (1982)

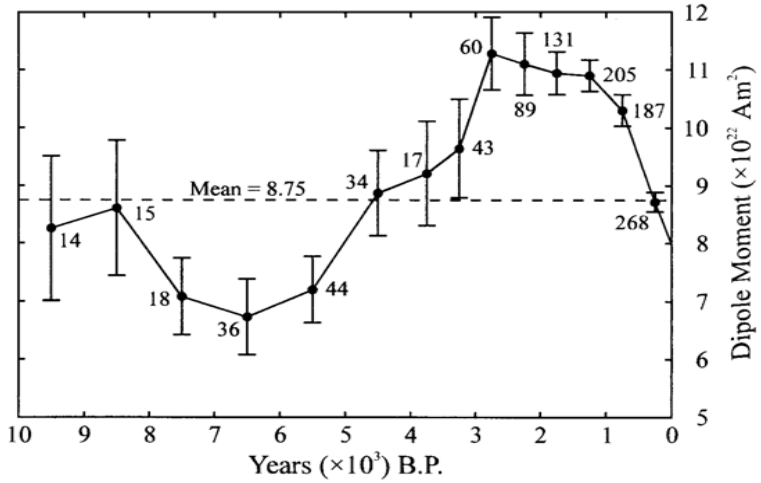

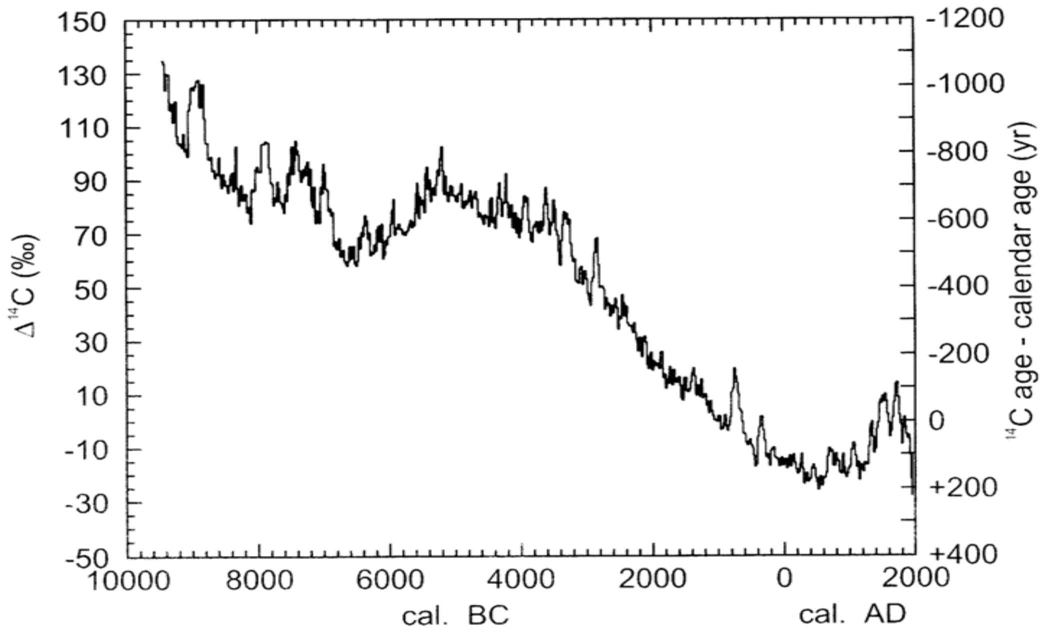

Stuiver and Reimer (1993)

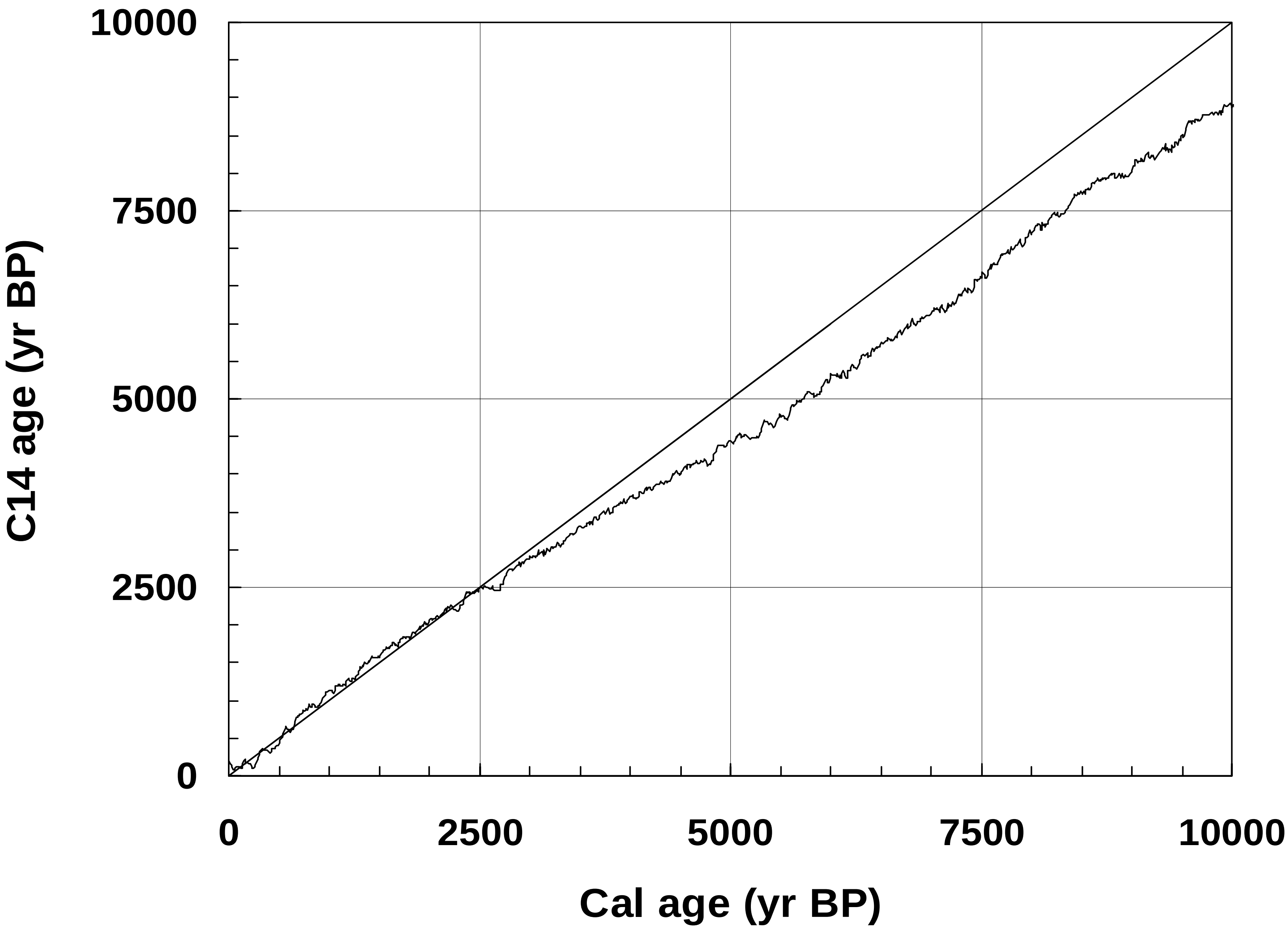
10000
7500
5000
2500
0
C14 age (yr BP)
0
2500
5000
7500
10000
Cal age (yr BP)

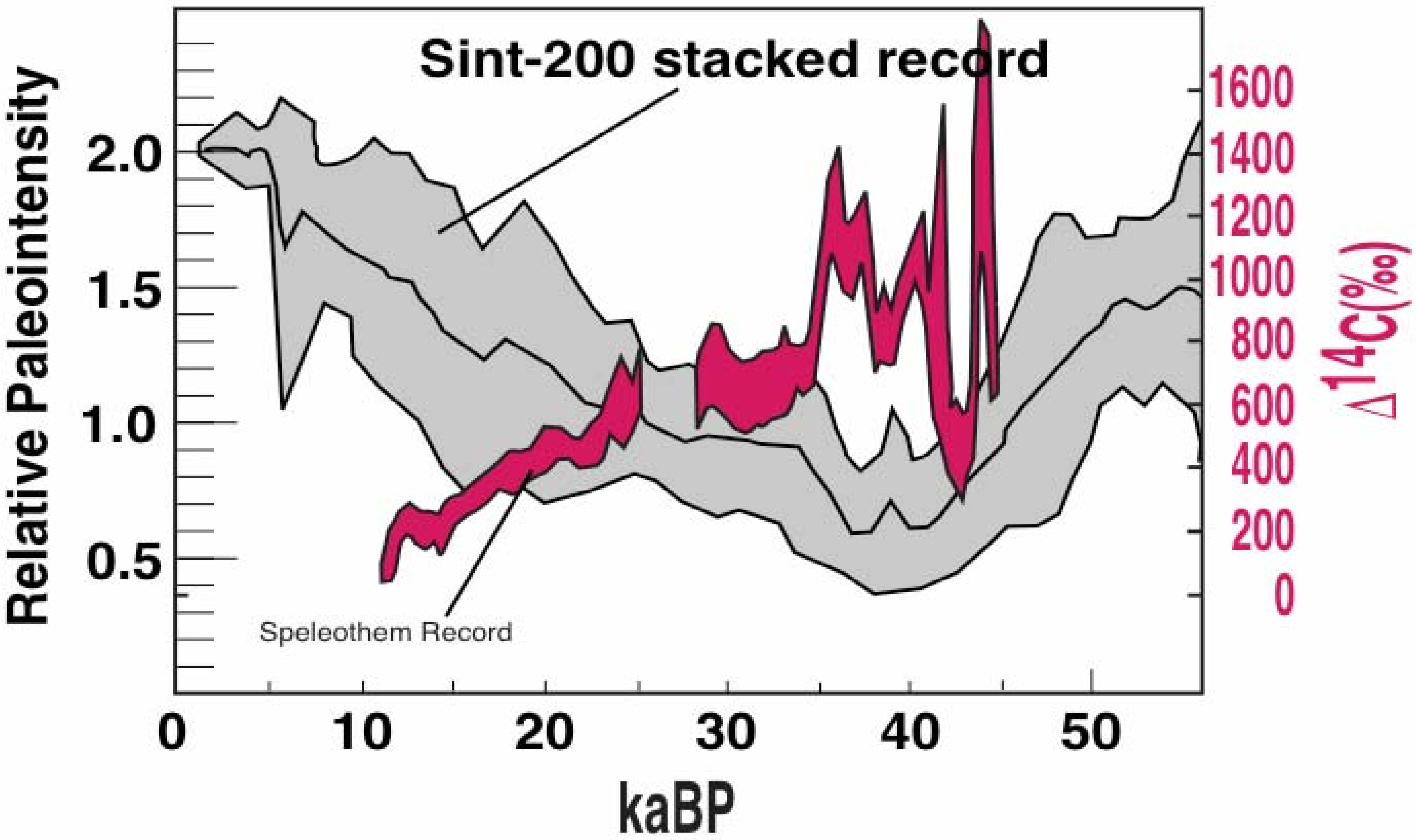
Sint-200 stacked record
Speleothem Record
Relative Paleointensity
2.0
1.5
1.0
0.5
0
10
20
30
40
50
kaBP
1600
1400
1200
1000
800
600
400
200
0
Δ14C(‰)

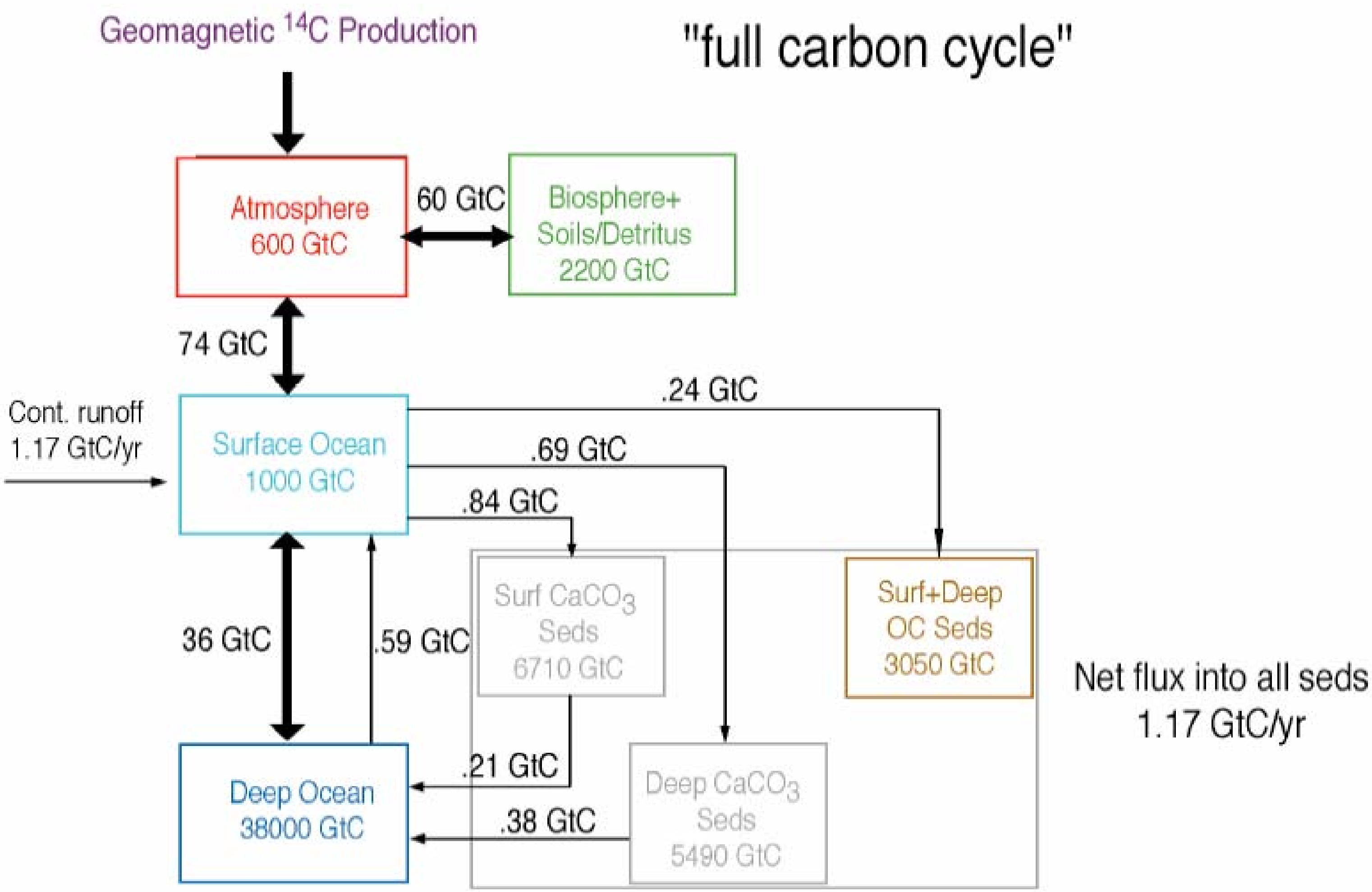

From Hughen et al., 2004

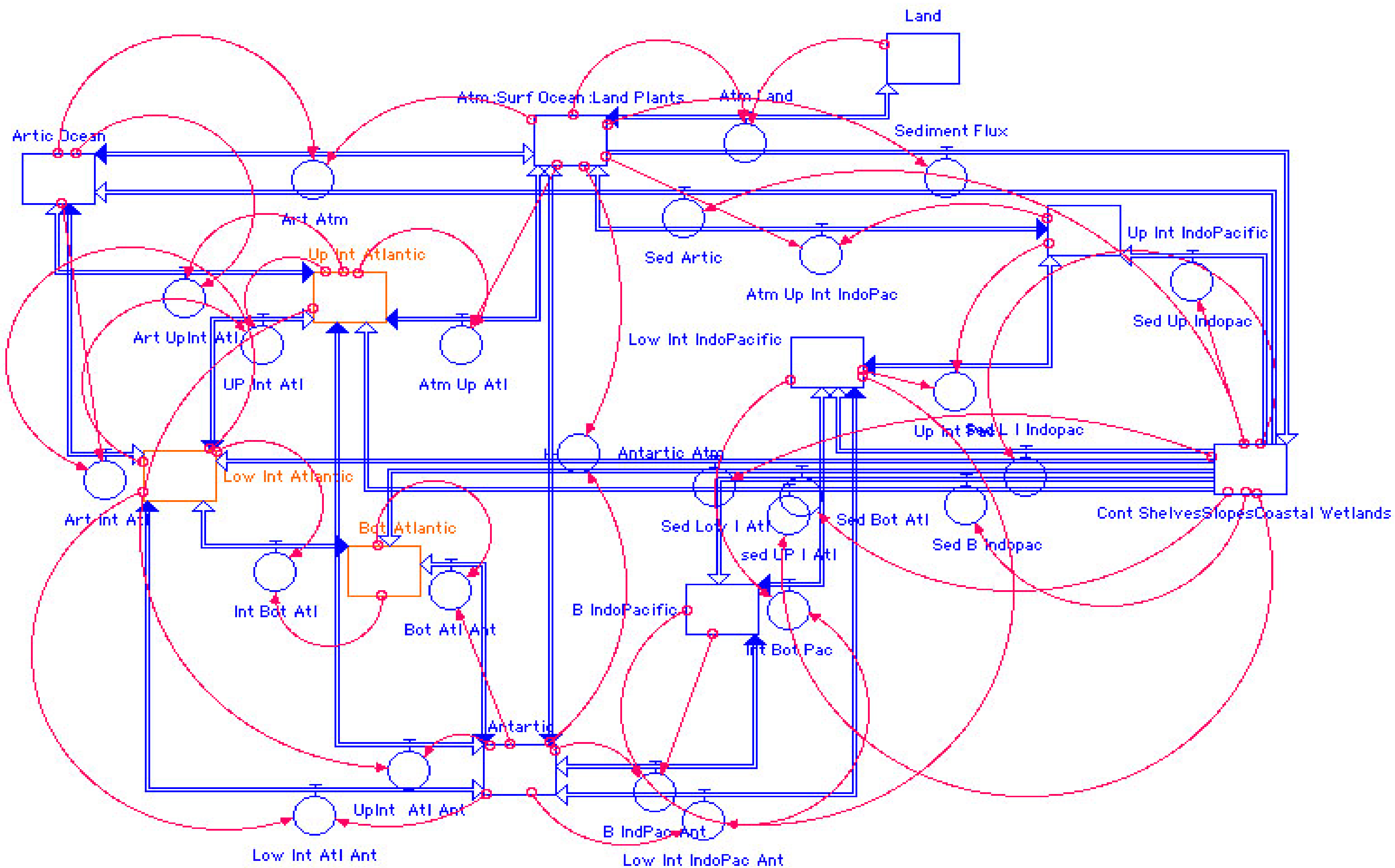

Land
Atm :Surf Ocean :Land Plants
Atm Land
Sediment Flux
Artic Ocean
Art Atm
Sed Artic
Atm Up Int IndoPac
Up Int IndoPacific
Up Int Atlantic
Art UpInt Atl
UP Int Atl
Atm Up Atl
Sed Up Indopac
Low Int IndoPacific
Up Int Pac
Sed L I Indopac
Antartic Atm
Low Int Atlantic
Art Int Atl
Sed Low I Atl
sed UP I Atl
Sed Bot Atl
Sed B Indopac
Cont ShelvesSlopesCoastal Wetlands
Bot Atlantic
Int Bot Atl
Bot Atl Ant
B IndoPacific
Int Bot Pac
Antartic
UpInt Atl Ant
Low Int Atl Ant
B IndPac Ant
Low Int IndoPac Ant

Model vs data comparison

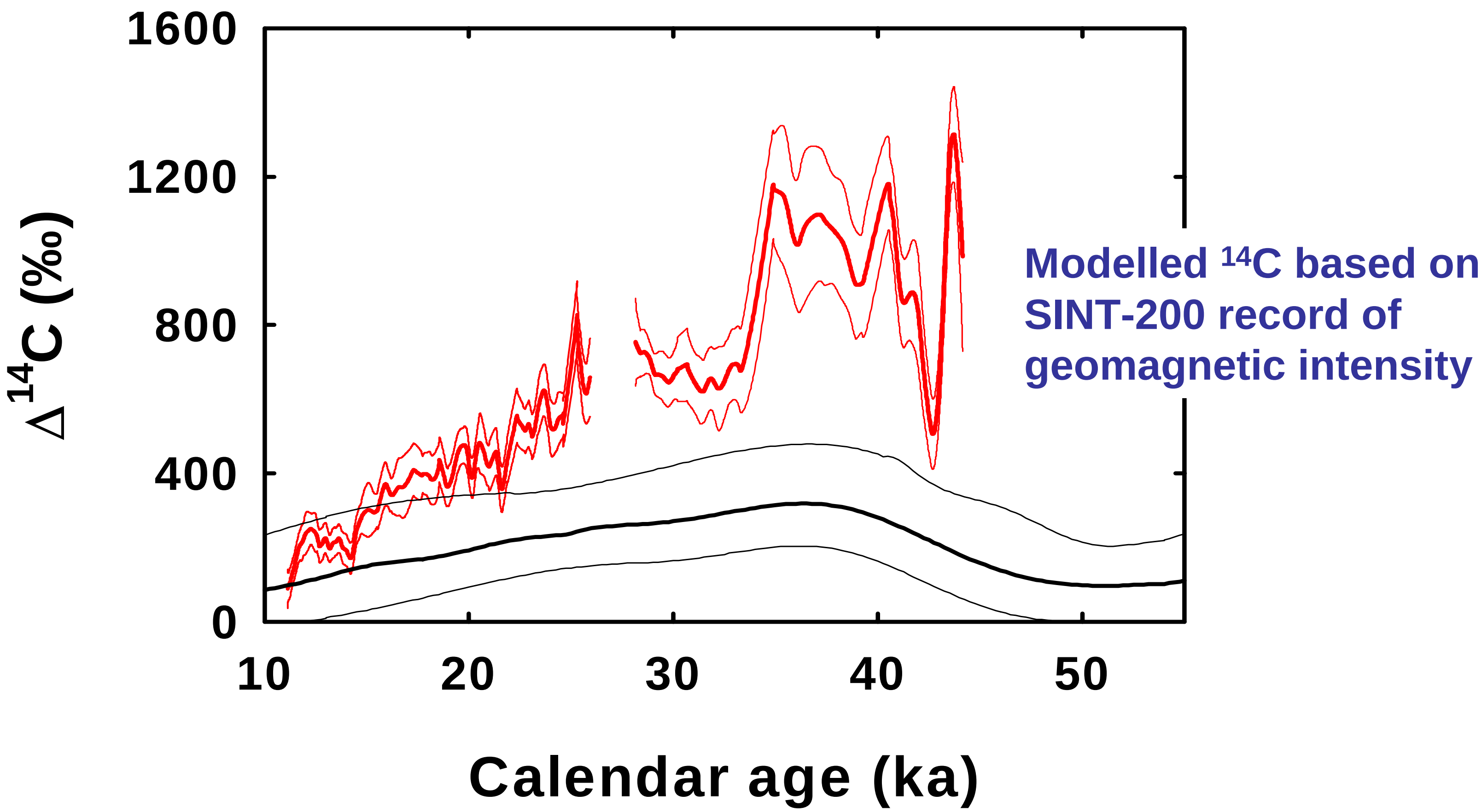

Radiocarbon during the last glacial maximum and deglaciation

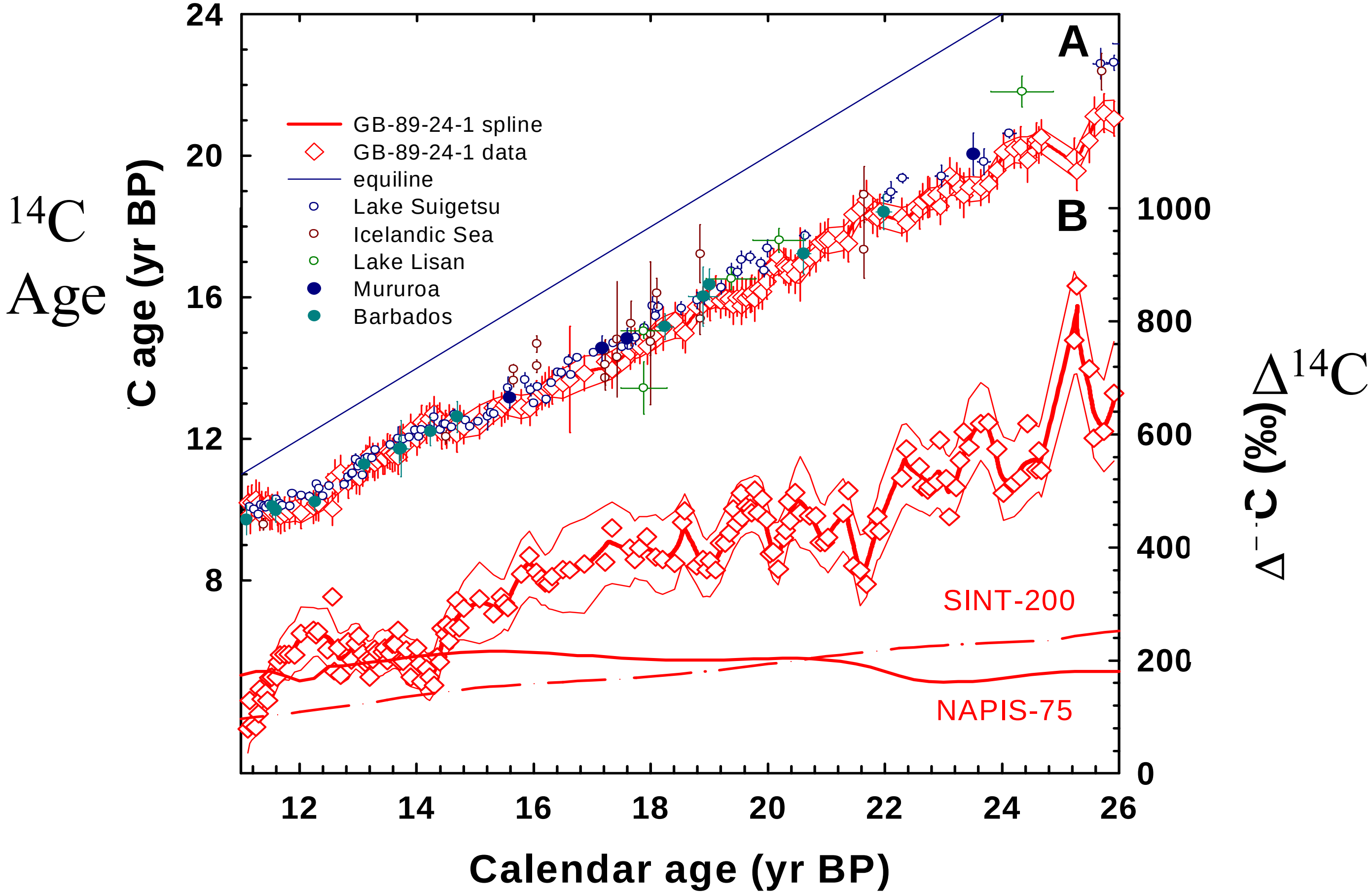

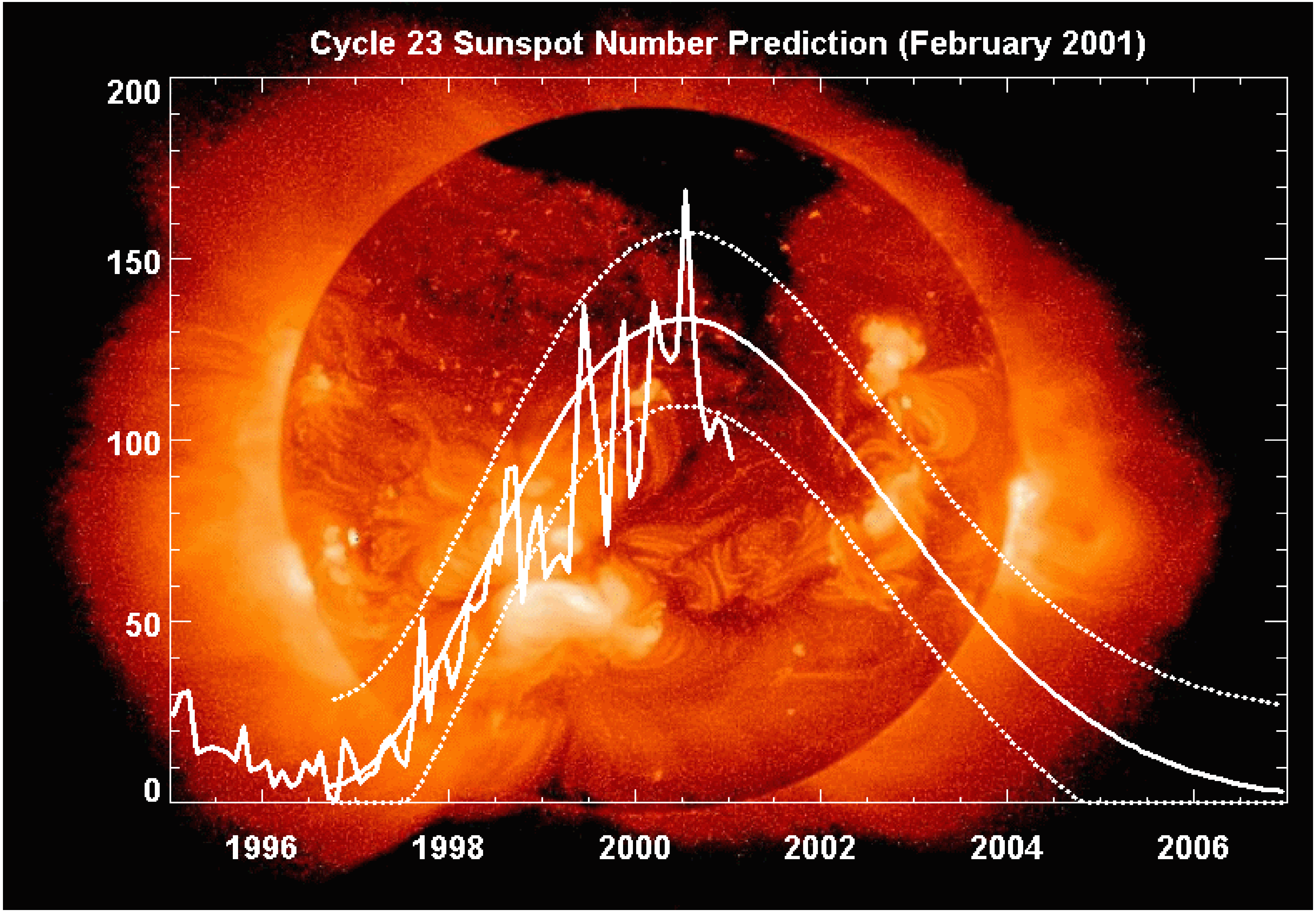
Cycle 23 Sunspot Number Prediction (February 2001)
200
150
100
50
0
1996
1998
2000
2002
2004
2006

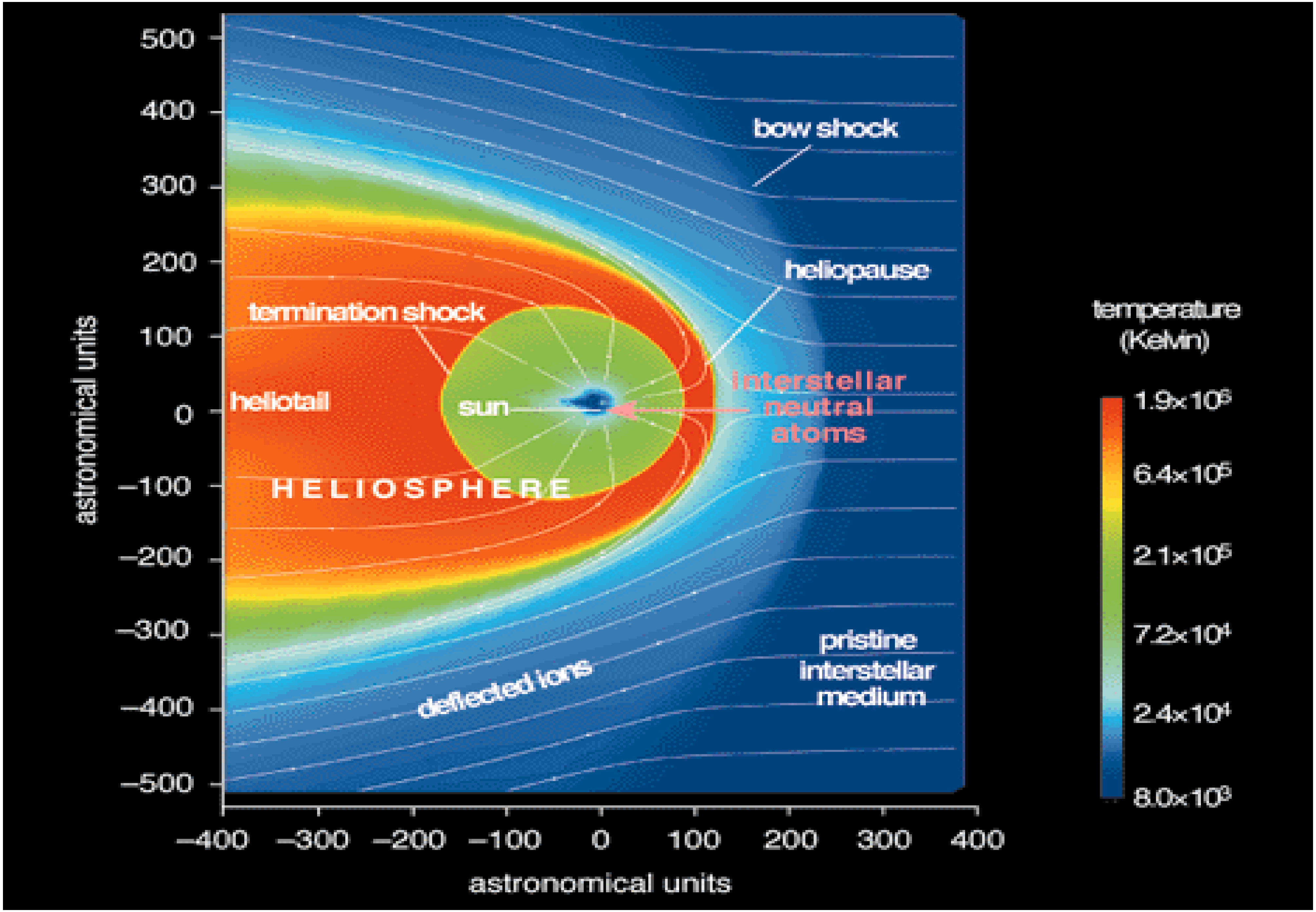

bow shock
heliopause
termination shock
interstellar
neutral
atoms
heliotail
sun
HELIOSPHERE
deflected ions
pristine
interstellar
medium
temperature
(Kelvin)
1.9×10^6
6.4×10^5
2.1×10^5
7.2×10^4
2.4×10^4
8.0×10^3
astronomical units
astronomical units
500
400
300
200
100
0
−100
−200
−300
−400
−500
−400 −300 −200 −100 0 100 200 300 400

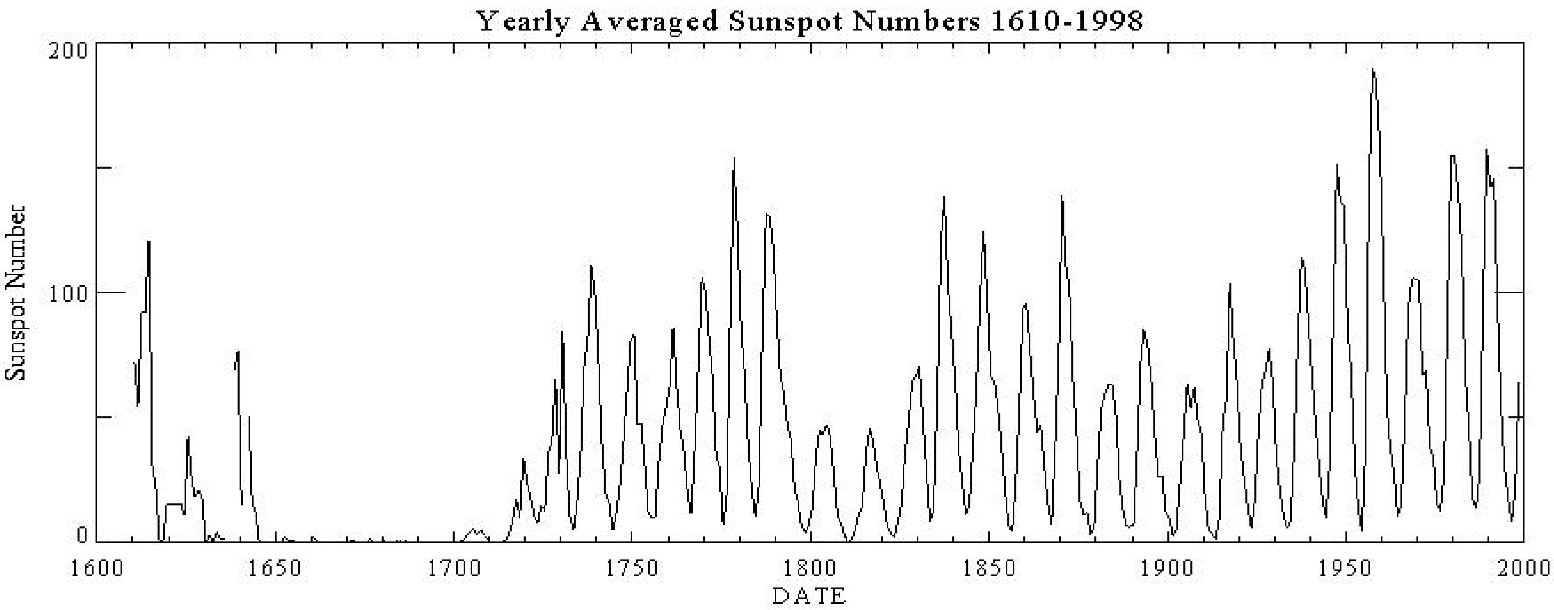

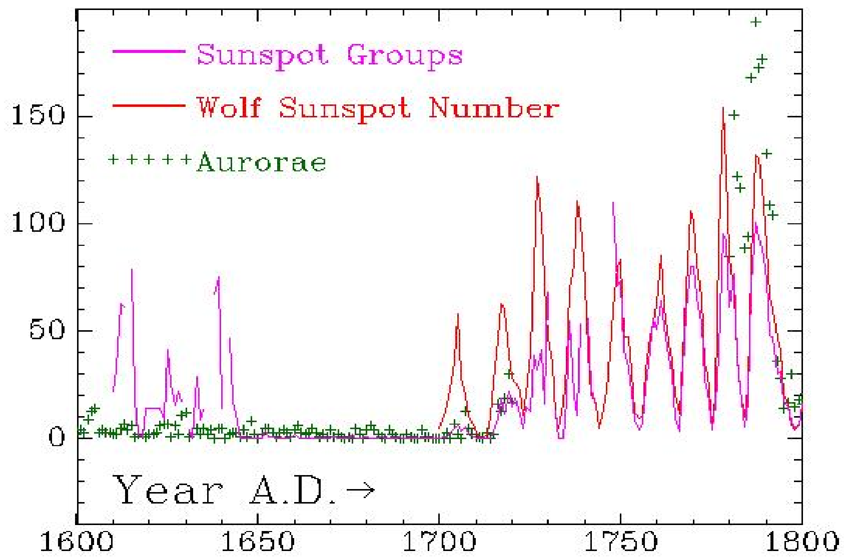

Maunder Minimum: a period when sunspots vanished

$\Delta^{14}C$ for the last millennium

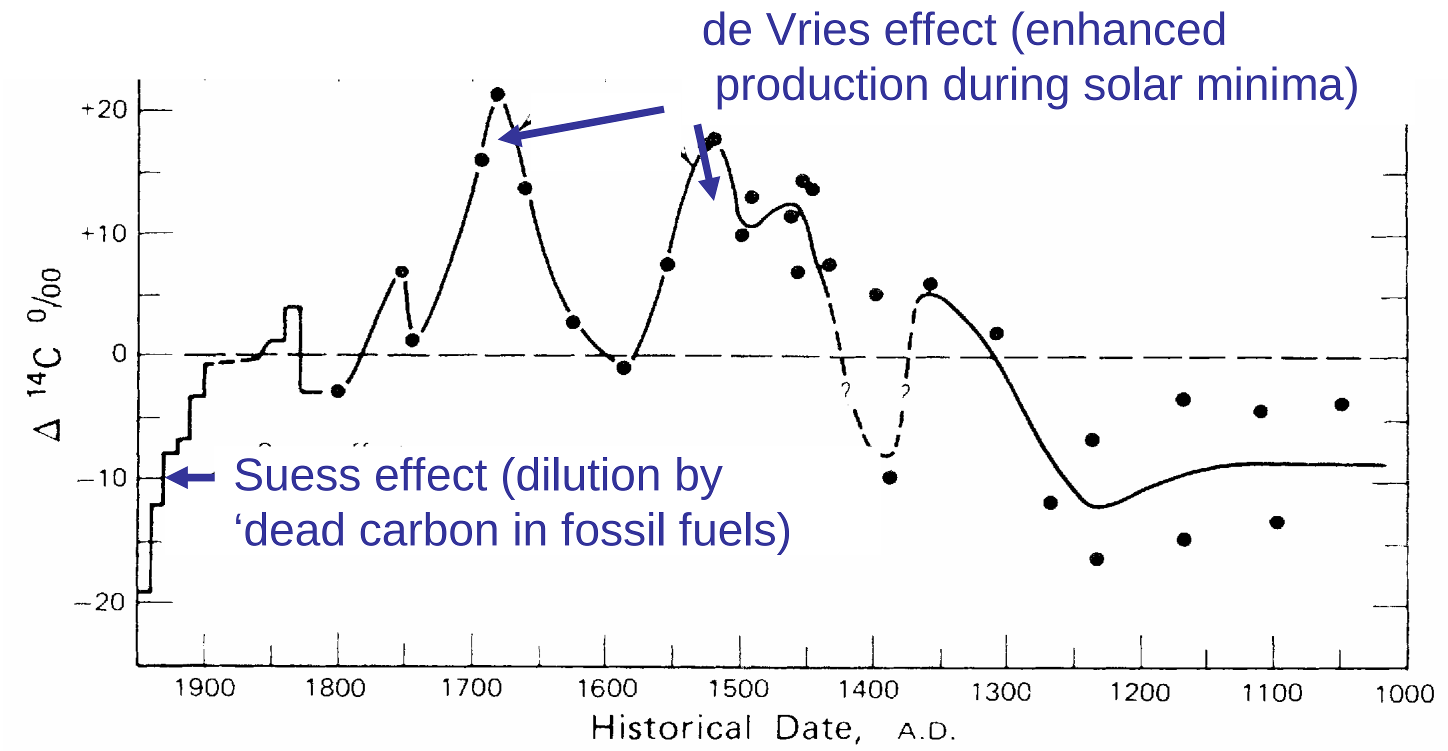

$\Delta^{14}C$: relative concentration of ^{14}C with respect to pre-industrial wood in parts per mil (‰)

Model vs data comparison

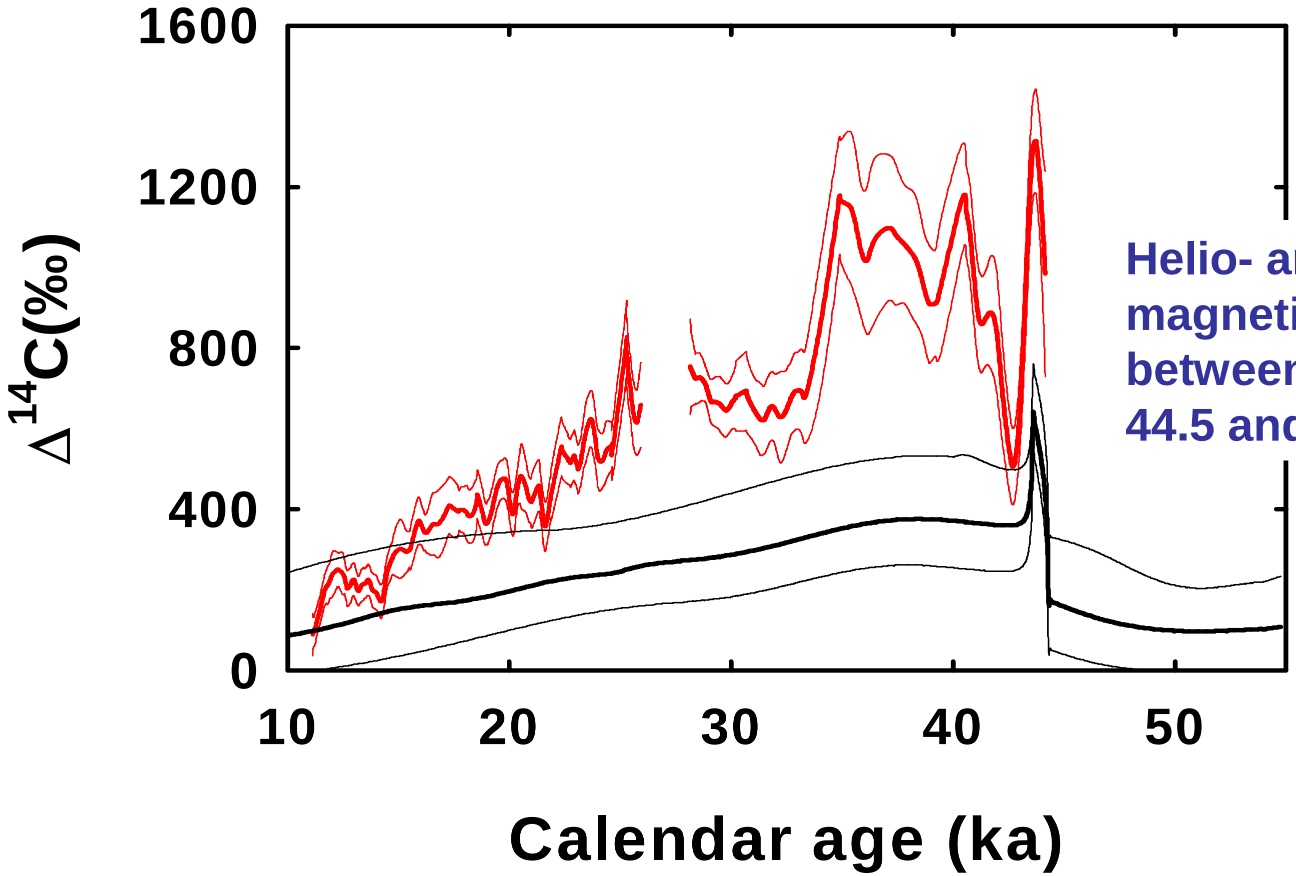

Helio- and geo-magnetic intensity = 0 between 44.5 and 43.8 ka

Why is $\Delta^{14}C$ so high during the last glacial age?

- Galactic cosmic ray flux was higher
- Geomagnetic field was lower
- Solar magnetic field was lower
- Ocean/atmosphere CO_2 exchange rate was significantly slower
- Carbon export from the ocean mixed layer was slower.

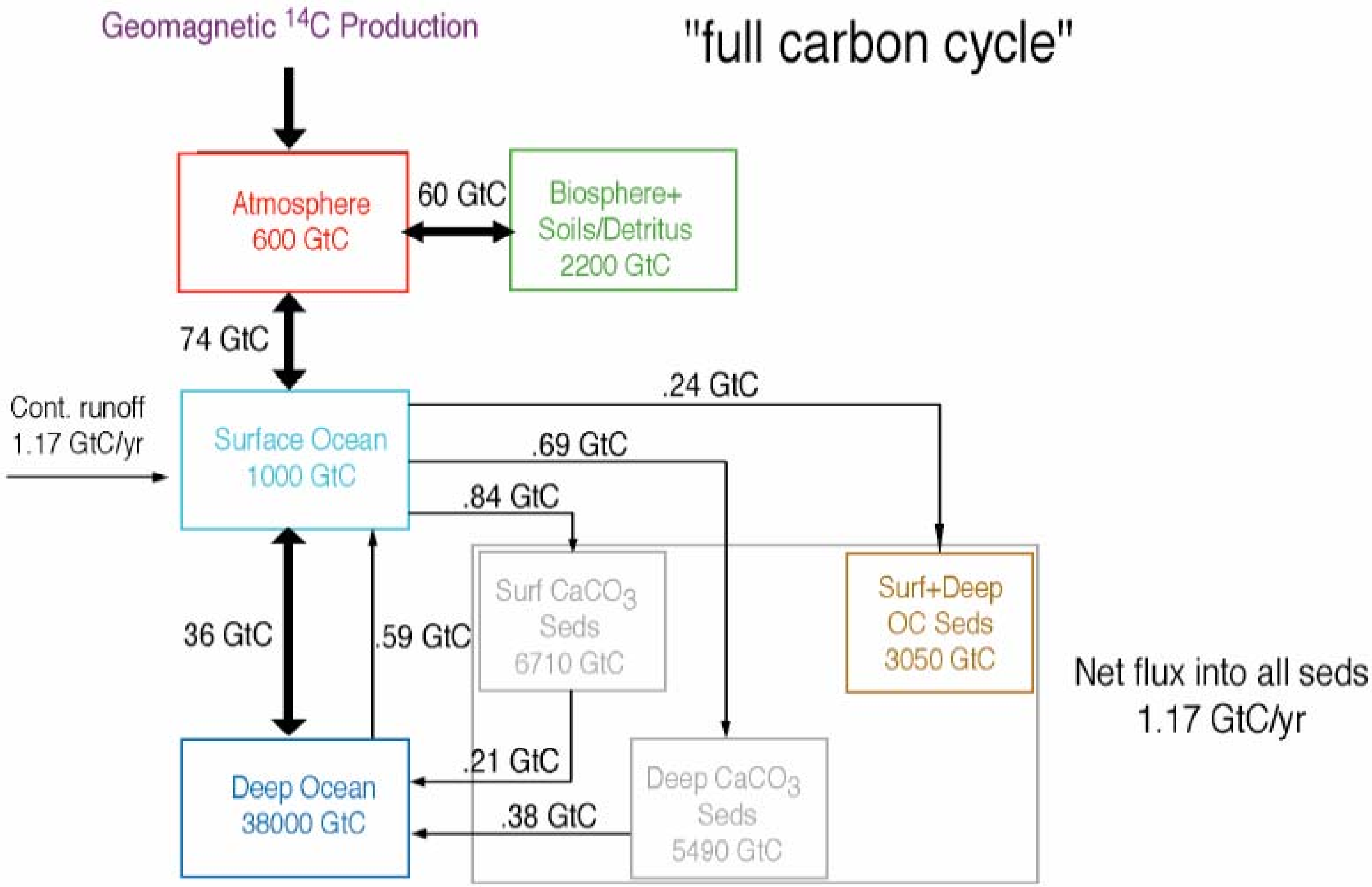

From Hughen et al., 2004

"minimum carbon cycle"

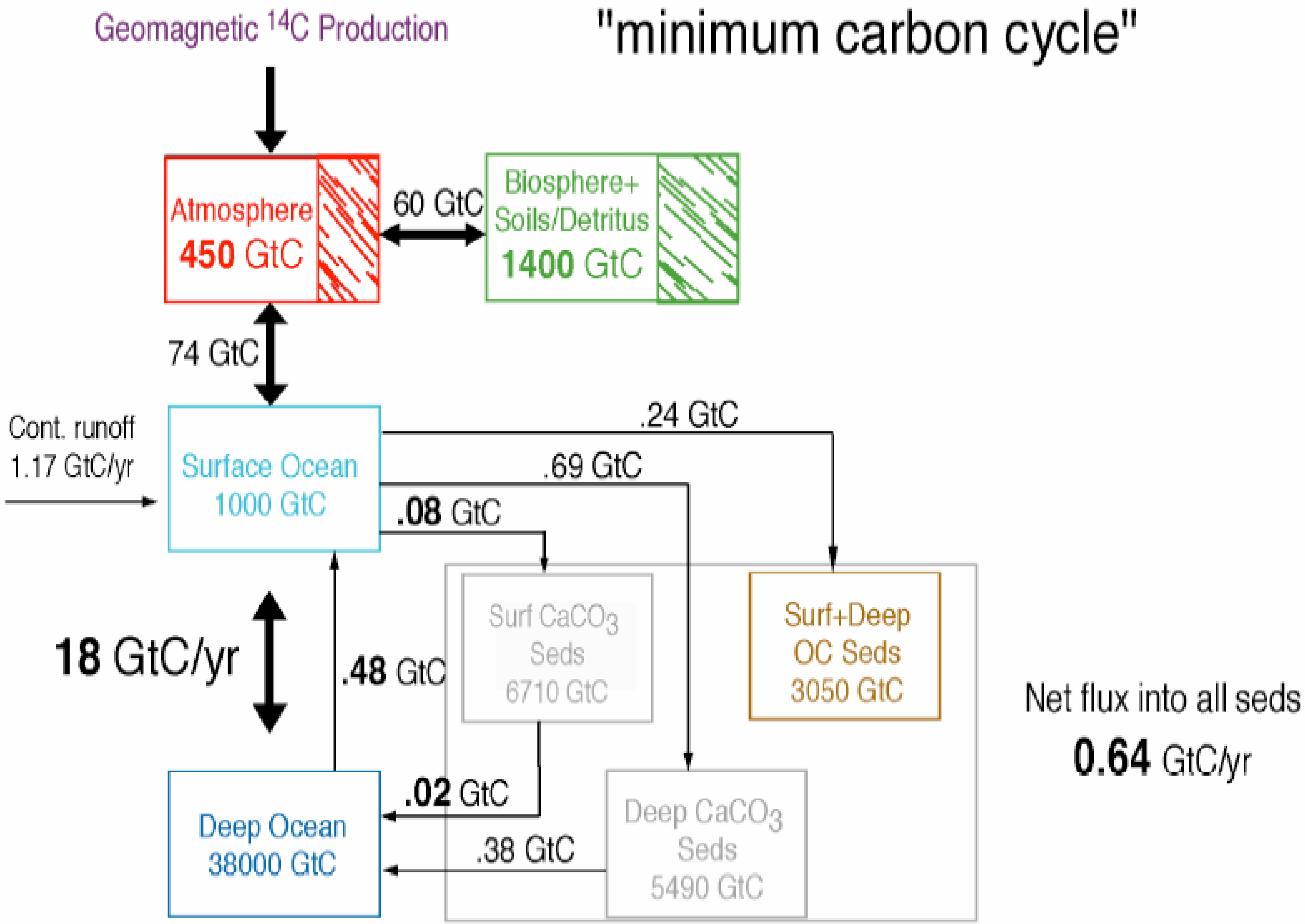

From Hughen et al . (2004)

Model vs data comparison

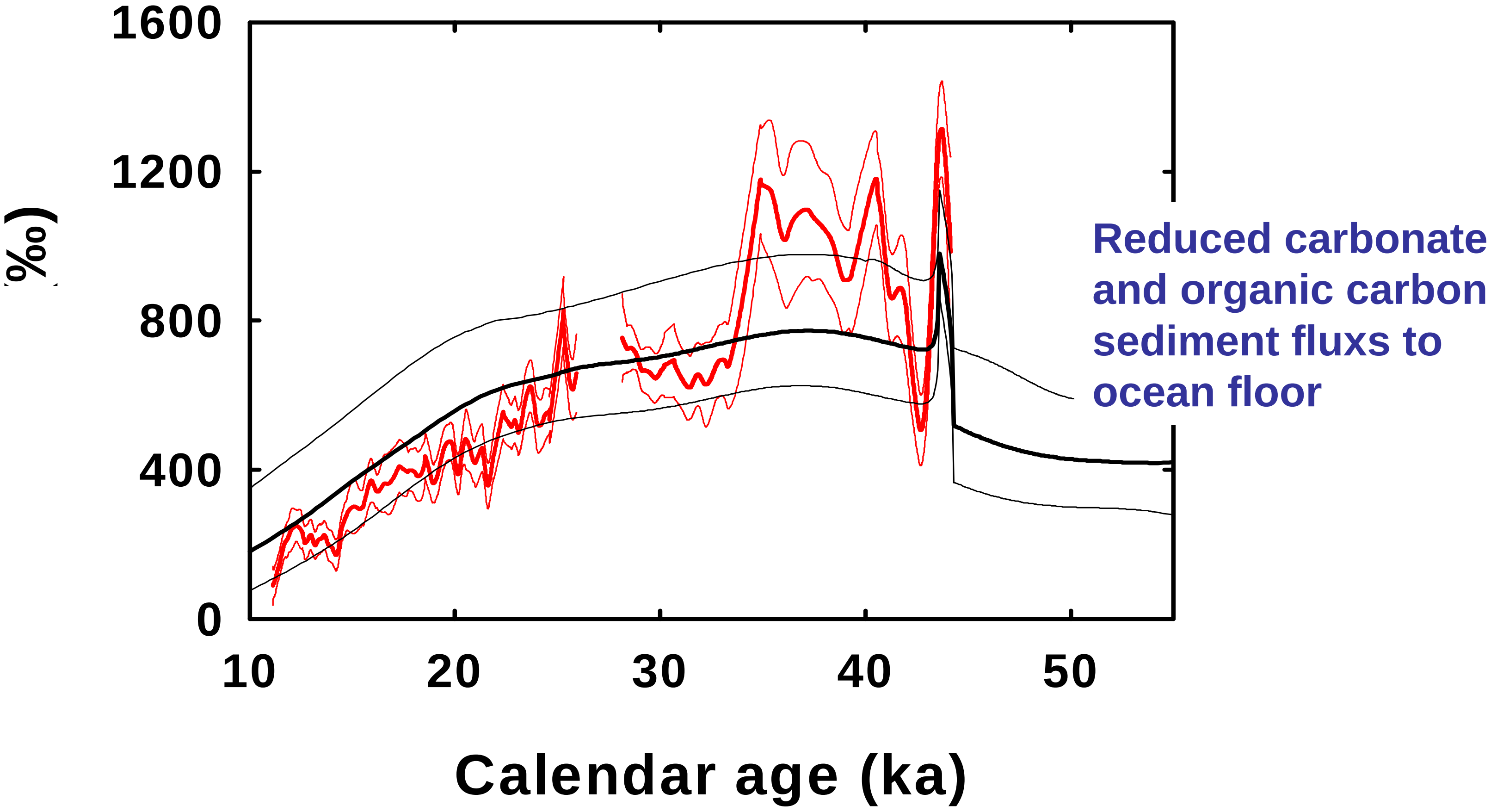

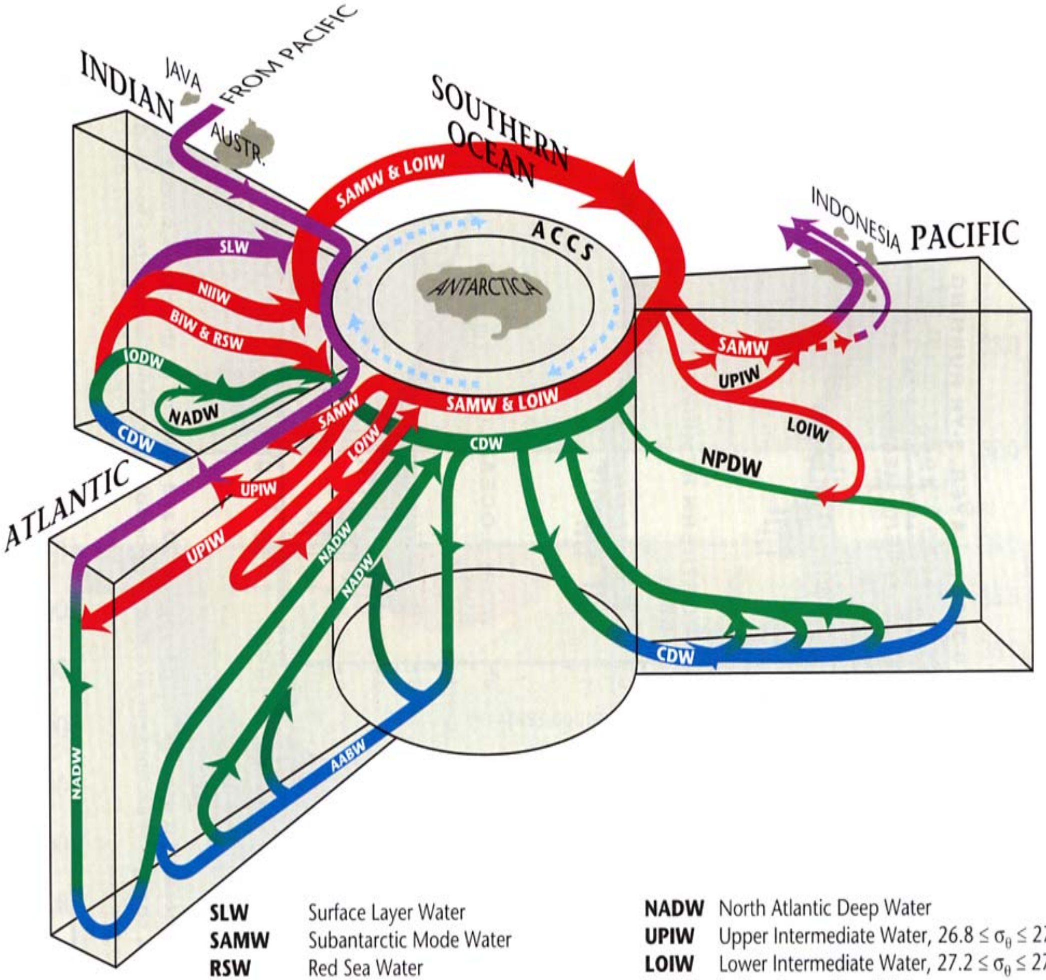

SLW	Surface Layer Water	**NADW**	North Atlantic Deep Water
SAMW	Subantarctic Mode Water	**UPIW**	Upper Intermediate Water, $26.8 \leq \sigma_\theta \leq 27.2$
RSW	Red Sea Water	**LOIW**	Lower Intermediate Water, $27.2 \leq \sigma_\theta \leq 27.5$
AABW	Antarctic Bottom Water	**IODW**	Indian Ocean Deep Water
NPDW	North Pacific Deep Water	**BIW**	Banda Intermediate Water
ACCS	Antarctic Circumpolar Current System	**NIIW**	Northwest Indian Intermediate Water
CDW	Circumpolar Deep Water		

Plate 1.2.7 (see p. 22) A three-dimensional schematic showing the meridional overturning circulation in each of the oceans and the horizontal connections in the Southern Ocean and the Indonesian Throughflow. The surface layer circulations are in purple, intermediate and SAMW are in red, deep in green and near-bottom in blue. From Schmitz (1996b).

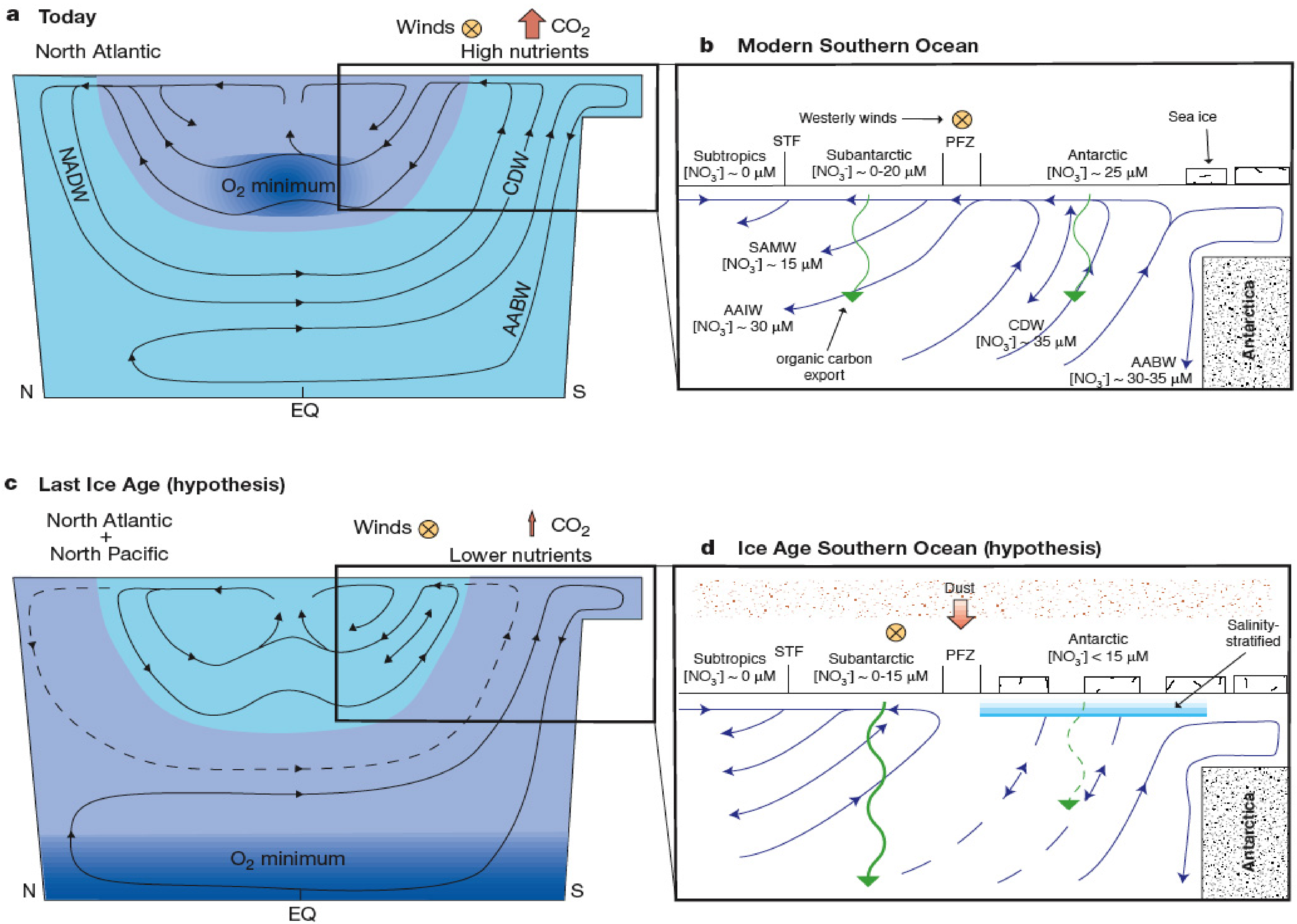

From Sigman & Boyle, 2001.

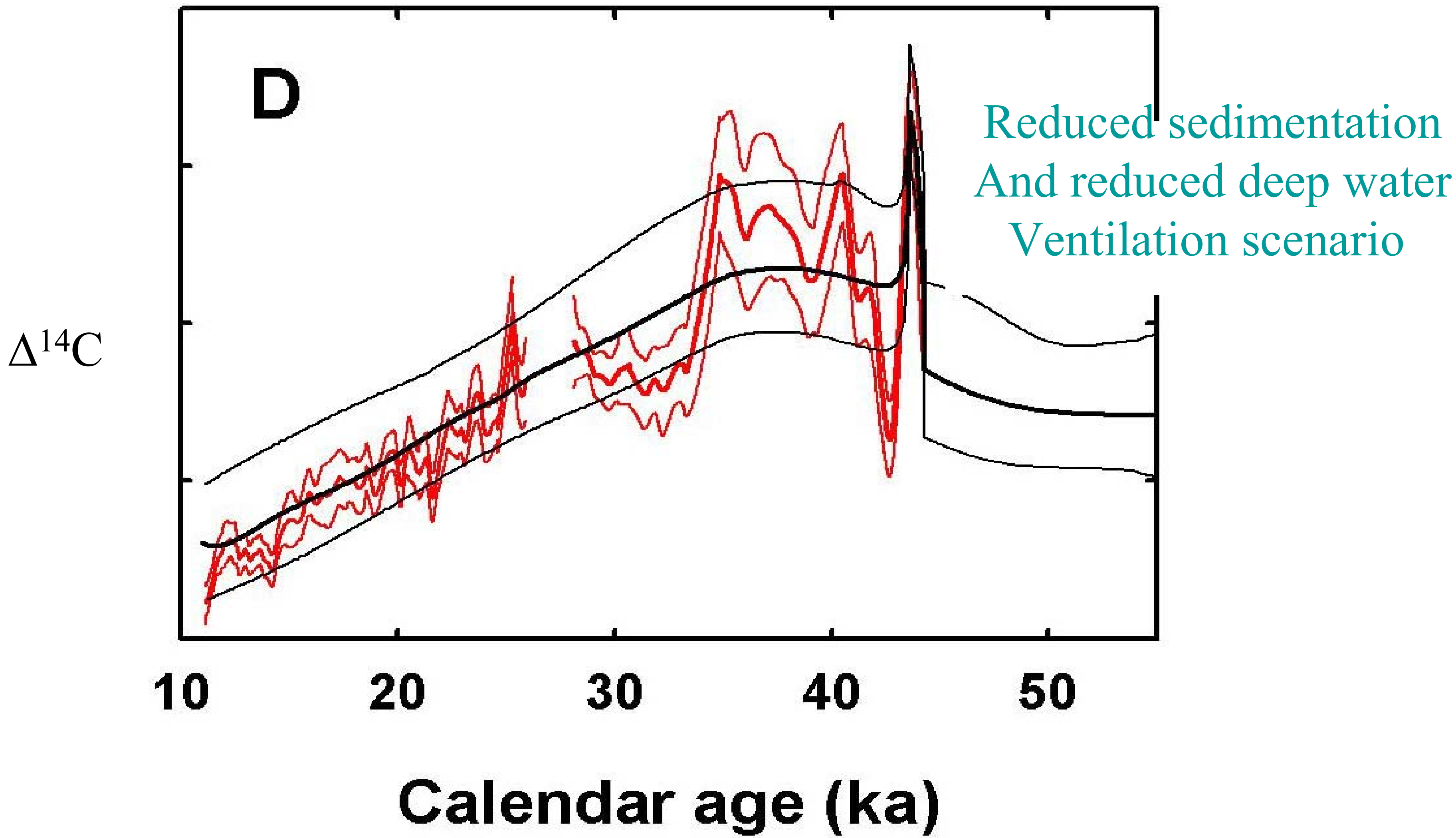

D
Reduced sedimentation
And reduced deep water
Ventilation scenario
$\Delta^{14}C$
10
20
30
40
50
Calendar age (ka)

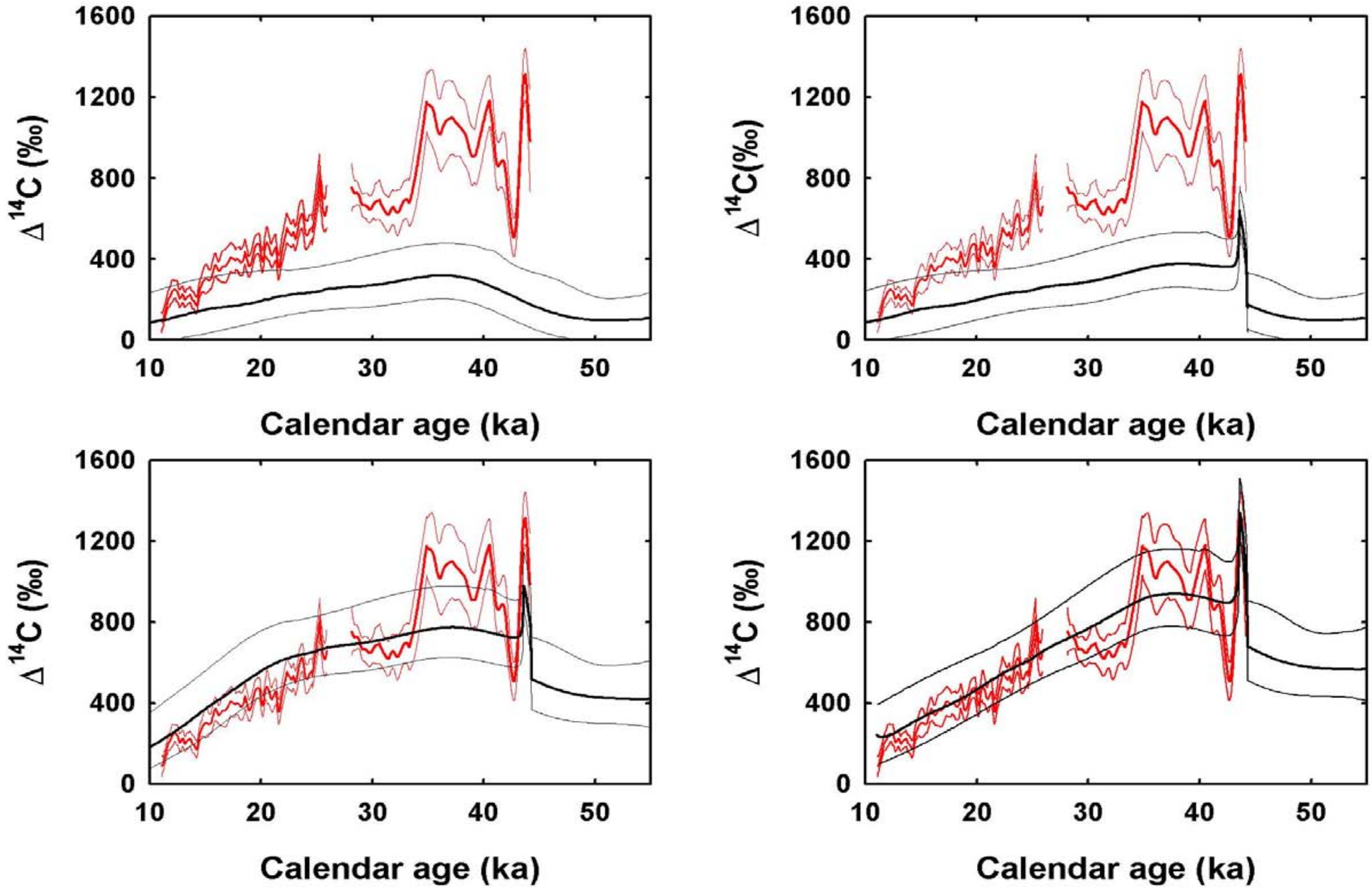

Δ14C (‰)
Calendar age (ka)
0
400
800
1200
1600
10
20
30
40
50

Radiocarbon during the last glacial maximum and deglaciation

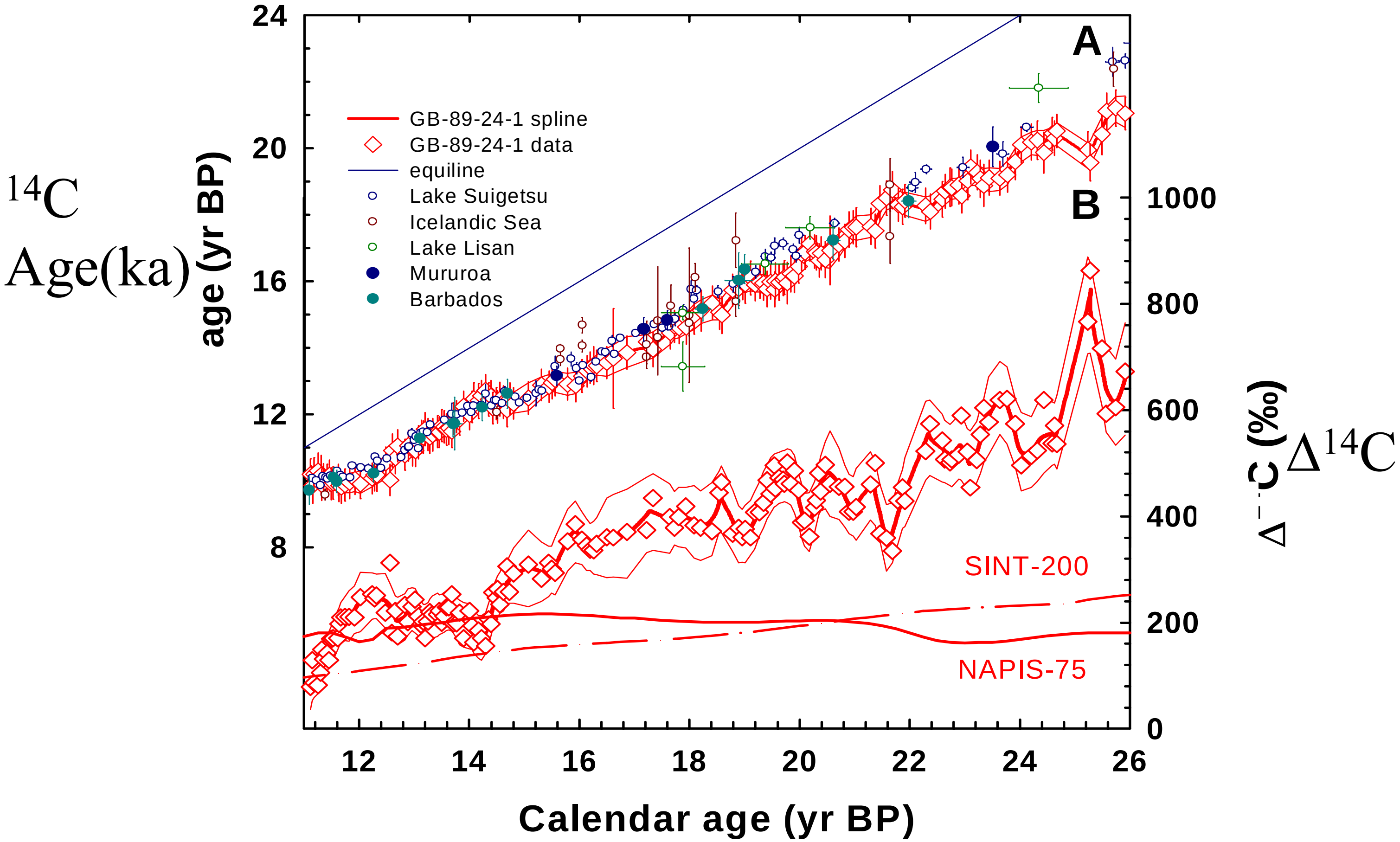

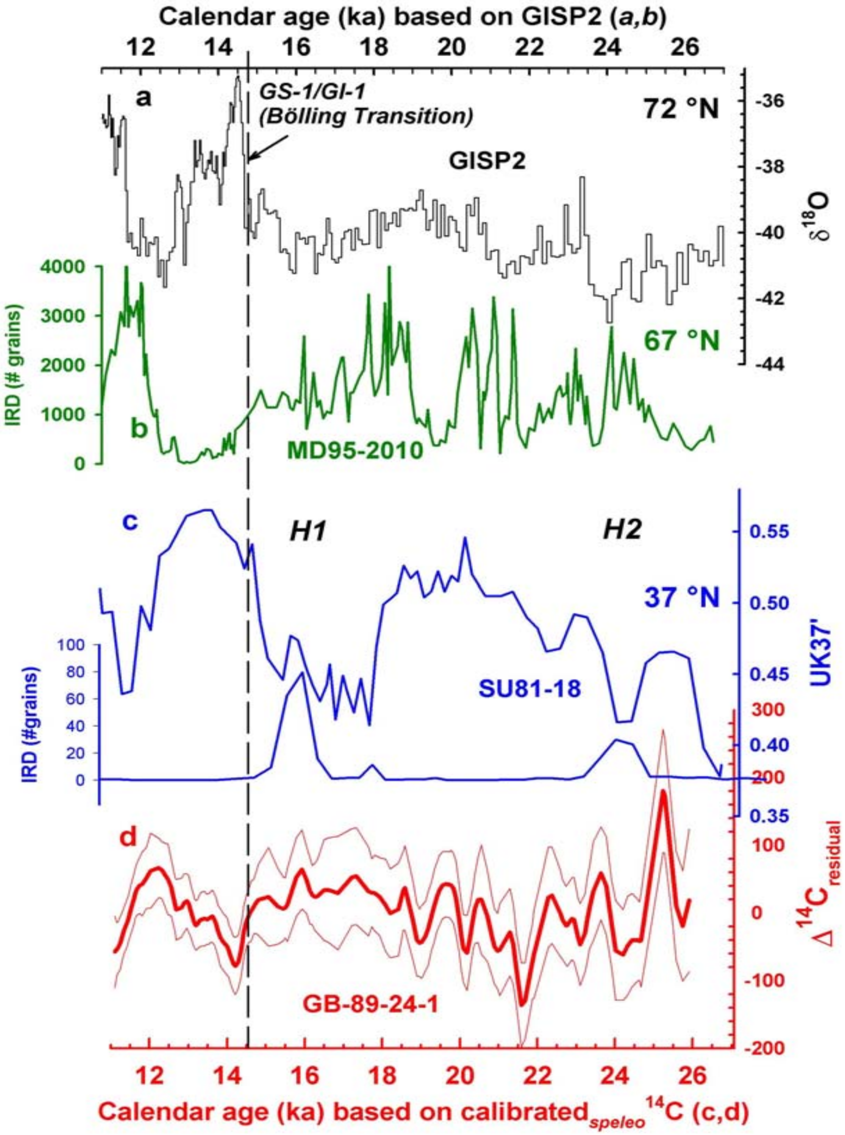
Calendar age (ka) based on GISP2 (a,b)
12 14 16 18 20 22 24 26
a
GS-1/GI-1
(Bölling Transition)
72 °N
GISP2
-36
-38
-40
-42
-44
δ18O
4000
3000
2000
1000
0
IRD (# grains)
b
MD95-2010
67 °N
c
H1
H2
37 °N
0.55
0.50
0.45
0.40
0.35
UK37'
100
80
60
40
20
0
IRD (#grains)
SU81-18
d
300
200
100
0
-100
-200
Δ14Cresidual
GB-89-24-1
12 14 16 18 20 22 24 26
Calendar age (ka) based on calibratedspeleo14C (c,d)

Different mode of circulation during the last glacial period

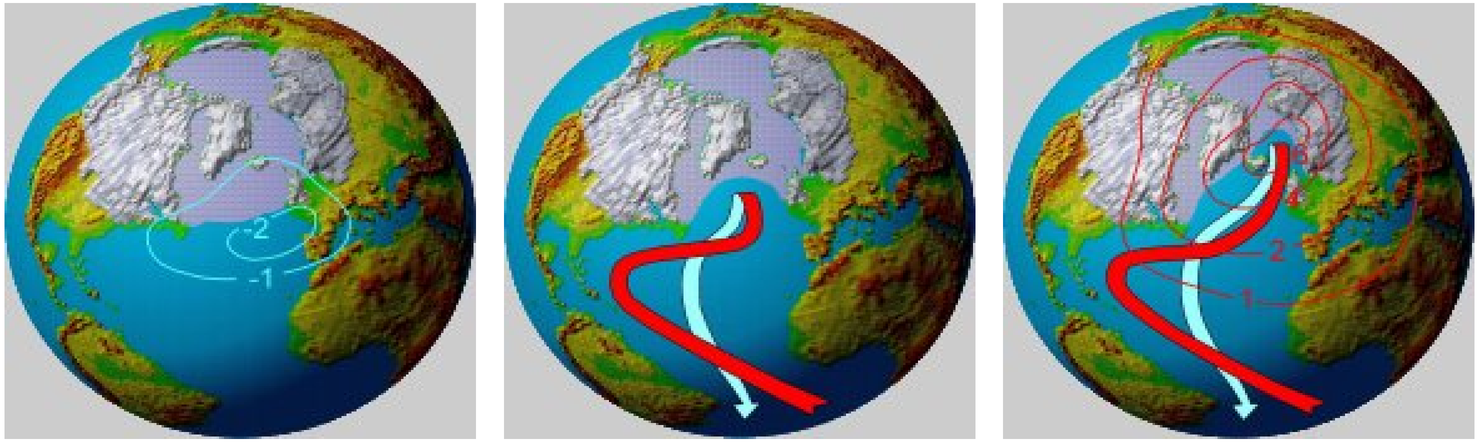

Heinrich event
'meltwater cap' halts thermohaline circulation - colder

Normal glacial mode
thermohaline circulation active

Dansgaard-Oeschger event
enhanced convection, further north in Norwegian Sea, hence warmer

Ganopolski, A. and S. Rahmstorf, 2001: Simulation of rapid glacial climate changes in a coupled climate model. *Nature*, **409**, 153-158.

Modelled ocean convection

Modern/Holocene

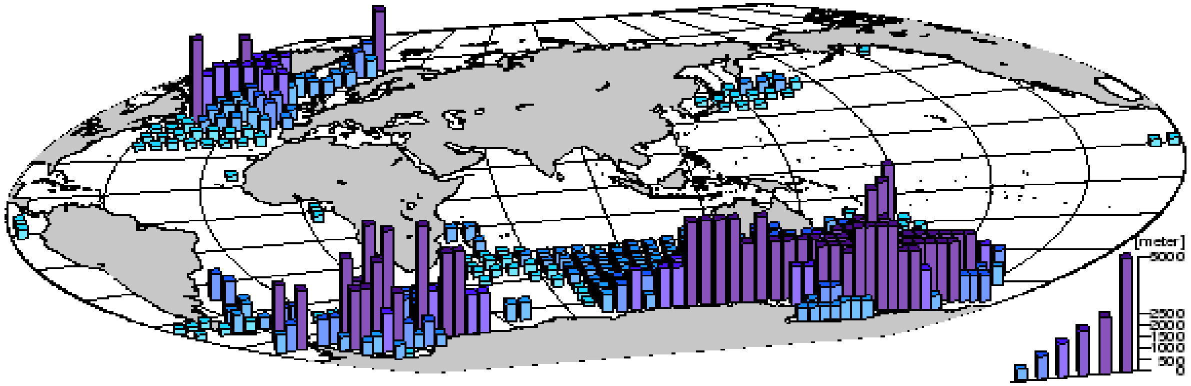

The heights of the bars are equal to the depth of convection.

Meltwater event

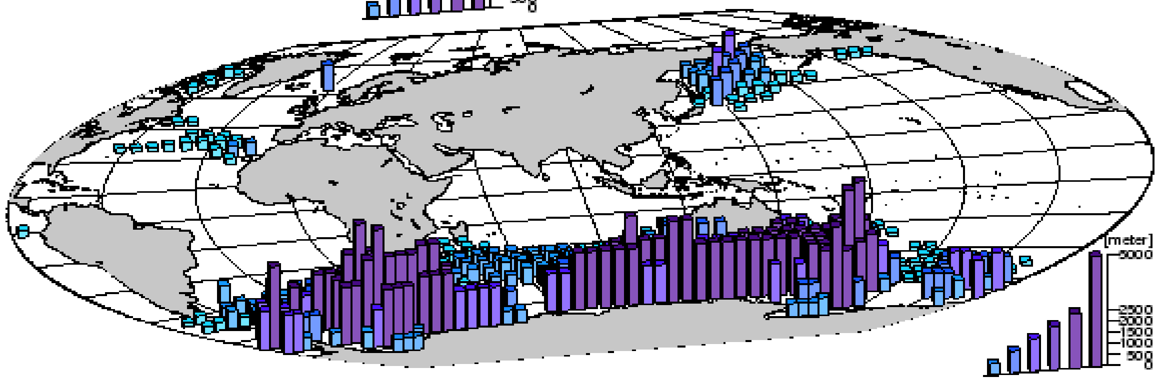

Numerical study of glacial and meltwater global ocean thermohaline conveyor by Seidov, D and Haupt, B. J. in Computerized Modeling of Sedimentary Systems, Ed. J. Harff, W. Lemke, and K. Stattegger, 1999, ISBN 3-540-64109-2, pages 79-113

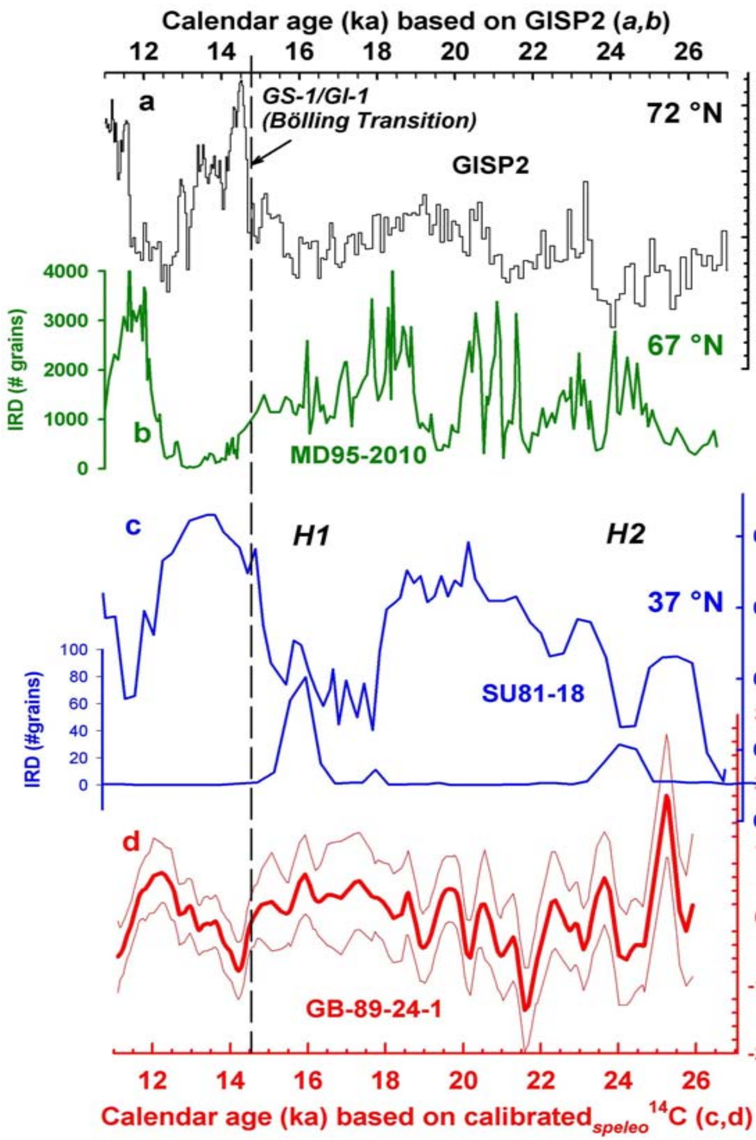

Calendar age (ka) based on GISP2 (a,b)
12 14 16 18 20 22 24 26
a
GS-1/GI-1
(Bölling Transition)
72 °N
GISP2
-36
-38
-40
-42
-44
δ18O
4000
3000
2000
1000
0
IRD (# grains)
b
MD95-2010
67 °N
c
H1
H2
37 °N
0.55
0.50
0.45
0.40
0.35
UK37'
100
80
60
40
20
0
IRD (#grains)
SU81-18
300
200
100
0
-100
-200
d
Δ14C residual
GB-89-24-1
12 14 16 18 20 22 24 26
Calendar age (ka) based on calibrated speleo 14C (c,d)

(After McManus et al, 2004)

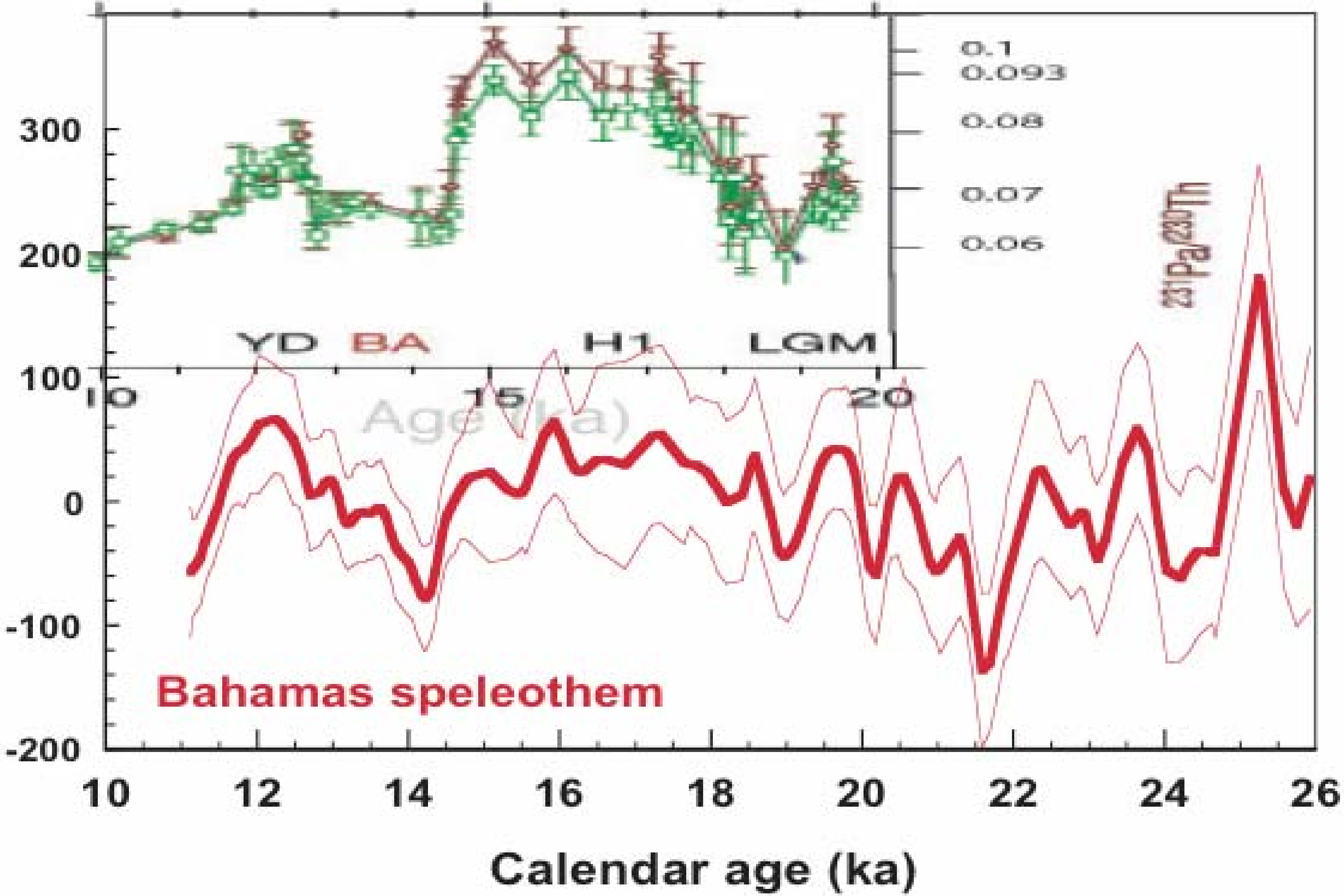

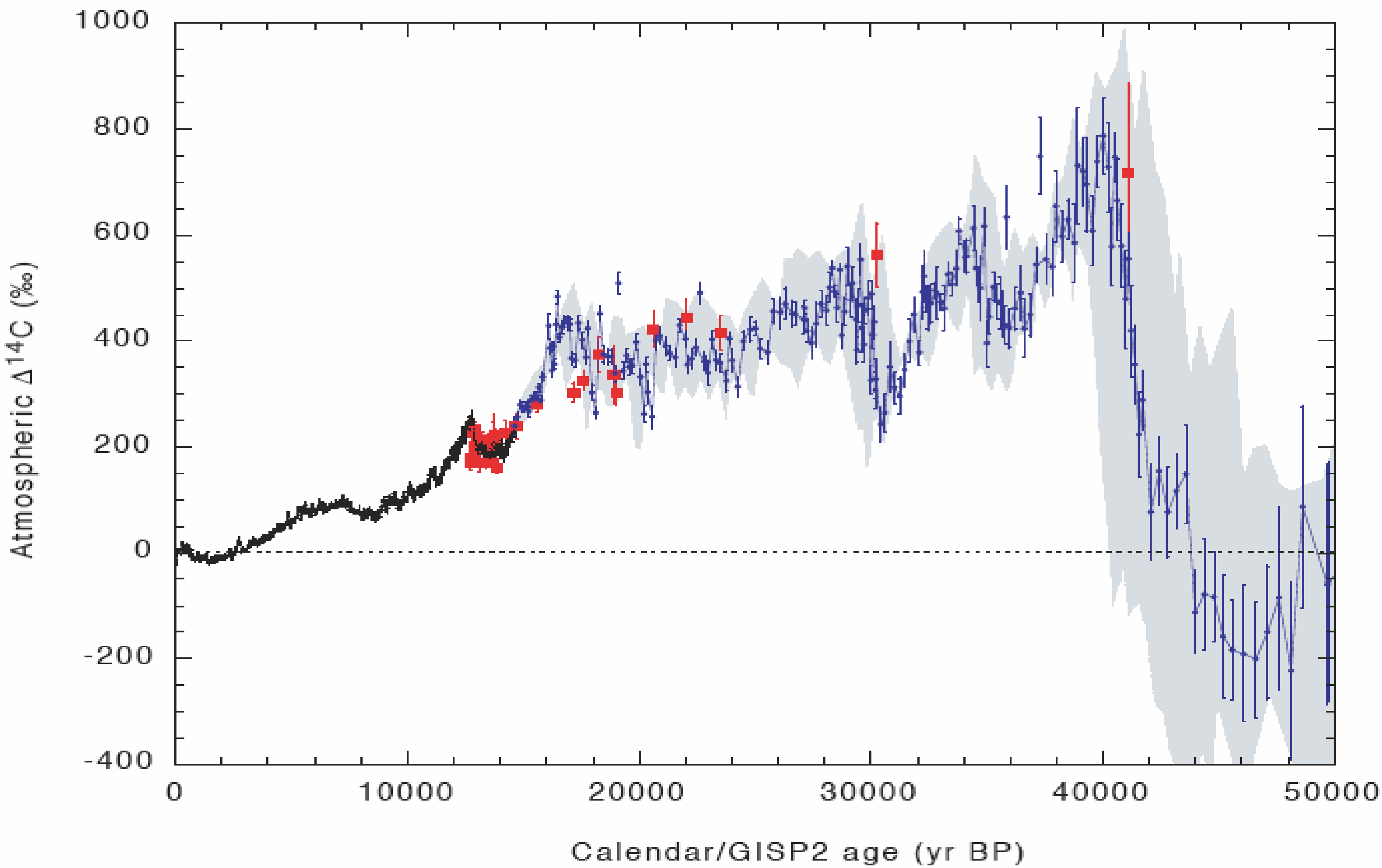

Fig. 3. Atmospheric $\Delta^{14}C$ for the past 50 cal. ka B.P. Symbols are the same as those in Fig. 2A. Cariaco error bars represent independent uncertainty in $\Delta^{14}C$ due to 1-σ ^{14}C age error. Light gray shading shows additional uncertainty in Cariaco $\Delta^{14}C$ due to calendar-age error that is not independent from sample to sample, but rather would shift sections of the curve together within the limits of the shading. Dotted line is modern preindustrial atmospheric $\Delta^{14}C$, defined as 0‰. Upper and lower limits were determined by adding and subtracting 1–σ errors to the calendar age and recalculating $\Delta^{14}C$ with the use of the new calendar ages.

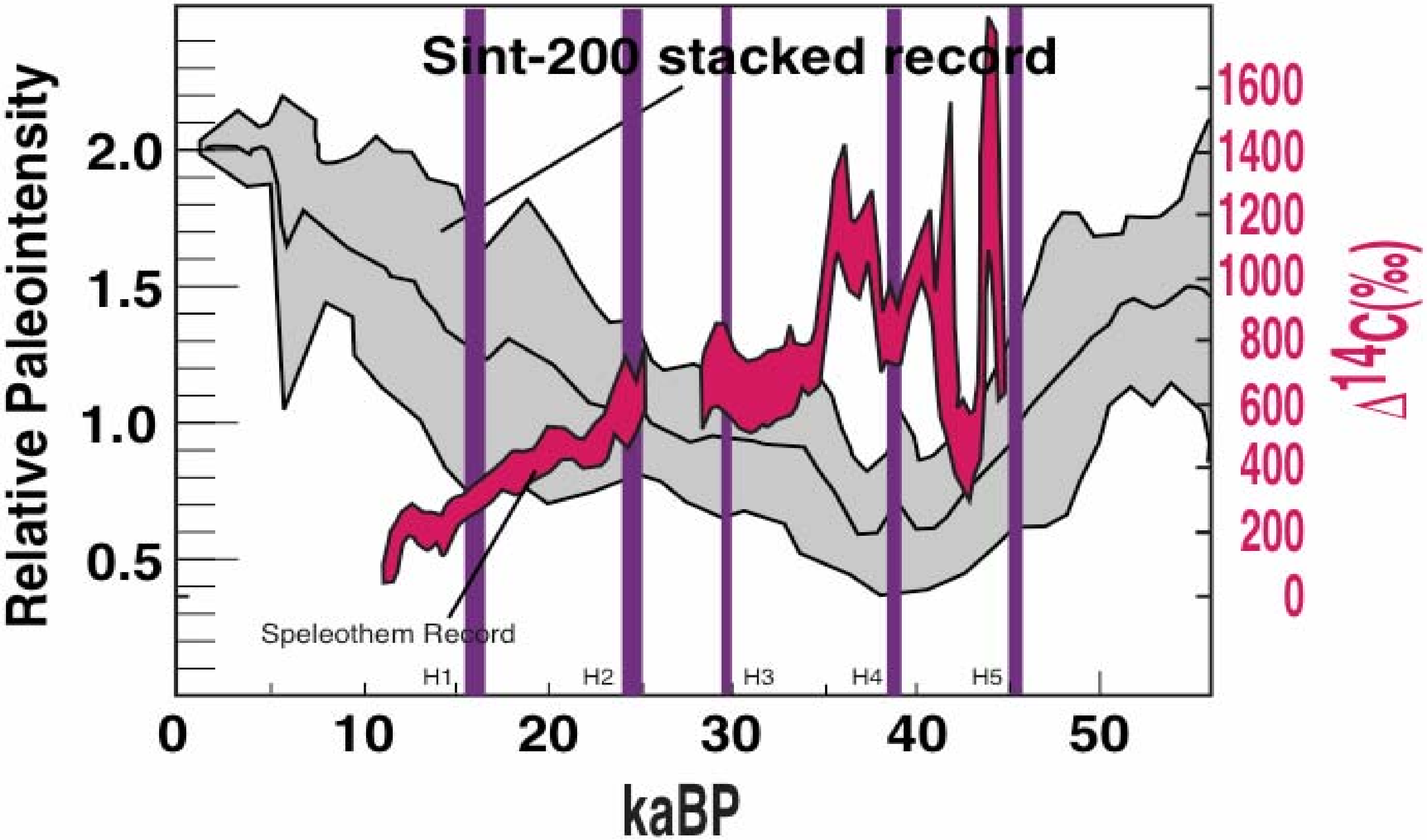

Sint-200 stacked record
Relative Paleointensity
2.0
1.5
1.0
0.5
1600
1400
1200
1000
800
600
400
200
0
Δ14C(‰)
Speleothem Record
H1
H2
H3
H4
H5
0
10
20
30
40
50
kaBP

Conclusions

Atmospheric ^{14}C rose to very high levels during MIS3
This was in part due to low geomagnetic field, but
Carbon cycle box models show that either
carbon sedimentation rate or ocean overturing rate
Or both must have been significantly lower (~1/3 lower)
In order to achieve such high $\Delta^{14}C$.

Smaller fluctuations in the ^{14}C records appear synchronous
With Heinrich events, suggesting that shutdown of deep
Ocean ventilation associated with these events was significant
And prolonged.